STUDIES OF INTERSTELLAR REDDENING.

BY

J. W. HARRIS.

A thesis for the degree of Master of Science submitted to the University of Edinburgh.

AUGUST 1969.

SUMMARY.

The wavelength dependence of interstellar obscuration, in magnitudes against reciprocal wavelength, is known to be well represented, over the visible part of the spectrum, by two straight lines intersecting at or near the broad interstellar absorption band at 4430A. The existing measures, obtained principally from low dispersion objective prism spectra, have a bandwidth of about 50A so that the question arises as to whether the observed "corner" is simply the unresolved band or is a separate feature of the extinction law. If the latter, it is important to know how sharp the corner is and to see if the linearity of the two parts of the curve holds good at higher resolution. The extinction law has therefore been observed with a continuous distribution of measured points at a resolution of 6A which is sufficient to give a number of points within the interstellar band. The data were obtained from photographic slit spectra of reddened and comparison stars in Perseus, taken at a dispersion of 120A/mm.

It appears that the corner of the extinction law and the 4430A interstellar band are separate features, provided that the band is completely contained within 50A. Between 2.0 and 2.7 μ^{-1} at a resolution of 6A, the intersecting straight lines representation is still valid, while the intersection point is defined to 17A. At the level of the observational errors in extinction, the change of slope is shown to occur within the resolution bandwidth. The sharpness of the corner and the straightness of each section of the curve, as found here, confirms the suggestion that existing theories of extinction, based on classical scattering by interstellar grains, are not entirely adequate.

PREFACE.

A summary of the results of the investigation recorded here has been communicated to "Nature" and is now in press.

Thanks are due to Professor H.A. Brück for the use of the facilities of the Royal Observatory Edinburgh, where this work was carried out. The author acknowledges with pleasure the help and advice of Dr.V.C. Reddish and would like to thank him and Dr.K. Nandy for valuable discussions.

John W. Harris.

Royal Observatory,

Edinburgh.

August 1969.

CONTENTS.

CONTENTS.

1. THE CORNER OF THE EXTINCTION LAW.

1.1 INTRODUCTION.

A proportion of the matter in the Galaxy exists in the form of gas and dust between the stars. This , so called, interstellar medium plays an important role in the structure and evolution of the Galaxy and in the formation of stars. The understanding of these topics requires a knowledge of the nature and properties of the medium but, while the gas component of the medium is known to consist mainly of hydrogen, the identity of the dust particles is still not certain.

The light of distant stars is dimmed and reddened by the dust, which tends to be present in the form of clouds, and estimates of stellar distances are very dependent on the assumed obscuration. Trumpler (1), in 1930, was able to show the existence of a general obscuration by setting up a distance scale which was independent of photometric measurements and based on the angular diameter of open clusters. He found the photographic extinction to be about 1 mag./kpc and discovered that extinction is always accompanied by reddening. By assuming a universal wavelength dependence for the interstellar obscuration, the total extinction for a star can be derived from the difference between the observed and intrinsic colours of the star. This assumption was shown to be approximately correct by Stebbins, Huffer and Whitford (2) who investigated the wavelength dependence of extinction using three colour photometry. They compared the UBV colours of heavily reddened and little reddened stars of the same spectral type and demonstrated that the extinction in magnitudes varied inversely as the wavelength. Observations over an extended wavelength range have since shown deviations from this simple proportionality, particularly in the infra-red and ultra-violet, and it is also evident that the extinction law is not uniform across the sky.

The premise that dust particles are responsible for extinction, stems from the need to explain the approximate inverse wavelength dependence of the extinction in magnitudes and to obtain a photographic extinction of the order of 1 mag./kpc from material having an overall mass density less than about 3×10^{-24} gm/cm . The latter figure is an upper limit to the local density of the interstellar medium which was derived by Oort (3) from a study of stellar motions perpendicular to the plane of the Galaxy. Metallic particles with sizes of the order of 0.01 μ and dielectric particles with sizes of the order of 0.5 μ will both produce the right form of extinction by classical scattering and absorption. About one per cent of the mass of the interstellar medium is then required to be in the form of solid particles.

Because of the association of gas and dust clouds, Lindblad (4), in 1935, suggested that the dust particles, or interstellar grains, condense out of the interstellar gas. Until recently, most theories of grain formation were based on these ideas. When the expected interstellar element abundances are taken into account, the most likely composition for the grains appears to be an ice contaminated by compounds containing the elements H, C and N, as proposed by Van de Hulst (5). An alternative particle based on theories of grain formation consists of an aggregate of free radicles. These Platt (6) particles are very small and would cause extinction by a quantum mechanical process.

The discovery, in 1948 by Hiltner and Hall (7), that the interstellar medium produces partial plane polarisation of star light gives further evidence for the existence of grains. Polarisation is supposed to be produced by aligned grains, the alignment being caused by Galactic magnetic fields. To explain the high ratio of polarisation to extinction, which can reach 3 per cent per magnitude of extinction,

Cayrel and Schatzman (8) put forward the idea that a proportion of the grains are graphite flakes. These would readily align and strongly polarise, on account of the marked electrical anisotropy of graphite. Hoyle and Wickramasinghe (9) have taken the suggestion further and have developed a theory for the formation of graphite grains on the surfaces of cool carbon stars.

Observational work during the last decade has been aimed at extending the wavelength range of extinction measurements and at increasing their accuracy, particularly in the visible. Measurements have also been made of the wavelength dependence of polarisation. As a result of the improved observations, it is possible to distinguish between the various proposed grain theories and dielectric grains having a graphite core are now perhaps the most plausible. The argument for such a grain model turns, to some extent, on a very characteristic feature of the extinction law which is detailed in Section 1.4 . Since the same feature also raises doubts as to the assumed nature of the extinction mechanism, it forms the subject of the present observational investigation.

1.2 THE OBSERVED EXTINCTION LAW.

In principle, the form of the extinction law is readily found by comparing the observed spectral energy distributions of a reddened star and unreddened star having the same spectral type and luminosity class. O and B stars have generally been used for this purpose because of their brightness, small range of intrinsic colours and comparatively featureless spectra. Unless the stars are at the same or known distances, it is only possible to determine the relative attenuation at different wavelengths and it is therefore usual to arbitrarily define the magnitude of extinction as zero at some chosen wavelength.

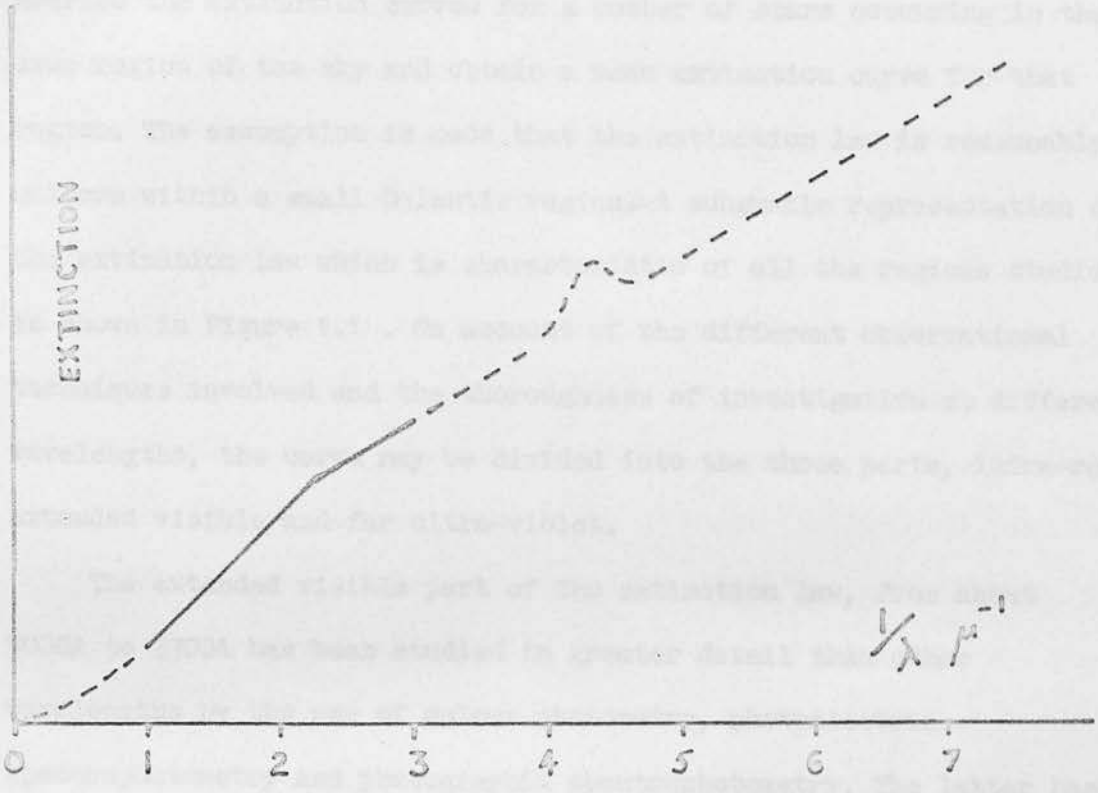

FIGURE 1.1

Schematic extinction law.

The solid line indicates the best known part of the curve.

In order to compare the extinction curves derived from different pairs of stars, it is also usual to choose a second reference wavelength and normalise the measurements to give unit colour excess between the two reference wavelengths.

Because it is difficult to match pairs of stars and find comparison stars with little or no reddening, it is necessary to average the extinction curves for a number of stars occurring in the same region of the sky and obtain a mean extinction curve for that region. The assumption is made that the extinction law is reasonably uniform within a small Galactic region. A schematic representation of the extinction law which is characteristic of all the regions studied, is shown in Figure 1.1 . On account of the different observational techniques involved and the thoroughness of investigation at different wavelengths, the curve may be divided into the three parts, infra-red, extended visible and far ultra-violet.

The extended visible part of the extinction law, from about 9000A to 3300A has been studied in greater detail than other wavelengths by the use of colour photometry, photoelectric spectrophotometry and photographic spectrophotometry. The latter has provided the most detailed information regarding the shape of the extinction law, the most definitive observations to date being those of Nandy (10 – 14) . As indicated in Figure 1.1, the extinction law is nearly linear with an abrupt change in slope at about 2.3 μ^{-1}. It appears that the amount by which the slope changes is a function of Galactic longitude, a result in accord with the variations shown by the earlier wide band measures of Johnson and Morgan (15), Borgman (16) and Wampler (17).

Wide band infra-red observations which extend to wavelengths of a few microns have been made by Johnson and Borgman (18) and

Johnson (19). The interpretation of these measures is not straightforward owing to the change in effective wavelength of the filters with the colour of the star observed and the difficulty of finding suitable test objects. However, it would appear that the extinction law has a small positive slope at long wavelengths and shows considerable variation between Galactic regions.

Since, for any mechanism whatever, extinction must be zero at infinite wavelengths, extrapolation of the infra-red part of the extinction law to infinite wavelengths gives the zero point for the otherwise arbitrary scale of extinction. The ratio of the absolute extinction at one wavelength to the relative extinction between two wavelengths can then be estimated. This, so called, ratio of total to selective extinction is in general agreement with the average value found by other methods, such as star counts, and is much used to correct stellar distances on the basis of colour excess measurements.

At wavelengths shorter than 3000A, observations must be made from above the earth's atmosphere. Because such observations are far from extensive, little is known of the intrinsic ultra-violet colours of stars and their relation to the visual spectral types. The extinction curve for this region is therefore very uncertain. Boggess and Borgman (20) compared stellar fluxes in the ultra-violet with model atmosphere calculations, while Stecher (21) has derived extinction estimates from pairs of stars at wavelengths down to 1200A. Two features of the extinction law emerge; the general rise in extinction towards the far ultra-violet, which roughly follows the trend established in the near ultra-violet, and what may be taken to be a superposed peak in the extinction at $4.4\ \mu^{-1}$.

1.3 THE GRAPHITE CORE - ICE MANTLE MODEL.

Apart from a scaling factor, the extinction law would represent the extinction cross section of individual interstellar grains if these were all identical. For the real case of a distribution of particle sizes, an integrated cross section is applicable. In fitting a grain model to the observed extinction law, the classical scattering and absorption of radiation is calculated on the basis of Maxwell's equations using the complex index of refraction of the assumed grain material. It is also necessary to furnish a model for the grain size distribution. Though element abundance considerations restrict the choice of possible chemical compositions for the grain material, constraints on the physical constitution of the grains are less certain, so that scope exists for various combinations of material and size distributions.

Grains comprised of a graphite core coated with a mantle of dirty ice provide a reasonable fit with the entire wavelength range of the observed extinction and are consistent with the wavelength dependence of polarisation, as shown by the calculations of Wickramasinghe and others (22). The metallic like absorption by the core accounts for all the infra-red extinction and gives a linear extinction curve in the visible. At short wavelengths, scattering by the mantle becomes increasingly effective and maintains the rise in extinction in the far ultra-violet. Typical sizes for the core and mantle are 0.05 μ for the core radius and 0.16 μ for the outer radius of the mantle. By adjusting these dimensions, the change in slope that occurs towards the ultra-violet can be altered to agree with the regional Galactic variations given by Nandy (23) .

The success of the model depends on the ability of graphite particles to produce a change of slope similar to the "corner" of the

extinction law at 2.3 μ^{-1}. This effect is a property of the refractive index of graphite and occurs for particles of radius of the order of 0.05 μ and above. However, the strongest case for the presence of graphite relates to the peak in the extinction curve at 4.4 μ^{-1}. Graphite has a strong ultra-violet absorption band which causes a maximum in the cross section of small particles at a wavelength which coincides with the observed extinction peak (24). The two conspicuous features of the extinction law therefore seem to provide fairly direct evidence that graphite is at least in part responsible for interstellar extinction.

1.4 THE CORNER OF THE EXTINCTION LAW.

It was first pointed out by Whitford (25) and later confirmed by Nandy (10) that the change in slope of the extinction law takes place over a narrow range of wavelengths. In fact, the observations of Nandy show that the change is confined to less than 200A and that extrapolation of the linear section of the curve each side of the corner yields an intersection point which does not appear to change with Galactic longitude. By comparing the absolute spectral energy measures of O stars obtained by Oke (26) and Willstrop (27) with model atmospheres, Underhill and Walker (28) have derived a similar corner.

Though the presence of the corner can be explained in terms of a specific refractive index effect of graphite particles, its close proximity to the 4430A interstellar band raises further questions. One might ask whether the unresolved band gives rise to the observed corner, or, if the corner is real, what effect it might have on measured profiles of the band. In determining the band profile, the necessary continuum fitting could be easily disturbed by the corner. Quite apart from the interstellar band, it proves difficult to match

the sharpness of the corner by theoretical extinction curves (23).

A matter not unrelated to the reality and sharpness of the corner concerns the linearity of the curve each side of the corner. According to Nandy (14), the departure from linearity over the range 1.2 μ^{-1} to 2.9 μ^{-1} is less than 0.005 magnitude when the curve is normalised to make the blue–visible slope unity. This implies that the integrated cross section of the grains is linear with reciprocal wavelength to better than one per cent. Even if some features of the curve are hidden for want of resolution, it is difficult to account for the lack of curvature, particularly as this applies to both sides of the corner. This aspect of the extinction curve, taken in conjunction with the comparative sharpness of the corner, suggests that existing theories based on classical scattering may not be entirely correct.

As the only characteristic of the extinction curve, other than the feature at 4.4 μ^{-1}, which might be directly associated with a particular element or compound, the corner merits examination. If the corner should prove to be a separate entity to the 4430A interstellar band, its position and sharpness would be required to establish the agent or mechanism responsible. The extinction law has therefore been measured over 2000A in the vicinity of the corner, with a resolution and density of datum points sufficient to resolve the interstellar band. The range of wavelengths permits the validity of Nandy's straight lines to be tested at higher resolution. Emphasis has been placed on the estimation of errors in order to provide figures which will be of physical significance.

2. OBSERVATIONS.

2.1 TELESCOPE AND SPECTROGRAPH.

The Edinburgh 36 inch reflector is a Cassegrain instrument with a focal ratio of F/18 giving images which are typically 3 arc seconds across. A particularly useful facility provides for rotation of the spectrograph about the telescope axis. By setting the spectrograph slit vertical, atmospheric dispersion in the image is along the slit length and has no effect on continuum spectroscopy.

The grating spectrograph is, in the configuration used, basically an all mirror instrument which transmits in the ultra-violet beyond the usual glass cut off at 4000A . A high camera to collimator focal length ratio of 18 is obtained with an F/1 schmidt camera of 10 cm aperture. The high ratio gives emulsion limited resolution for all but the widest slit widths. A field flattening lens permits the use of flat photographic plates measuring 15 mm by 22 mm and up to five spectra can be exposed on one plate. Spectra are widened by the use of a quartz rocking plate of two seconds period which is placed beneath the slit. For the purpose of controlling exposure, a small amount of light is abstracted from the collimator beam and passed into a photomultiplier. Electronic integration of the photomultiplier current provides a measure of the total light flux incident on the photographic plate.

The spectrograph was set up with a grating having 600 lines/mm blazed at 5000A to give a dispersion of 120A/mm in the first order, while the rocking plate mechanism was adjusted to give spectra 0.3mm wide. It was decided to sacrifice resolution to a small extent in order to pass as much starlight as possible through the spectrograph slit. Therefore, the projected slit width was matched to the photographic spread function which was taken to have a half depth width of 15 μ .

With a slit width of 270 μ equivalent to 3.4 arc seconds on the sky, practically all the starlight enters the slit unless observing conditions are very poor.

2.2 CALIBRATION SPECTROGRAPH.

The calibration plates were exposed for times comparable to the stellar exposures in a multiple slit grating spectrograph which has a dispersion of 50 A/mm, and gives spectra having a total brightness range of about 5 magnitudes. There are 14 slits 0.75 mm high and separated by the same amount while the widest slit is 2 mm in width. Both collimator and camera mirrors have a focal length of 122 cm and work at F/16 . The only transmitting component is a field lens which was changed to match the light source required by this work. It was replaced by quartz, rather than glass, so as to obtain spectra below 4000A wavelength. Exposures can be timed to the nearest half minute by a shutter placed before the slits which is worked from an electrical time switch.

Since the stellar spectra are widened by using a rocking plate, the exposures are of an intermittent nature, there being two exposures per cycle of the rocking plate. To roughly simulate this in the calibration spectrograph, a chopper with appropiate rate is placed before the entrance slits. In the stellar spectrograph, the projected visual width of star images on the photographic plate, perpendicular to the direction of dispersion, is calculated to be about 15 u and is subject to seeing and guiding errors, but the image spreads beyond this because of light scattering in the emulsion. As the stellar spectra are widened to some 300 μ, a chopper mark-space ratio of the order of, say, 1:15 is indicated. A simple on off type chopper does not correctly reproduce the exposing conditions, so the ratio is even less well

defined. However, the actual ratio used is not very critical (29), any resulting photographic effect being similar to reciprocity failure and the same for all plates. The ratio was set to 1:5 which may seem low, but it has the practical advantage of allowing more light to enter the calibrator.

2.3 CALIBRATOR LIGHT SOURCE.

It seemed desirable that the colour of the light source should not be too different from one exposure to the next so that comparison of characteristic curves from one plate to another and from wavelength to wavelength would be meaningful. In fact, if the colour was quite stable then the calibration spectra could be used to detect any differences in wavelength sensitivity and allow direct comparison of stellar spectra on different plates. The existing light source was inadequate in this respect, so a light source was therefore sought which would ensure that the colour of the light reaching the spectrograph slits would vary as little as possible. Advantage was taken of the decision to change the light source by extending the wavelength coverage into the ultra-violet to match that of the stellar spectrograph.

A 12 volt 100 watt tungsten-iodine lamp was chosen as a suitable source of light. Since the filament of such a lamp does not evaporate, the colour ought to remain constant. Also no metal film forms on the envelope so there is no progressive dimming of the output or change in the colour transmission properties of the envelope. The quartz envelope permits the use of radiation at wavelengths below 4000A , while such radiation is greater than normal on account of the higher filament temperature.

Calibration exposure times are roughly matched to stellar ones

so some means must be provided for attenuating the output of the light source but in a neutral manner if the colour is to be preserved. Neutral filters tend to be opaque below about 4000A and so cannot be used. However, the inverse square law can be made use of. In the arrangement adopted, light from the lamp, passing over a variable distance, illuminates a magnesium carbonate diffusing surface which in turn is focussed on to the spectrograph grating via a quartz field lens in front of the slits. The field lens ensures that the slit ratios are invariant to any lack of uniformity of the grating or in the illumination of the diffusing surface, provided also that the distance between the slits and diffusing surface is great enough to give almost uniform illumination of the slits; in this case set to better than one per cent. As a further precaution, the smallest distance between the lamp and diffusing surface is such that the surface is still substantially uniformly illuminated. Meeting these requirements involves a considerable loss of light, while the maximum distance between the lamp and diffusing surface places a restriction on the range of brightness levels possible. In practice, the large output and small physical size of the lamp allows a range of brightness of 5 magnitudes, while the shortest stellar exposure can be matched.

It was necessary, before using the light source, to produce a calibration of light intensity at the calibrator slits against the distance between the lamp and diffusing surface. The calibration should equally well apply to the intensity at the camera focus and it ought to obey the inverse square law. A photomultiplier was set up at the zero order focus. The reciprocal of the square root of the cell output is plotted against the inter lamp diffusing-surface distance in Figure 2.1. Within the errors of measurement, the inverse square law is obeyed, except when the lamp is so close up to the diffusing surface

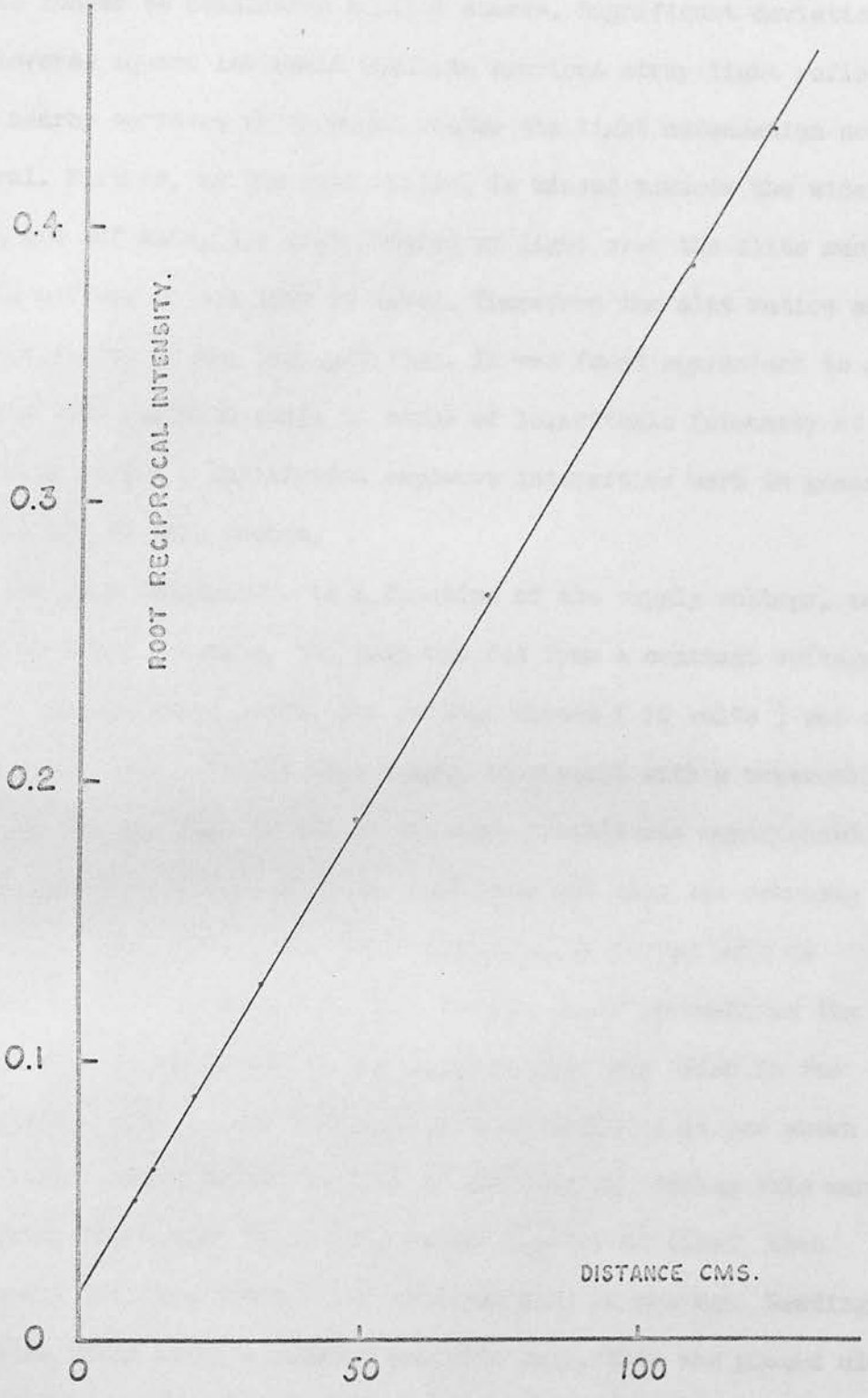

FIGURE 2.1

Inverse square law attenuation of calibrator light source.

that the latter is no longer uniformly illuminated and the lamp filament can no longer be considered a point source. Significant deviations from the inverse square law would indicate spurious stray light reflected from nearby surfaces which might render the light attenuation non neutral. Further, as the cell reading is biased towards the widest slits which are off axis, the distribution of light over the slits must remain uniform as the lamp is moved. Therefore the slit ratios should be independent of the lamp position. It was found convenient to mark off the lamp position scale in terms of logarithmic intensity at intervals of 0.1 . Calibration exposure intensities were in general rounded off to this amount.

The lamp temperature is a function of the supply voltage, so, to minimise colour changes, the lamp was fed from a constant voltage D.C. source through heavy leads. The voltage chosen (10 volts) was one which would give a fairly high output consistent with a reasonable lifetime for the lamp of 400 hours. Some trouble was experienced in making good connections with the lamp pins but this was overcome by putting the pins into heavy brass clamps which served both as connections and the lamp mounting. Despite these precautions the lamp was not stable. By measuring the light in the zero order in the spectrograph with a blue sensitive photomultiplier, it was shown that most change occurs within an hour of swithing on. During this warming up period, the output falls off, rather rapidly at first, then apparently drifting about 4 per cent per hour on average. Readings were also taken using a cadmium sulphide cell. This was placed close to the lamp and the light heavily attenuated by filters so that the current and hence heating of the cell should be small. Since the cadmium cell is red sensitive, comparison of the readings of photomultiplier and cadmium sulphide cell allowed changes in lamp colour to be observed.

On constant voltage, although the light output appeared to vary somewhat, the colour remained substantially constant. When the voltage was purposely changed, changes in colour were quite evident. It was hoped to use a bridge circuit with two cadmium sulphide cells to monitor and correct colour, using feedback to the lamp supply. However, the sensitivity of the cells in the blue is not so high and all the blue filters available let through too much red light to be of any use. Attempts were therefore made to stabilise the output by feedback, because if this is constant, the colour can be supposed constant. An amplifier circuit was arranged to do this but, although it held the current constant in a monitoring cadmium sulphide cell, there was some change in the output according to the photomultiplier installed in the calibrator. Inspection of the lamp filament through a filter revealed that the effective temperature at the ends of the coil filament would not be the same as that on the surface of the coil. Since the cadmium sulphide cells faced the ends of the coil and the calibrator the surface, the different cells would not "see" the same colour.

By the time these investigations had been made, the observing season was well under way and many plates had been calibrated by feeding the lamp from the constant voltage supply. It was therefore thought advisable to calibrate the rest of the plates in the same manner, even though no satisfactory conclusion had been reached regarding the stability of the lamp. The lamp was always used at least an hour after switching on, to allow initial conditions to settle down.

One can place a limit on colour changes accompanying the drift in lamp output by assuming that the lamp is very approximately a black body radiator. From the lamp manufacturer's data, the colour temperature is 3000° K. Then for the 4 per cent variation in output per hour in the blue (4500A), the difference in output between 3300A and 5000A amounts

to about 0.018 magnitude. This is comparable to other sources of error and, in general, calibration exposures were less than an hour, so that colour changes would be smaller. However, this takes no account of possibly larger variations between different periods of lamp operation. These could only be examined in retrospect by consideration of the calibration plates.

For the purposes of wavelength identification on the calibration plates, light from a mercury discharge lamp falls onto the diffusing surface in front of the slits of the calibration spectrograph. Emission lines are thereby superposed on the continuous spectrum. The light is attenuated, as required, by neutral density filters.

2.4 CALIBRATOR SLIT RATIOS.

The light transmitted into the spectrum by the slits of the calibration spectrograph is proportional to their width. However, the "slit ratios" determined from the slit widths do not, in general, give the actual relative brightness of the spectra. It is better to measure the brightness of the spectra to give apparent slit ratios. This takes into account non uniform illumination of the slits, vignetting, contamination by dirt of the fine slits and diffraction losses from the latter. Deterioration in the quality of the grating and mirror surfaces may cause the slit ratios to change a little. Partly for this reason, but mainly because of the change of light source, the slit ratios were determined anew.

There is astigmatism present in the spectrograph and the focus is set mid way between the two astigmatic foci. This has the effect of reducing changes in brightness across the width of spectra on account of lack of parallelism of the slits and of blurring out any streaks that would result from particles of dirt caught in the finer slits.

Also, the extremes of wavelength resolution between the bright and faint spectra are less. Since the edges of the spectra are not sharply focussed, the light intensity is only sufficiently uniform for photometry across a certain proportion of their width. It is thus very necessary to use a suitably chosen width of spectrum for the measurement of the photographic calibration spectra in the densitometer. The slit ratios are only meaningful for the particular width used for their measurement. Further, the analysing slit must always take the same position across the width of any particular spectrum. This can be done objectively by maximising the reading of light intensity, in the case of measurement of slit ratios, or photographic density in the case of photographic spectra. Since the photographic process is non linear, the positions obtained for the analysing slits are not quite the same for the two cases but the difference can be ignored unless the spectra are very non uniform.

The slit ratios were measured photo-electrically with a 1P21 photomultiplier fed from a stable E.H.T. supply unit with the light source set to pass as much light as possible into the calibrator. A slit was mounted in a plateholder so that it occupied the same plane as that normally taken by the emulsion of a photographic plate. The slit height was set at 430 μ after consideration of densitometer tracings of photographs of the calibration spectra which had been traced across the direction of dispersion. Light passed by the slit was imaged onto the photo cell cathode with a field lens to form an image of the grating. This field lens imposed a limit on the slit length of 5.8 mm . To obtain large enough readings for accurate measurement with a galvanometer, the slit was positioned at the wavelength which gave the greatest reading (about 4700A). No attempt was made to measure the slit ratios at other wavelengths since previous measurements did

not show any significant wavelength dependence from 4000A to 7000A, and the range covered by the stellar spectra in this work is very much smaller and includes the wavelength at which the slits were measured.

The plateholder mounting was moved across the spectra, using a fine screw, so that the slit was passed successively through the spectra and the maximum galvanometer readings on each were then recorded. To check for constancy in the light source output, readings were repeated at the finish of each run on the first spectrum measured, this being the brightest. Where the light source had drifted, the readings were then interpolated to correspond with the time when any other particular spectrum was being measured. The mean slit ratios, derived from three runs, are shown in Table 2.1 and are on a magnitude scale with the brightest spectrum (slit 1) corresponding to zero magnitude. They do not differ significantly from previously derived slit ratios and are accurate to better than 0.01 magnitude.

TABLE 2.1

Slit ratios of calibration spectrograph.

SLIT	1	2	3	4	5	6	7	8	9	10	11	12	13	14
MAG.	0	0.37	0.75	1.13	1.50	1.94	2.32	2.67	3.18	3.53	3.94	4.42	4.88	5.04

A small amount of stray light was apparent between the spectra when the slit ratios were being measured. An over exposed plate showed this to be light scattered through small angles, probably by dust on the mirrors. Stray light included in the measurement of brightness of a spectrum at a particular wavelength therefore has much the same wavelength as the spectrum. Although it will change the slit ratios a little, the derived values will still be the correct ones to use.

2.5 SELECTION OF STARS FOR REDDENING PAIRS.

Stars in the Perseus region were chosen for this work partly on account of the large change in slope of the reddening curve each side of the corner. Cygnus might have been more suitable as it contains more heavily reddened stars but it was too low in the sky when the telescope became available. With the spectrograph set to give a dispersion of 120A/mm, as described in Section 2.1, the practical limiting B magnitude was estimated to be about 9 using the Kodak IIa-O emulsion. Therefore, only Perseus O and B stars brighter than this were examined with a view to forming reddening pairs. Data on classification and UBV magnitudes were taken from a paper by Hiltner (30). Because of the need to match star pairs and the restriction on brightness, only about 30 stars could be considered. It was apparent that the scarcity of stars with small colour excess placed a limit on the total differential reddening that could be measured and that each comparison star would have to be paired with more than one well reddened star. It was decided for practical reasons to match most of the stars into groups of three containing two reddened stars and one comparison star. A further practical consideration was that the stars in each group should not have widely differing exposure times. In the final selection there were 20 pairs and 10 independent comparison stars. Except in the case of the O stars, for which thermal colours are nearly all equal, the stars were for the most part matched to better than one spectral type subclass and one luminosity class. See Table 2.2 . When the groups were placed in order of merit, in terms of differential colour excess per unit of exposure time, it was evident that observing effort should be concentrated on the first eight groups.

TABLE 2.2

Stars selected for observation.

Reddened stars.				Comparison stars.			
No.	Star.	Sp. Type.	E_{B-V}	No.	Star.	Sp. Type.	E_{B-V}
1	HD 16429	O9.5 III	0.92	3	HD 13268	O8 V	0.44
2	HD 15558	O6	0.84				
4	HD 15690	B1.5 Ib	0.90	6	HD 13841	B2 Ib	0.47
5	HD 13402	B0.5 I	0.89				
7	HD 14956	B2 Ia	0.96	9	HD 13866	B2 Ib	0.43
8	HD 14143	B2 Ia	0.76				
10	HD 14542	B8 Ia	0.70	12	HD 14322	B8 Ib	0.44
11	HD 17088	B9 Ia	0.88				
13	HD 14947	O6f	0.78	15	HD 14434	O6	0.48
14	HD 15570	O5f	1.02				
16	HD 15629	O5f	0.75	18	HD 12323	O9 V	0.29
17	HD 16691	O5f	0.80				
19	HD 15785	B1 Iab	0.83	21	HD 13854	B1 Iab	0.54
20	HD 15571	B1 II	0.83				
22	BD 60° 493	B0.5 Ia	1.07	24	HD 14818	B2 Ia	0.55
23	HD 16808	B0.5 Ib	0.84				
25	HD 13036	B0.5 III	0.81	27	BD 55° 554	B0 III	0.46
26	HD 15752	B0 III	0.79				
28	HD 13716	B0.5 III	0.61	30	HD 13544	B0.5 IV	0.27
29	HD 15325	B1 IV	0.68				

2.6 DETAILS OF THE STELLAR AND CALIBRATION PLATES.

During the period December 1965 to February 1966, a total of 42 useable stellar spectra were obtained on 19 plates. Details are given in Table 2.3 . To simplify the photometry, it was hoped that each plate would carry the exposures of the three stars in a matched group, and that these would be taken in succession to minimise extinction corrections. Observing conditions did not in general permit more than a few plates to be exposed in this manner. The aim of at least two exposures per star was nearly achieved. This was done to check identification, to detect plate faults and reduce photometric errors and grain noise.

The small plates for the stellar spectrograph were cut from standard 4 × 5 inch Kodak IIa-O plates, so that the stellar spectra and their corresponding calibration spectra were obtained from the same material. Care was taken that the stellar plates did not come from near the edge of the original plates where the emulsion may not be uniform. Exposures were intended to give photographic densities of the order of 0.6 over the middle range of the spectra, as experience shows that grain noise and photometric errors have the least effect at this level of density. The integrating exposure meter was calibrated by trial exposures on a bright programme star but as no corrections were made for star colours or reciprocity failure, the reddest stars are slightly underexposed in the ultra-violet. To avoid the effects of atmospheric dispersion, the spectrograph was always rotated so that the slit was vertical during the middle of an exposure.

For every calibration plate cut from a standard plate, a number of plates were cut suitable for use in the stellar spectrograph and on each of these more than one stellar spectrum could be exposed. Therefore, as only three exposures could be taken on a calibration

TABLE 2.3

Details of useable spectra. The exposure time is in minutes.

Star	Plate	Sec Z	Exp.	Plate	Sec Z	Exp.	Plate	Sec Z	Exp.
1	3/66	1.37	35	4/66	1.04	32			
2	4/66	1.08	37	5/66	1.15	34			
3	38/65	1.22	18	6/66	1.28	25			
5	37/65	1.03	23	9/66	1.10	35			
6	37/65	1.02	11	44/65	1.14	23			
7	36/65	1.00	11	46/65	1.17	12			
8	46/65	1.16	6	4/66	1.53	11			
9	36/65	1.00	13	44/65	1.21	24	46/65	1.15	12
10	39/65	1.35	9	44/65	1.09	11	47/65	1.28	12
11	39/65	1.35	18	47/65	1.30	28			
12	39/65	1.53	8	4/66	1.44	11			
13	40/65	1.61	25	9/66	1.17	28			
14	40/65	1.67	38	41/65	1.01	27			
15	4/66	1.30	49	9/66	1.51	37			
16	42/65	1.01	36						
17	42/65	1.10	61						
18	42/65	1.06	47						
19	42/65	1.20	42	1/66	1.08	51			
20	1/66	1.18	51	10/66	1.40	59			
21	42/65	1.42	14	44/65	1.17	11	1/66	1.16	7
22	2/66	1.27	40						
24	45/65	1.11	5						

TABLE 2.4

Details of calbration plates, developed with the given stellar plates.

Plate	Stellar plates.	Calibration No.	Exposure Time (minutes)
1	36/65, 37/65, 38/65	1	45
		2	20
		3	11
2	39/65, 40/65	4	21
		5	38
		6	8
3	41/65, 42/65, 43/65	7	50
		8	30
		9	14
4	44/65, 45/65	10	23
		11	11
5	46/65, 47/65	12	33
		13	16
		14	7
6	1/66, 2/66	15	51
		16	7
7	3/66	17	35
8	4/66	18	49
		19	34
		20	11
9	5/66, 6/66, 9/66	21	99
		22	36
		23	26
10	10/66	24	59

plate, it was not possible to match every stellar exposure with a calibration spectrum having an equal exposure time. Instead, like stellar exposures were grouped and the calibration time made equal to the mean exposure time of the group. The calibrator light source was adjusted for each exposure time to give nearly constant exposures to each plate, the logarithm of the intensity being rounded off to 0.1 . A total of 24 calibration spectra were obtained on 10 plates. See Table 2.4 .

During the calibration of the plates, it was noticed that the chopper rate was sometimes erratic. The motor speed control was unreliable so that the speed could vary from one period of operation to the next and also during the course of a single exposure. This being an intermittency effect, the exposure would be changed in a manner equivalent to that of reciprocity failure.

Many of the calibration spectra with long exposures were found to be blurred across the direction of dispersion and the longer the exposure the worse the degree of blurring. The effect was intermittent and so difficult to trace but was probably due to temperature changes causing warping of the calibrator base relative to the supports. Calibrations with exposure times greater than about 40 minutes are therefore suspect.

Plates were brush developed for 5 minutes in Kodak D19b developer at a temperature of 20° C. To ensure that the calibration and stellar plates would have the same development, they were held in a perspex jig during development and developed together. The camel hair brush was suspended at a fixed distance above the plates with the bristles just touching the surface of the plates. A brushing rate of the order of 100 strokes per minute was used. Brush development was adopted as it is normal practice for spectroscopy where the Åberhard effect must

plate, it was not possible to match every stellar exposure with a calibration spectrum having an equal exposure time. Instead, like stellar exposures were grouped and the calibration time made equal to the mean exposure time of the group. The calibrator light source was adjusted for each exposure time to give nearly constant exposures to each plate, the logarithm of the intensity being rounded off to 0.1 . A total of 24 calibration spectra were obtained on 10 plates. See Table 2.4 .

During the calibration of the plates, it was noticed that the chopper rate was sometimes erratic. The motor speed control was unreliable so that the speed could vary from one period of operation to the next and also during the course of a single exposure. This being an intermittency effect, the exposure would be changed in a manner equivalent to that of reciprocity failure.

Many of the calibration spectra with long exposures were found to be blurred across the direction of dispersion and the longer the exposure the worse the degree of blurring. The effect was intermittent and so difficult to trace but was probably due to temperature changes causing warping of the calibrator base relative to the supports. Calibrations with exposure times greater than about 40 minutes are therefore suspect.

Plates were brush developed for 5 minutes in Kodak D19b developer at a temperature of 20° C. To ensure that the calibration and stellar plates would have the same development, they were held in a perspex jig during development and developed together. The camel hair brush was suspended at a fixed distance above the plates with the bristles just touching the surface of the plates. A brushing rate of the order of 100 strokes per minute was used. Brush development was adopted as it is normal practice for spectroscopy where the Eberhard effect must

be minimised in order not to alter line profiles too much. In this instance, this is of no great consequence but the uniform development which is supposed to be had from brush development was required.

A number of calibration plates show a distinct drop in fog level at the violet end of the spectrum which is quite close to the edge of the plate. Either, the edge in question is that of the original standard size plate and therefore liable to uneven coating of the emulsion, or, the plate is so orientated during development that the edge is near the end of travel of the developer brush where development may not be uniform. Subsequent analysis of the calibration plates shows that there may be non uniform development.

3 MEASUREMENT.

3.1 DENSITY TRACINGS OF STELLAR AND CALIBRATION PLATES.

Both calibration and stellar spectra with their associated fog levels were traced in a Joyce Loebl double beam microdensitometer. In this instrument, light passing through the photographic plate is balanced against a comparison beam which is attenuated by means of a servo controlled linear density wedge. The wedge motion is directly transmitted to the recording pen so that the output is on a linear density scale. The density range can be selected by using alternative wedges. As the tracing table is coupled by a lever to the plate carriage, distances along the tracings are strictly proportional to distances along the spectra.

The resolution obtained on the tracings and the extent to which photographic grain noise is integrated depend on the size of the densitometer slit. For tracing the stellar spectra, the slit width was set to 40 μ in order to approximately match the resolution limitations set by the spectrograph slit and the photographic spread function. In the case of the calibration spectra, the slit was set to the maximum possible width of 200 μ to reduce the effect of grain noise. As mentioned before, in connection with slit ratios, the height of the slit and its position across the width of the calibration spectra are important (see Section 2.4). The slit was set 430 μ high to match the slit used for the measurement of calibrator slit ratios, while the position was set by finding the position of the maximum density reading.

As a matter of convenience in digitising the tracings, the density wedge was chosen so that correctly exposed stellar spectra would give maximum readings above fog level a little more than half way across the recording paper, or about 10 cms. Again, for convenience, magnification in the direction of dispersion was made equal to five for

the calibration spectra and fifty for the stellar spectra. Tracings of the latter required spectra to be scanned in three sections and occupy three recording sheets. It was necessary to arrange a small overlap between these sheets to allow for any backlash in the paper drive and to permit the sheets to be correctly positioned with respect to each other.

3.2 DIGITISATION OF THE STELLAR TRACINGS.

As a preliminary to digitising the tracings of the stellar spectra, an estimate was made of the grain noise expected at particular density levels so that a suitable digitising increment could be chosen. A typical set of calibration spectra were traced over a short wavelength range with the densitometer arrangements the same as were used for the stellar spectra. Smooth curves were drawn through the tracings and the dispersion about these curves derived at a number of densities. It was concluded that grain noise would always swamp digitising errors if the stellar tracings could be read to an accuracy of 0.5 mm, corresponding to half the size of the grid printed on the recording paper.

Practically all spectrum lines on plates taken at a dispersion of 120A/mm have the same profile, the resolution being basically emulsion limited. Therefore, the spectrum lines on the tracings give an indication of the overall resolution obtained. In this case, the width of lines at half depth is about 2.5 mm on the tracings which in terms of wavelength is 6A. The resolution is further degraded by sampling unless the sampling interval is small enough. A sampling interval of 1.2 mm is suggested from a consideration of Shannon's sampling theorem and the observation that the spectrum lines can be crudely represented by triangular functions. As the recording paper is printed with a

millimeter grid, it was decided to use the convenient sampling interval of one millimeter.

Although each spectrogram carries a printed grid, which is well suited to both the sampling interval and digitising increment, the relation between spectral features and the grid is arbitrary. Further, each spectrum is divided into three sections so that the grids on the three separate spectrograms are arbitrarily related. By matching the regions of overlap between consecutive sheets, the distances between spectral features can be established. Therefore, a number of spectra with strong lines were selected and the mean distances between the lines found to an accuracy of 0.1 mm . It was then an easy matter to fix the position of any grid with respect to the set of spectrum lines. For convenience this was done with the aid of a perspex graticule marked out with the positions of the principal lines. The spectrum line H_γ was chosen as origin and the position of every grid reckoned from this line to the nearest millimeter. Thus the position of any point in a spectrum can be specified to an accuracy of 0.5 mm . The position relative to adjacent points is, of course, very much better.

With the relative positions of the grids known, the tracings of each spectrum were read at intervals of one millimeter, giving a total of 700 points per spectrum. In order to find the spectrum densities above fog level, the associated fog levels were fitted by straight lines and read in the same way as the spectra. Where prominent spectrum lines were encountered, the measuring grid was locally displaced across the extent of the line so that the line centre coincided with the nearest grid line. This was necessary in order that strong lines would be properly matched in wavelength. Failure to do this would result in large residuals in the difference between two spectra. Even so, it is still possible to accumulate an error of a millimeter between the

assigned positions of the same line occuring in different spectra. When the spectra are differenced by hand, the discrepancy is immediately obvious and can be allowed for but this is not so with computer reduction. There is a case for oversampling to improve the relative line positions. However, the extra labour did not seem to be justified.

3.3 THE DISPERSION CURVE OF THE STELLAR PLATES.

Because the dispersion in the spectrograph is low and is done with a grating, the relation between the wavelength of spectral features on the stellar plates and their position is nearly linear. The dispersion curve calculated from the spectrograph optical arrangement is, for practical purposes, a quadratic. Therefore the wavelength of the strongest lines were fitted to a quadratic function of their positions. Some difficulty was experienced in obtaining a good fit, partly on account of the poor distribution of lines but more so because of errors in line positions. The complete absence of any visible lines on the tracings beyond the Balmer jump meant that at these wavelengths the dispersion curve was obtained by extrapolation. This dispersion curve was used for the initial reduction of the stellar plates. Graphical interpolation was used to find the 700 values of reciprocal wavelength that were required.

As a result of considerations given in Section 5.4 , the data on the stellar plates were subsequently prepared for computer processing. The dispersion curve used in the final stage of the work was readily fitted in the computer as follows. By adding all 42 spectra together, the effects of grain noise were greatly reduced and a number of weak lines became visible, particularly in the ultra-violet. The positions of these lines were then estimated from a plot and added to the existing list of lines. Since the errors associated with the lines are in their

positions and not their wavelengths, the positions were fitted to the wavelengths, rather than the other way about. A least squares fitting was obtained using orthogonal polynomials which, after examination of the residuals, were terminated at the fourth degree. The wavelength at each of the 700 sampling positions was calculated by solving the roots of the polynomial by the Newton-Raphson method.

3.4 MEASUREMENT OF CALIBRATION TRACINGS.

A preliminary investigation was made of the characteristic curves derived from a few representative tracings of calibration spectra. It showed that the photometric properties of the IIa-O emulsion change slowly with wavelength except in the vicinity of 5000A. Where the properties change faster, the wavelengths of measurement must be close enough to follow the changes. This consideration led to a maximum desirable spacing of reciprocal wavelength which was also compatible with the view that there should be at least five points of measurement corresponding to each of the two straight sections of the reddening curve. Although photometric properties change very slowly in the ultra-violet, the low levels of density mean that the numbers of measures can be increased to advantage.

Fifteen wavelengths between 4900A and 3200A were finally selected for measurement. On a reciprocal wavelength basis they are reasonably uniformly distributed but avoid the mercury emission lines used for wavelength identification. Also, they are closer spaced near 4300A, this being the approximate position of the corner of the reddening law. The positions for measurement on the tracings were found by measurement from the mercury lines. After fitting the fog levels by straight lines, the height of the calibration steps above fog level were read off to the nearest 0.5 mm, corresponding to 0.004 in logarithmic density.

4 ANALYSIS OF THE CALIBRATION MATERIAL.

4.1 INTRODUCTION.

To reduce the measures of blackening of the stellar spectra to measures of relative intensity, parts of the plates, from which the stellar plates had been cut, were exposed in a multiple slit spectrograph and developed together with the stellar spectrum plates. Photometric properties derived from the calibration plates ought then to apply to the stellar spectra; an assumption which must be examined, since the conditions of exposure and development were less than ideal. This question is dealt with both here and in Section 6.3.1. The investigation also includes a comparison of plates not developed together, since the stellar spectra forming a reddening pair may occur on plates developed quite separately. As well as identifying potential sources of error, consideration was given to the need to collate the calibration data with a view to simplifying the tedious hand reduction of the stellar spectra.

The relationship between photographic blackening, the intensity and colour of the exposing light and the exposure time is not a simple one, though the general pattern of behaviour is well known. Because only one developer and batch of plates has been used, a unique set of relations will exist, but they may well be obscured by lack of uniformity in the properties of the emulsion and development and by changes in the calibrator lamp. In order to represent the mean photometric properties of the calibration material by a small number of empirical functions, the data have been tested against the general expression derived by Van Kreveld and Ornstein (31), which follows:-

$$f(b) = \left(\log_{10} E + \phi_1(t) + \phi_2(\lambda) \right) / \left(F_1(t) + F_2(\lambda) \right)$$

where b is a measure of photographic blackening, E denotes exposure i.e. product of relative intensity and exposure time, t exposure time

and λ wavelength. For a given exposure time and wavelength, the resulting expression connecting blackening and exposure is an alternative way of representing the usual characteristic curve. Characteristics at different wavelengths are seen to have the same shape. This property, discovered by Webb (32), is most important in the present context. The general expression also embodies the result obtained by Webb (33) and others that reciprocity failure is almost independent of wavelength. Reciprocity failure is given by the functions ϕ_1 and F_1, though the effect of F_1 is very small. ϕ_2 combines the colour sensitivity of the emulsion with the colour composition of the exposing light, while the sum of the functions F_1 and F_2 is a measure of contrast.

If the expression of Van Kreveld and Ornstein is valid for the emulsion and developer used here, then the various functions involved should be invariant across a given plate. Provided that the properties of the emulsion and the development conditions are sufficiently uniform, the functions can also be expected to be invariant from plate to plate. Therefore, the manner in which the stellar spectra are reduced will depend on how constant these functions are.

4.2 LINEAR CHARACTERISTIC CURVES.

It is common practice to present the characteristic curves of an emulsion in terms of logarithmic exposure and logarithmic density, after the manner of Hurter and Driffield (34). The so called HD curves are not necessarily convenient for photometry on account of their pronounced curvature at low densities. By choosing another function of transmission, rather than logarithmic density, it is possible to derive nearly straight lines for the characteristic curves. This was done in the present investigation. A more linear relationship simplifies the

reduction of the stellar spectra and aids the comparison of characteristics from different plates and wavelengths.

A few representative calibration spectra were chosen and characteristics drawn for a number of wavelengths. The density scale used in this case was the Modified Density Δ of Baker (35), so chosen because of its approximately linear relation to logarithmic exposure. Δ is given by the expression:-

$$\Delta = \log_{10}\left(T^{-1} - 1\right)$$

where T is transmission with respect to fog level. Normally the fog level is measured in the vicinity of the density being measured. In this case the fog level was taken well clear of the calibration spectra because light scattered in the calibrator gives a false fog level near the spectra. Though curvature was not great it seemed worthwhile to attempt to straighten the characteristics still further, at least over the density range of most use for reducing the stellar spectra. Baker modified density is a special case of the empirical function:-

$$U^{-1}\log_{10}\left(T^{-u} - 1\right)$$

Using this function with the appropriate value of the parameter U, the straightness of the characteristics was found to be much improved. To facilitate the comparison of characteristics with different values of U and to retain a similarity with Δ over the middle range of densities, the above function was modified so that when plotted against Δ, the family of curves for different U are equal to zero and tangential to one another for Δ equal to zero, i.e. for T = 0.5 . The function then becomes:-

$$d_u = \frac{2^u - 1}{u\,2^{u-1}}\log_{10}\left(\frac{T^{-u} - 1}{2^u - 1}\right)$$

See Figure 4.1 . It was found that most characteristics could be made straight for densities d_u greater than about 0.2 using values of U

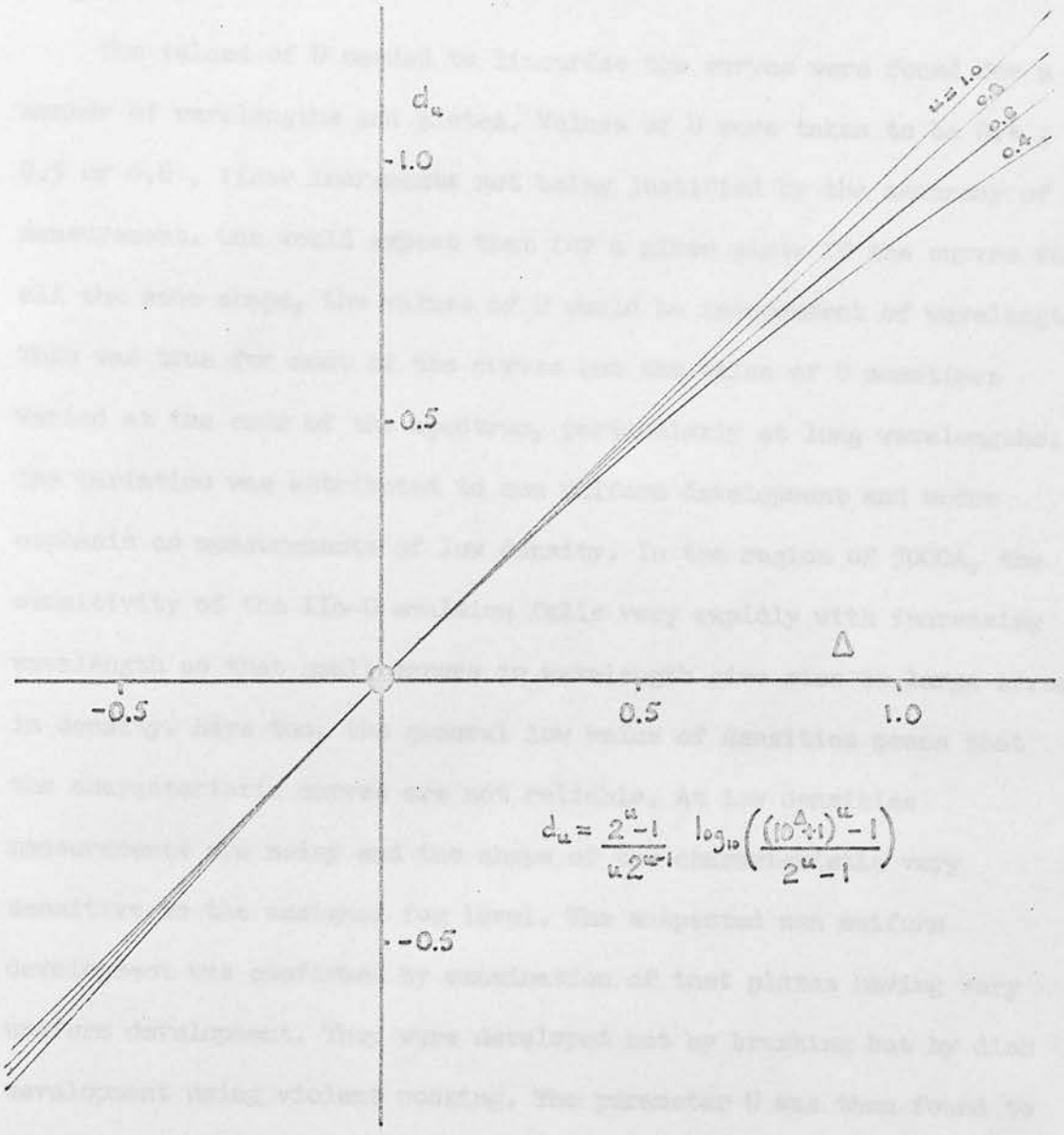

FIGURE 4.1

The photographic density d_u as a function of Baker density Δ.

between 0.4 and 0.6 . Densities below about 0.2 are not of great interest because of decreased accuracy and because the stellar spectra have densities above this value over most of the useful wavelength range.

The values of U needed to linearise the curves were found for a number of wavelengths and plates. Values of U were taken to be 0.4 , 0.5 or 0.6 , finer increments not being justified by the accuracy of measurement. One would expect that for a given plate if the curves were all the same shape, the values of U would be independent of wavelength. This was true for most of the curves but the value of U sometimes varied at the ends of the spectrum, particularly at long wavelengths. The variation was attributed to non uniform development and undue emphasis on measurements of low density. In the region of 5000A, the sensitivity of the IIa-O emulsion falls very rapidly with increasing wavelength so that small errors in wavelength give rise to large errors in density. Here too, the general low value of densities means that the characteristic curves are not reliable. At low densities measurements are noisy and the shape of the characteristic very sensitive to the assigned fog level. The suspected non uniform development was confirmed by examination of test plates having very uniform development. They were developed not by brushing but by dish development using violent rocking. The parameter U was then found to be independent of wavelength. The average value of U being about 0.5 , this value was chosen for the reduction of the calibration spectra. Thus the densities on the calibration tracings were converted to:-

$$d_{0.5} = \frac{2^{0.5} - 1}{0.5 \times 2^{-0.5}} \log_{10}\left(\frac{T^{-0.5} - 1}{2^{0.5} - 1} \right)$$

Characteristic curves were then drawn in terms of this density for all the calibration spectra at 15 wavelengths. Figure 4.2 is an example.

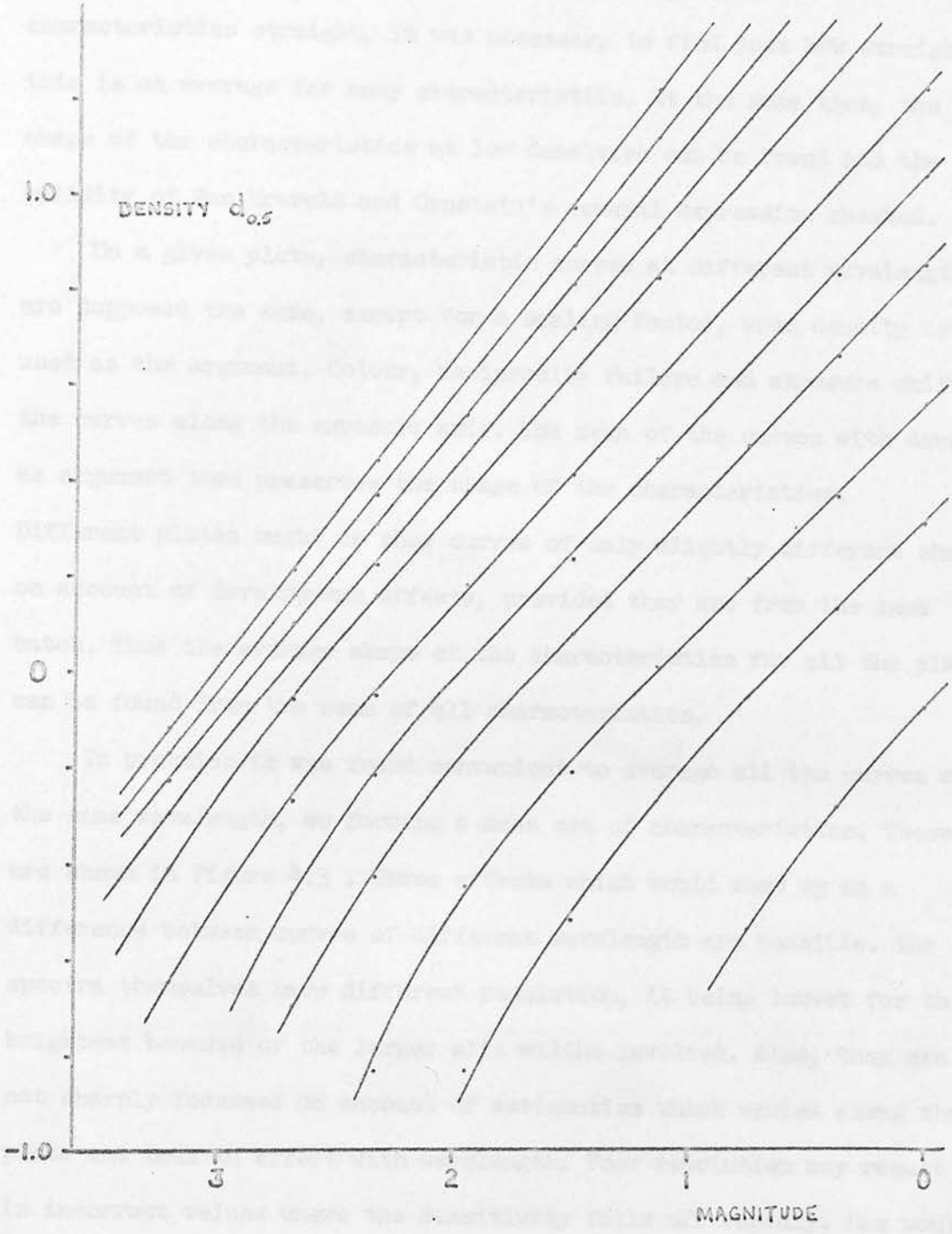

FIGURE 4.2

The semi-rectified characteristic curves of the IIa-O emulsion.

4.3 THE MEAN SHAPE OF THE CHARACTERISTIC CURVES.

Having attempted to make the most useful part of the characteristics straight, it was necessary to find just how straight this is on average for many characteristics. At the same time, the mean shape of the characteristics at low densities can be found and the validity of Van Kreveld and Ornstein's general expression checked.

On a given plate, characteristic curves at different wavelengths are supposed the same, except for a scaling factor, when density is used as the argument. Colour, reciprocity failure and exposure shift the curves along the exposure axis. The mean of the curves with density as argument then preserves the shape of the characteristics. Different plates ought to show curves of only slightly different shape, on account of development effects, provided they are from the same batch. Thus the average shape of the characteristics for all the plates can be found from the mean of all characteristics.

In practice it was found convenient to average all the curves of the same wavelength, so forming a mean set of characteristics. These are shown in Figure 4.3 . Three effects which would show up as a difference between curves of different wavelength are possible. The spectra themselves have different resolution, it being lowest for the brightest because of the larger slit widths involved. Also, they are not sharply focussed on account of astigmatism which varies along the plate and thus in effect with wavelength. Poor resolution may result in incorrect values where the sensitivity falls off rapidly. One would expect the characteristics to deviate at the upper end for these wavelengths. If serious enough, the lack of focus would change the effective relative slit ratios with wavelength. This would cause the characteristics to change shape and give a false scale to derived magnitudes. To check for such effects, the mean characteristics at a

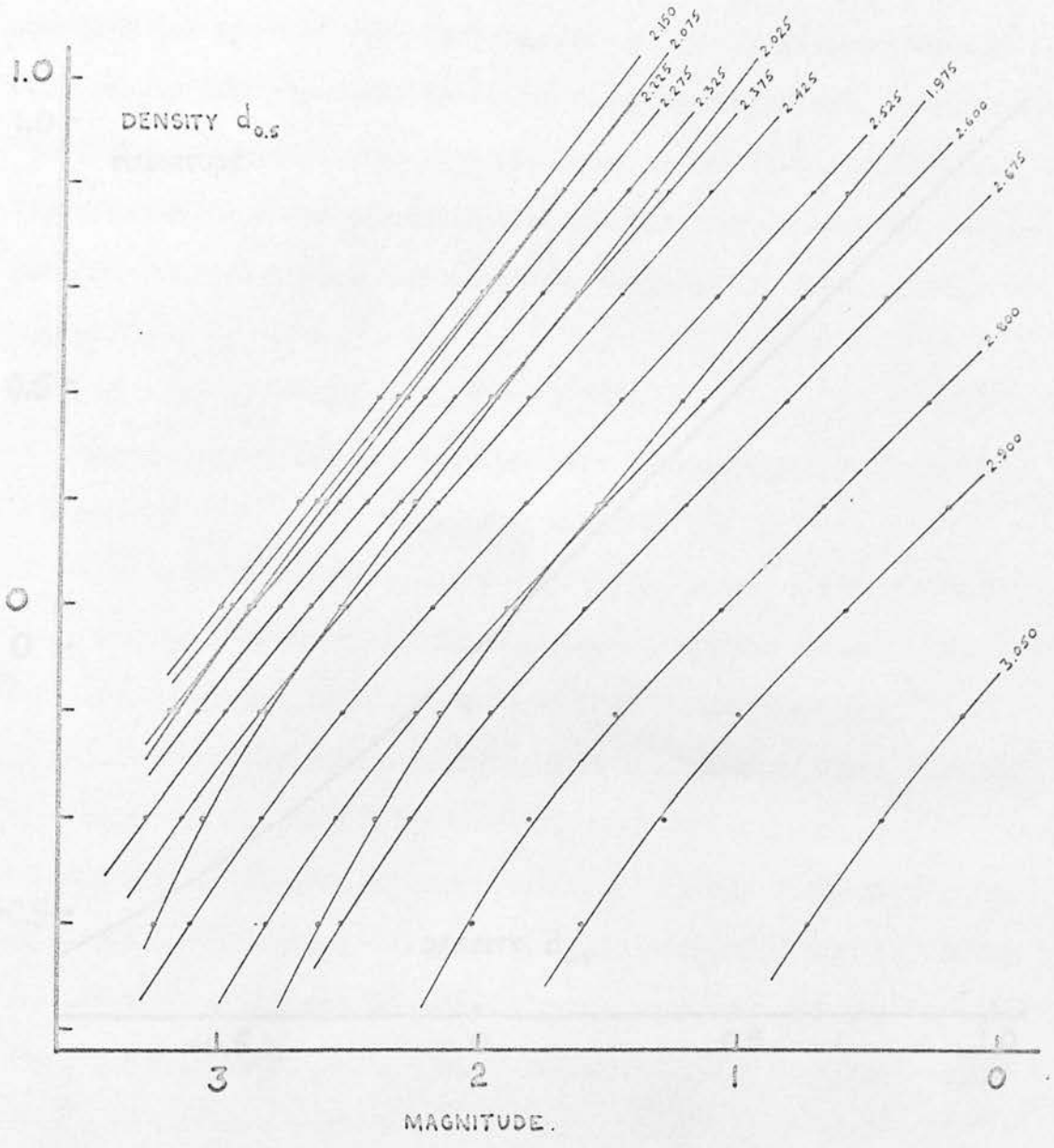

FIGURE 4.3

The mean set of characteristic curves at 15 reciprocal wavelengths.

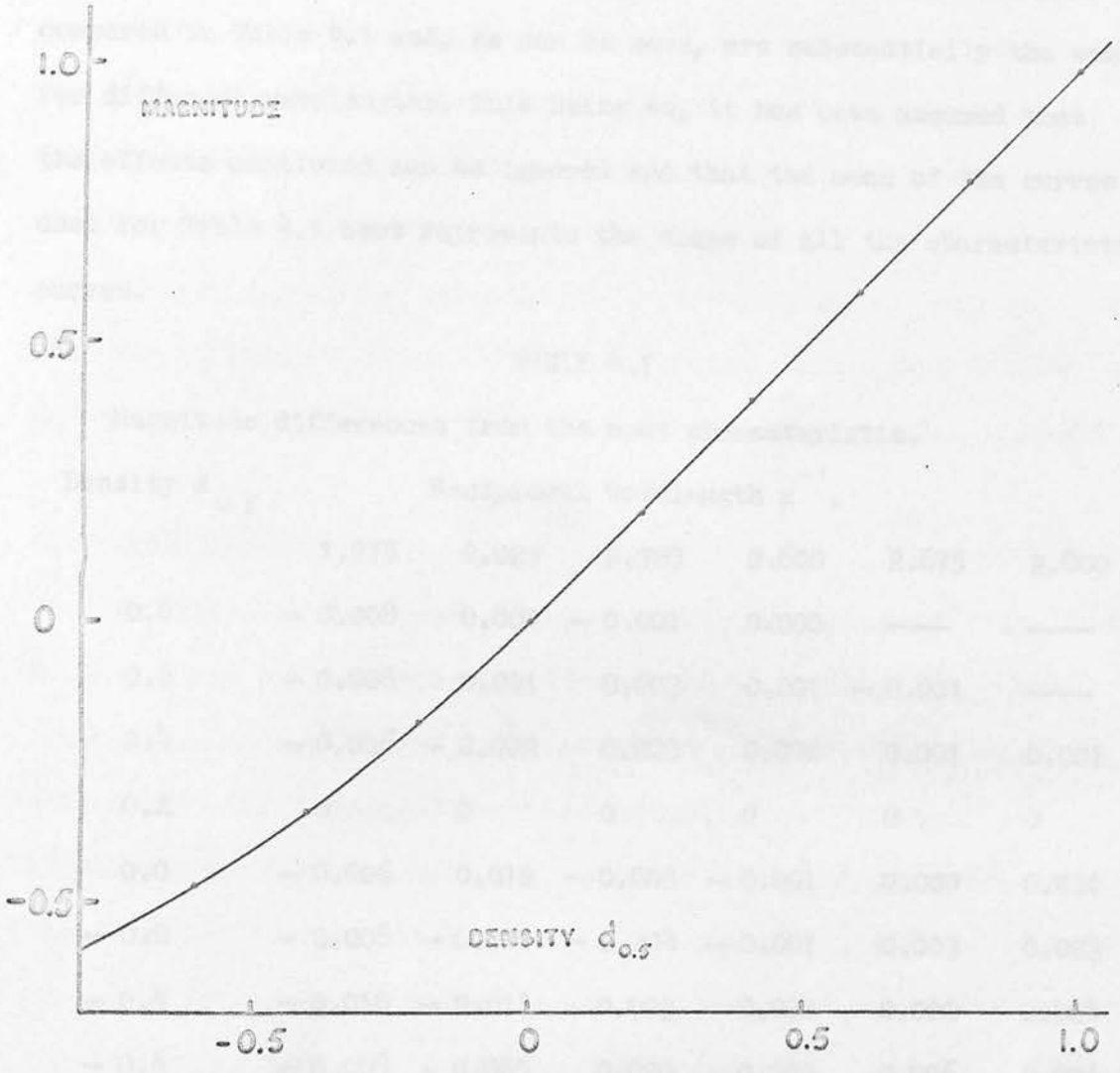

FIGURE 4.4

The mean shape of the characteristic curves.

number of wavelengths were normalised to make the straight line sections of slope unity and to pass through the point of density 0.2 with magnitude zero. Only those curves having both a lower curved portion and an upper straight part have been used. The characteristics are compared in Table 4.1 and, as can be seen, are substantially the same for different wavelengths. This being so, it has been assumed that the effects mentioned can be ignored and that the mean of the curves used for Table 4.1 best represents the shape of all the characteristic curves.

TABLE 4.1

Magnitude differences from the mean characteristic.

Density $d_{0.5}$	Reciprocal wavelength μ^{-1}.					
	1.975	2.025	2.525	2.600	2.675	2.800
0.8	- 0.008	0.000	- 0.001	0.000	——	——
0.6	- 0.006	0.001	0.003	0.001	- 0.001	——
0.4	- 0.006	- 0.002	0.003	0.002	0.001	0.001
0.2	0	0	0	0	0	0
0.0	- 0.006	0.012	- 0.003	- 0.001	0.000	0.001
- 0.2	- 0.008	- 0.011	- 0.004	- 0.001	0.003	0.023
- 0.4	- 0.010	- 0.011	0.003	0.000	0.002	0.024
- 0.6	- 0.008	- 0.025	0.020	0.009	0.006	0.006

The resulting mean curve is shown in Figure 4.4 . Since deviations from a straight line only appear for densities $d_{0.5}$ less than zero, the curve has been adjusted so that zero magnitude occurs at density zero. Individual calibration curves differ in shape from the mean, mainly because of irregular development across the plates and probable differences in development between the plates. The shape is also sensitive to the value given to the fog level, particularly at low

densities. For those plates having a noticeable drop in fog level near the blue end of the spectrum, it was difficult to decide where the fog level should be placed, so the variations in the shape of the characteristics are correspondingly greater. Thus, provided the other properties of the characteristic curves can be properly accounted for, the mean curve should be used in preference to curves derived from individual calibration plates, to represent the shape of the characteristics. To facilitate the reduction of the stellar spectra, the function called $d_{0.5}$ was modified empirically by the mean shape of the characteristics to give a density function which has a linear relation to logarithmic exposure for all the density levels measured.

4.4 MEASUREMENT OF CONTRAST AND SPEED.

In Figure 4.5 are representative curves of "contrast" F and "speed" S against reciprocal wavelength corresponding to Figure 4.2 . Here contrast is defined as the slope of the straight portion of the characteristic, while speed is the brightness level in magnitudes corresponding to zero density; the zero of the magnitude scale being taken as the level of brightness of the brightest calibration spectrum. The speed is measured relative to the spectral energy distribution of the calibrator lamp as modified by the calibrator.

Contrast and speed were taken directly from the linear parts of the plots where possible. For the shortest wavelengths, densities are low, so only the lower curved part of the characteristic is available. In such cases it was necessary to correlate the characteristic against one, from an adjacent wavelength, having a straight section. For curves at the two shortest wavelengths it was not always realistic to measure the speed, and the contrast was not measured at all.

A number of factors contribute to inaccuracies in the values of

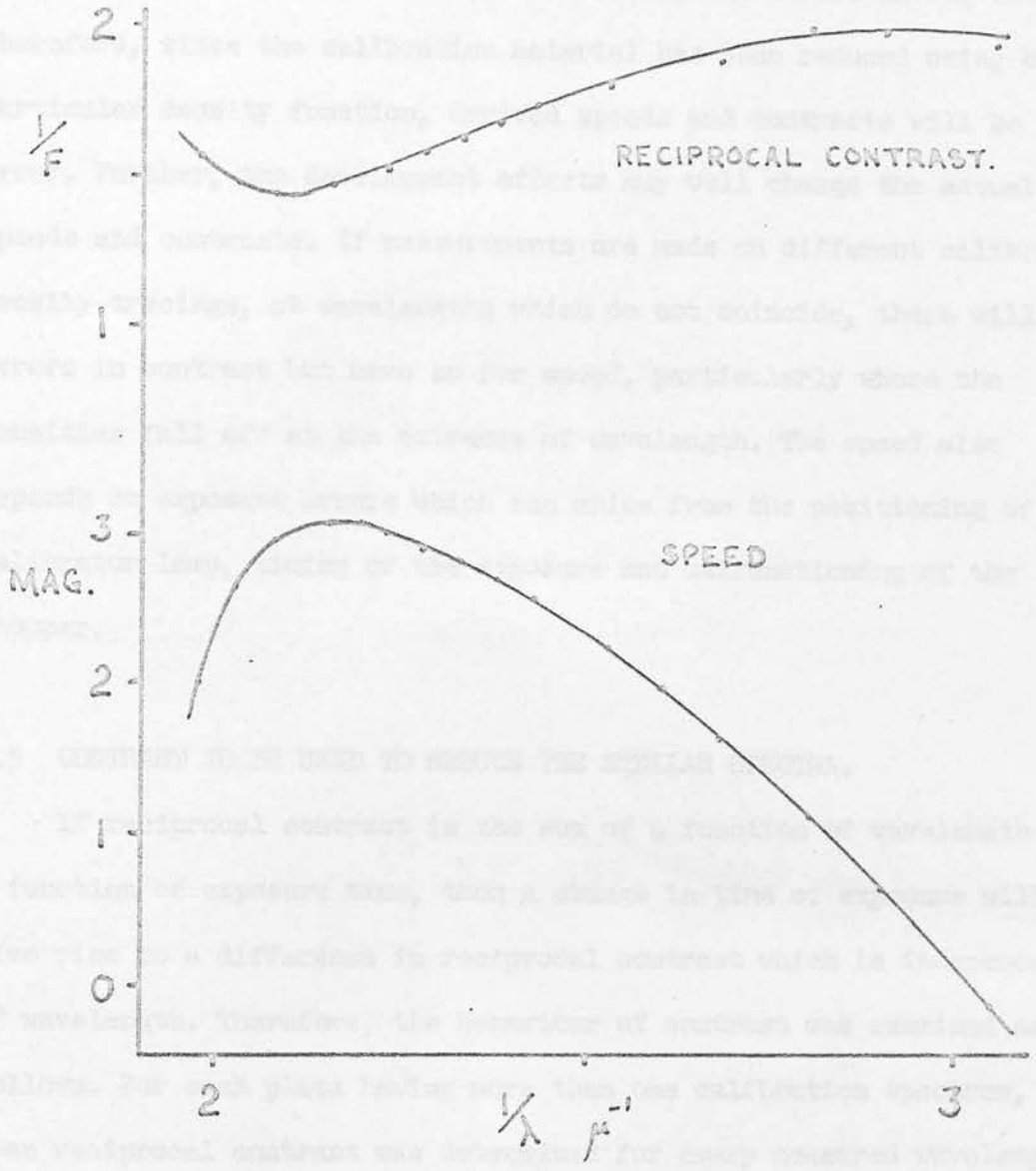

FIGURE 4.5

Example of the wavelength dependence of contrast F and speed S.

contrast and speed. The shapes of individual characteristic curves are different, on account of development effects and errors in fog level. Therefore, since the calibration material has been reduced using one particular density function, derived speeds and contrasts will be in error. Further, the development effects may well change the actual speeds and contrasts. If measurements are made on different calibration density tracings, at wavelengths which do not coincide, there will be errors in contrast but more so for speed, particularly where the densities fall off at the extremes of wavelength. The speed also depends on exposure errors which can arise from the positioning of the calibrator lamp, timing of the exposure and malfunctioning of the chopper.

4.5 CONTRAST TO BE USED TO REDUCE THE STELLAR SPECTRA.

If reciprocal contrast is the sum of a function of wavelength and a function of exposure time, then a change in time of exposure will give rise to a difference in reciprocal contrast which is independent of wavelength. Therefore, the behaviour of contrast was examined as follows. For each plate having more than one calibration spectrum, the mean reciprocal contrast was determined for every measured wavelength. The reciprocal contrast factors of the individual spectra were then differenced from the mean and plotted against reciprocal wavelength. In the same way, the plate means were compared to the overall mean. The results are shown in Figures 4.6 and 4.7 . Clearly, individual plates differ from one another and even on the same plate function F_2, the wavelength dependent part of the contrast, is not constant while the time dependent part, if present, is too small to be significant. Either the properties of the emulsion differ across a given plate or the development conditions give rise to the differences in F_2. As there

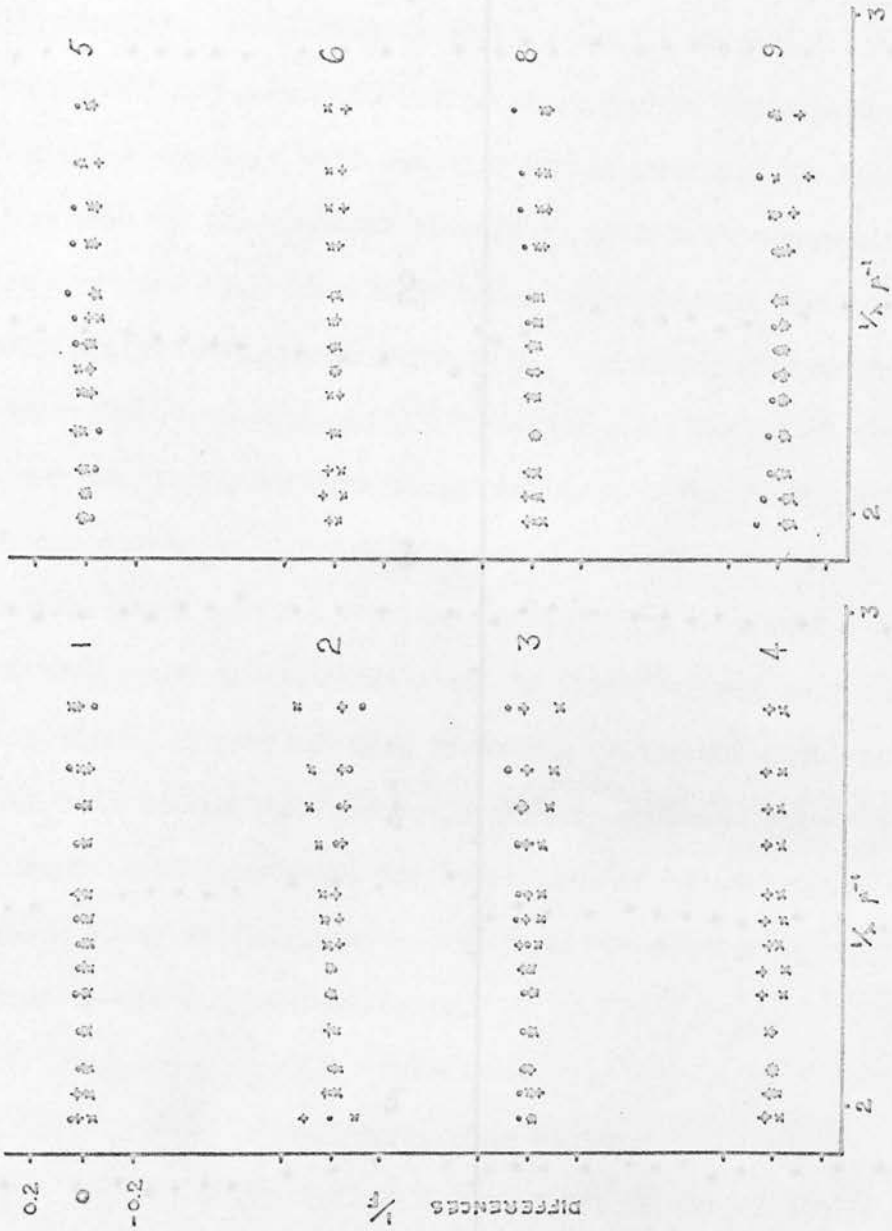

FIGURE 4.6

Dispersion in 1/F per plate.

The symbols × , + and ∘ denote shortest, intermediate and longest exposures respectively. Numbers are the calibration plate numbers.

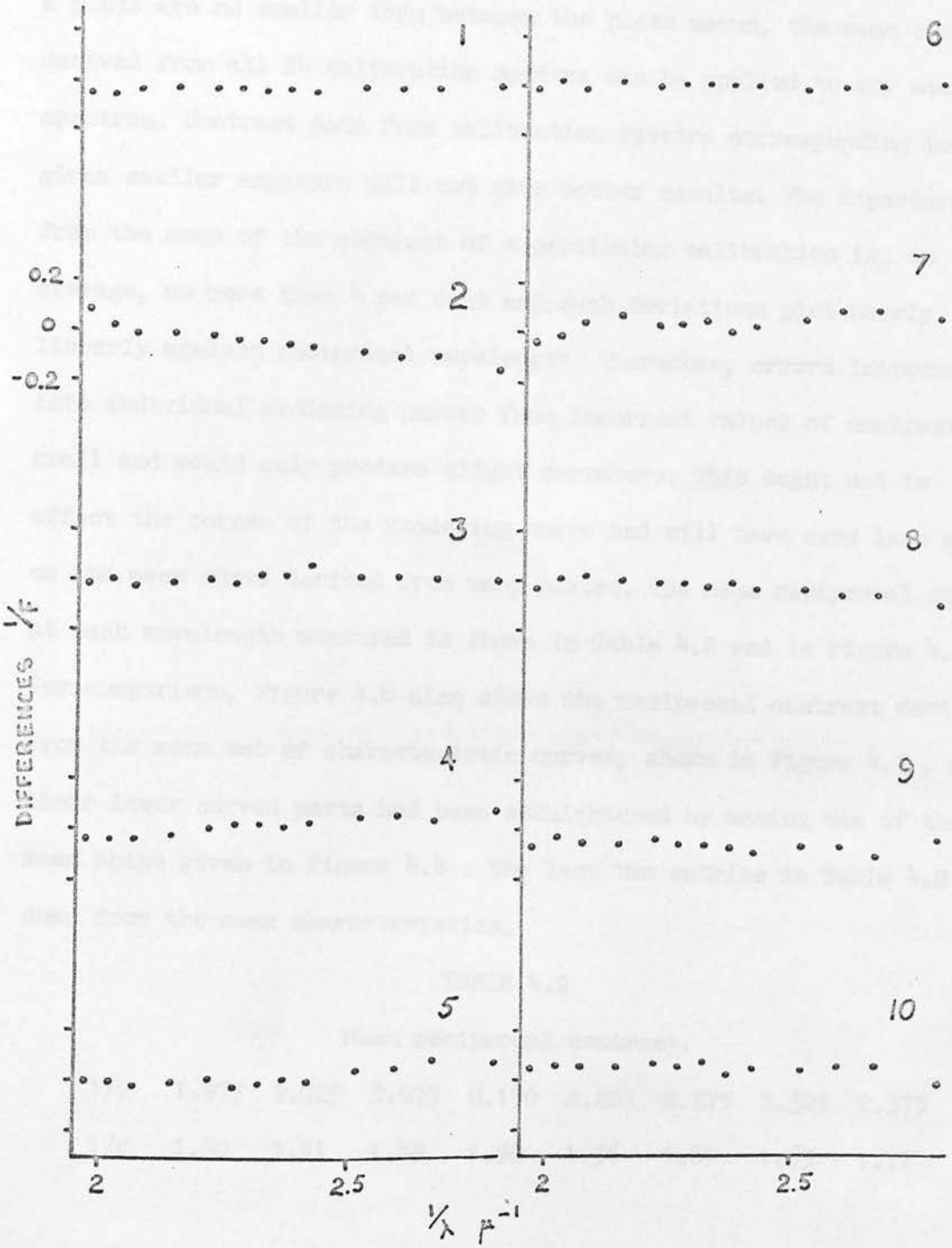

FIGURE 4.7

Comparison of 1/F between plates.

Numbers are the calibration plate numbers.

are variations in F_2 across the calibration plates there will be similar variations for the stellar plates. Since the variations in F_2 across a plate are no smaller than between the plate means, the mean contrast derived from all 24 calibration spectra can be applied to any stellar spectrum. Contrast data from calibration spectra corresponding to a given stellar exposure will not give better results. The departure from the mean of the contrast of a particular calibration is, on average, no more than 4 per cent and such deviations plot nearly linearly against reciprocal wavelength. Therefore, errors introduced into individual reddening curves from incorrect values of contrast are small and would only produce slight curvature. This ought not to affect the corner of the reddening curve and will have even less effect on the mean curve derived from many plates. The mean reciprocal contrast at each wavelength measured is shown in Table 4.2 and in Figure 4.8 . For comparison, Figure 4.8 also shows the reciprocal contrast derived from the mean set of characteristic curves, shown in Figure 4.3 , after their lower curved parts had been straightened by making use of the mean shape given in Figure 4.4 . The last two entries in Table 4.2 come from the mean characteristics.

TABLE 4.2

Mean reciprocal contrast.

$1/\lambda$	1.975	2.025	2.075	2.150	2.225	2.275	2.325	2.375
1/F	1.60	1.51	1.49	1.50	1.56	1.61	1.65	1.71

$1/\lambda$	2.425	2.525	2.600	2.675	2.800	2.900	3.050
1/F	1.75	1.84	1.89	1.93	1.99	(2.03)	(2.00)

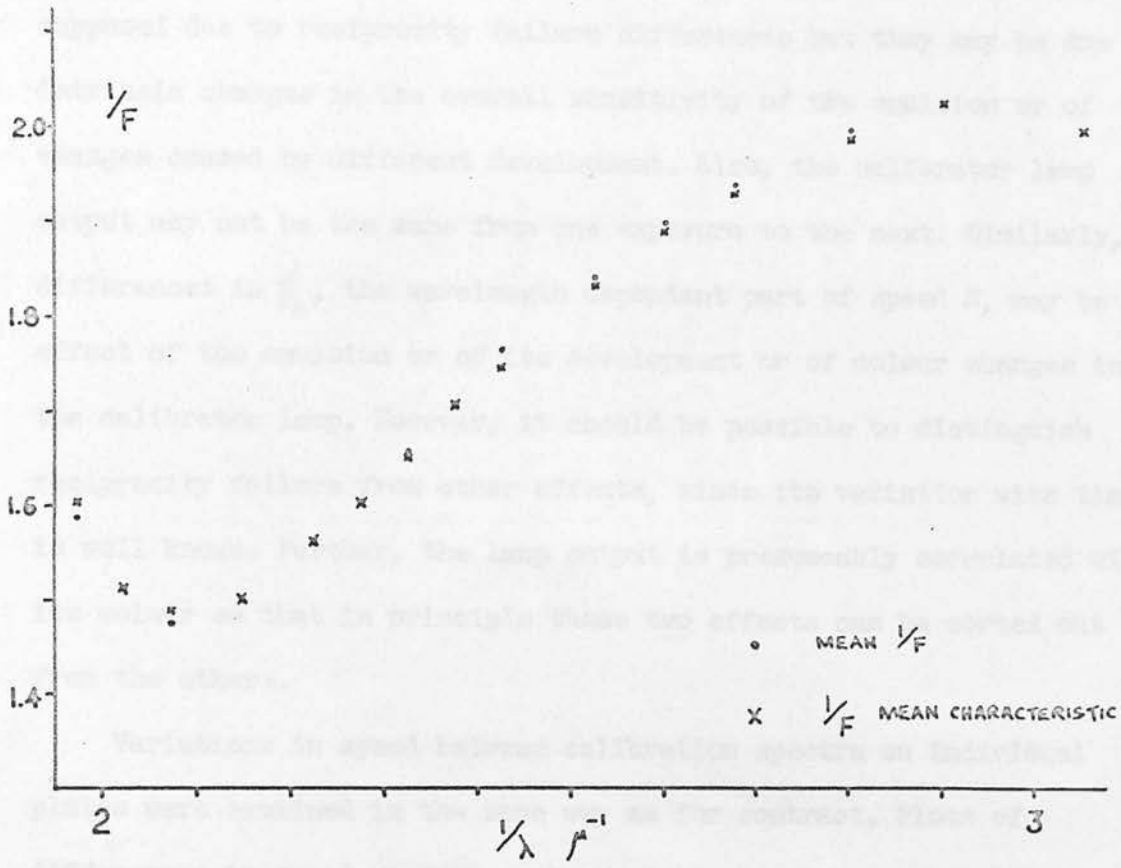

FIGURE 4.8

The mean reciprocal contrast as a function of reciprocal wavelength.

4.6 EMULSION SENSITIVITY, RECIPROCITY FAILURE & CALIBRATOR LAMP COLOUR.

Sensitivity, reciprocity failure and variations in the calibrator lamp output and colour are related. Differences in the function ϕ_1 are supposed due to reciprocity failure differences but they may be due to intrinsic changes in the overall sensitivity of the emulsion or of changes caused by different development. Also, the calibrator lamp output may not be the same from one exposure to the next. Similarly, differences in ϕ_2, the wavelength dependent part of speed S, may be an effect of the emulsion or of its development or of colour changes in the calibrator lamp. However, it should be possible to distinguish reciprocity failure from other effects, since its variation with time is well known. Further, the lamp output is presumeably correlated with its colour so that in principle these two effects can be sorted out from the others.

Variations in speed between calibration spectra on individual plates were examined in the same way as for contrast. Plots of differences in speed against reciprocal wavelength are shown in Figure 4.9 . The figures have been corrected for the small differences in exposure caused by rounding off the logarithm of light intensity to the nearest 0.1 when setting the calibrator lamp. As with contrast, the plots are nearly linear.

Low intensity reciprocity failure may be represented by Schwarzschild's law (36) which relates the exposure to reach a given photographic density with the exposure time. Then:-

$$It^p = \text{constant}.$$

where I is exposing intensity, t exposure time and p is Schwarzschild's constant, of the order 0.8 . Alternatively, the law can be given thus:-

$$\log It = (1-p)\log t + \text{constant}.$$

For the material here, the product of relative intensity and exposure

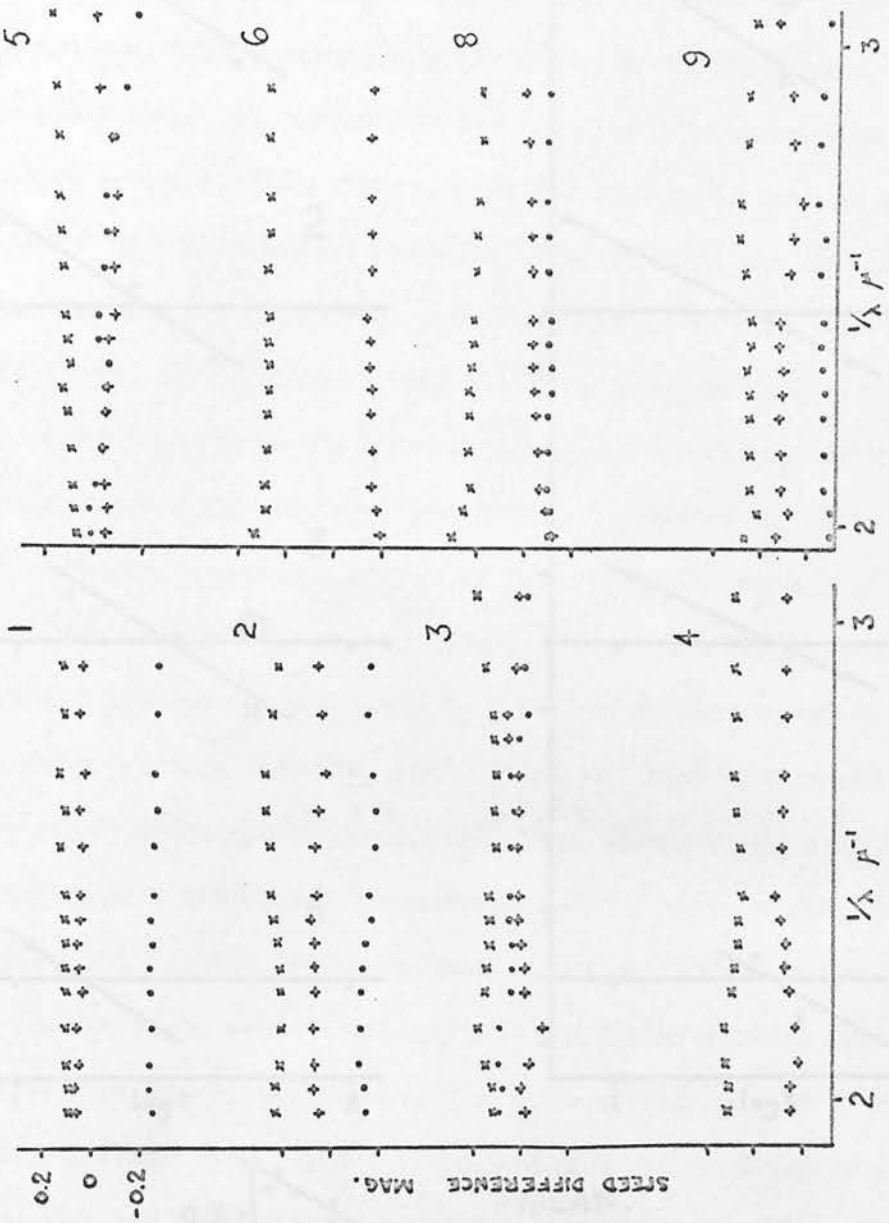

FIGURE 4.9

Dispersion in speed S per plate.

The symbols × , + and ∘ denote shortest, intermediate and longest exposures respectively. Numbers are calibration plate numbers.

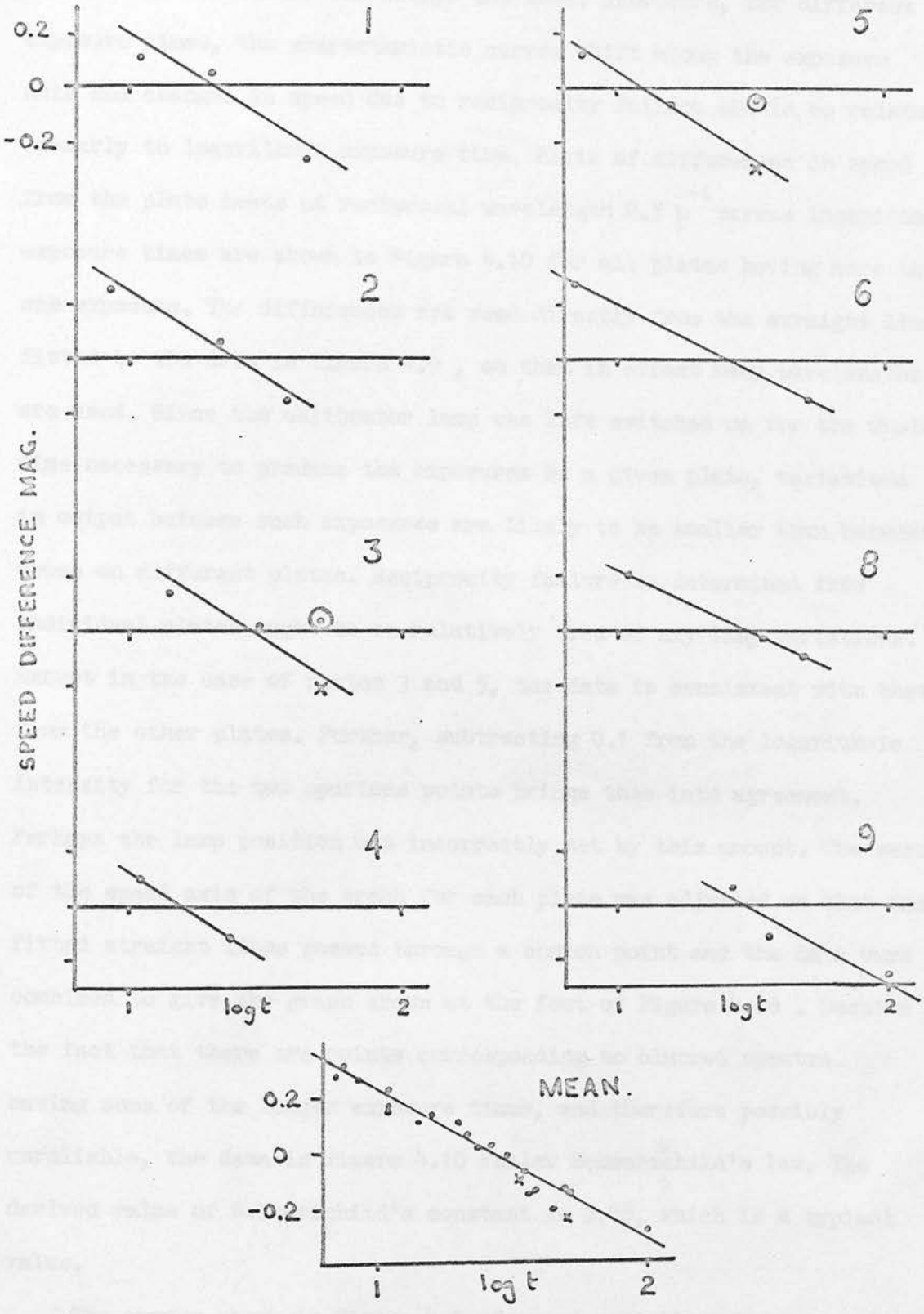

FIGURE 4.10

Reciprocity failure at 2.5 μ^{-1}.

Numbers are calibration plate numbers.

time in the calibrator was always the same. Therefore, for different exposure times, the characteristic curves shift along the exposure axis and changes in speed due to reciprocity failure should be related linearly to logarithmic exposure time. Plots of differences in speed from the plate means at reciprocal wavelength 2.5 μ^{-1} versus logarithmic exposure times are shown in Figure 4.10 for all plates having more than one exposure. The differences are read directly from the straight lines fitted to the data in Figure 4.9 , so that in effect many wavelengths are used. Since the calibrator lamp was left switched on for the whole time necessary to produce the exposures on a given plate, variations in output between such exposures are likely to be smaller than between those on different plates. Reciprocity failure as determined from individual plates ought to be relatively free of any lamp variations. Except in the case of plates 3 and 5, the data is consistent with that from the other plates. Further, subtracting 0.1 from the logarithmic intensity for the two spurious points brings them into agreement. Perhaps the lamp position was incorrectly set by this amount. The zero of the speed axis of the graph for each plate was adjusted so that the fitted straight lines passed through a common point and the data were combined to give the graph shown at the foot of Figure 4.10 . Despite the fact that there are points corresponding to blurred spectra having some of the longer exposure times, and therefore possibly unreliable, the data in Figure 4.10 follow Schwarzschild's law. The derived value of Schwarzschild's constant is 0.78, which is a typical value.

The curves shown in Figure 4.9 of speed variations between sets of calibration spectra taken on the same plates are shown again in Figure 4.11 but corrected for differences in reciprocity failure to an exposure time of 20 minutes. The remaining dispersion must be due

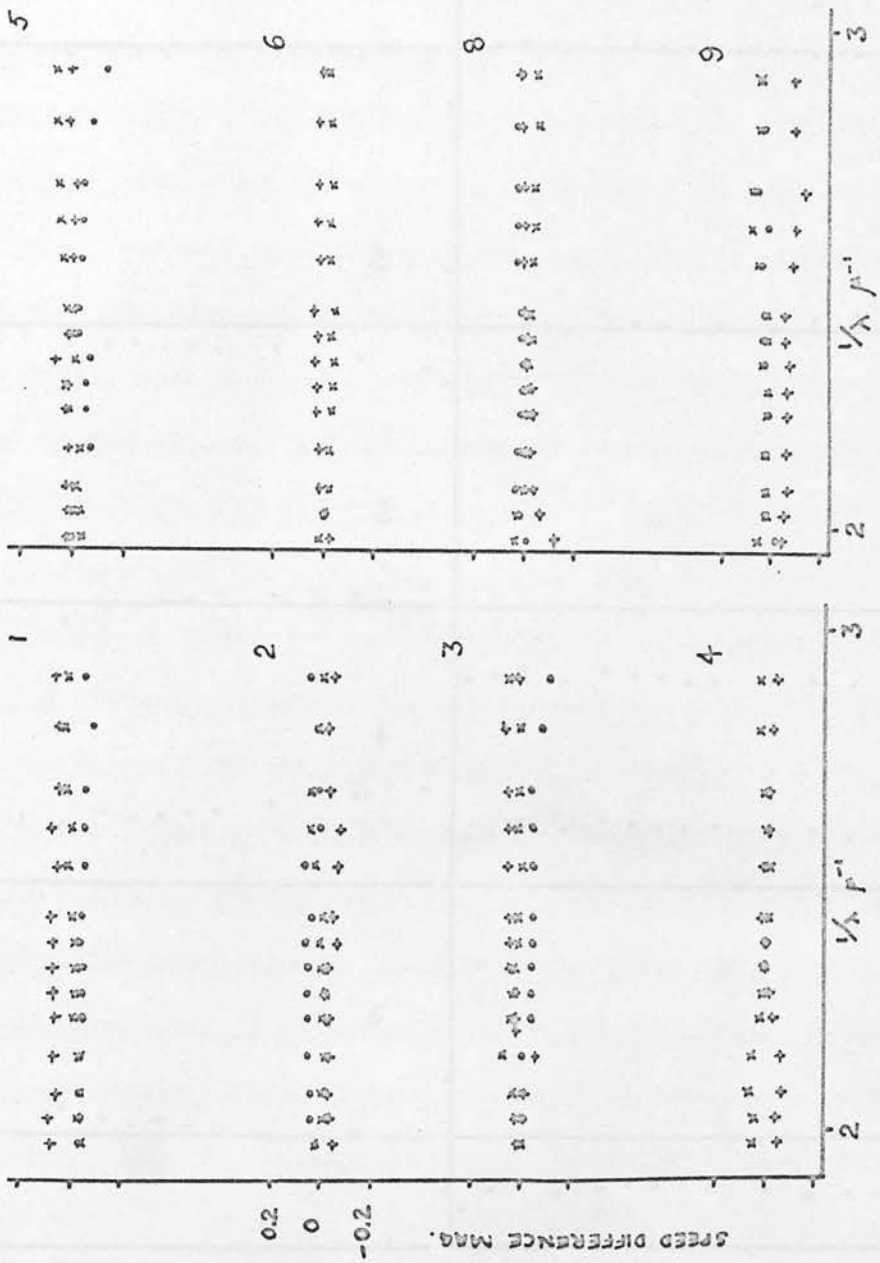

FIGURE 4.11

Dispersion in speed per plate corrected for reciprocity failure. The symbols × , + and ▪ denote shortest, intermediate and longest exposures respectively. Numbers are calibration plate numbers.

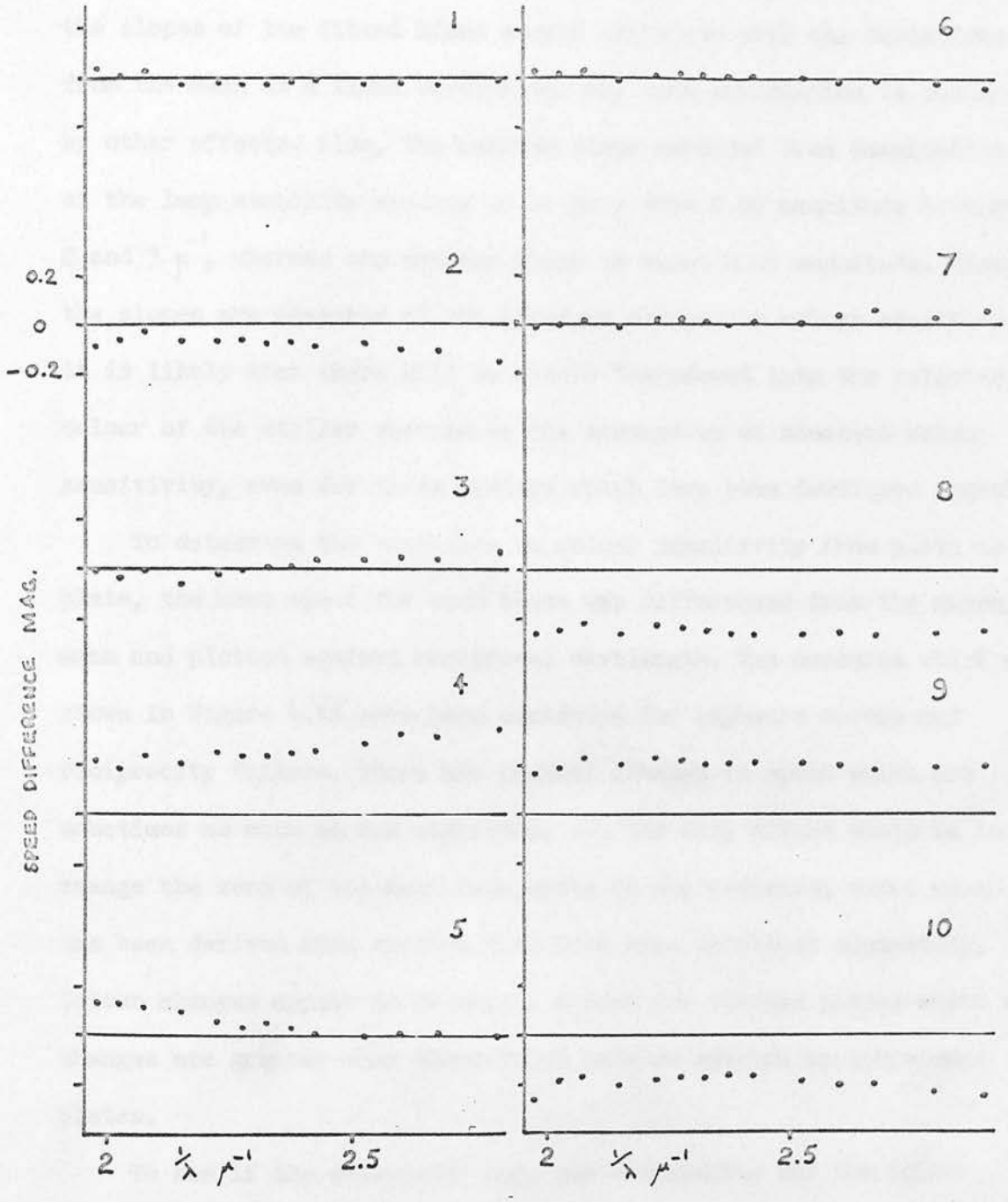

FIGURE 4.12

Comparison of plate speeds.

Numbers are calibration plate numbers.

to development effects, differences in emulsion sensitivity or changes in the calibrator lamp. As lamp colour ought to be related to output, the slopes of the fitted lines should correlate with the deviations from the mean at a fixed wavelength. Any such correlation is obscured by other effects. Also, the maximum slope expected from examination of the lamp stability amounts to no more than 0.02 magnitude between 2 and 3 μ^{-1}, whereas the average slope is about 0.05 magnitude. Since the slopes are measures of the apparent changes in colour sensitivity, it is likely that there will be errors introduced into the relative colour of the stellar spectra by the assumption of constant colour sensitivity, even for those spectra which have been developed together.

To determine the variation in colour sensitivity from plate to plate, the mean speed for each plate was differenced from the overall mean and plotted against reciprocal wavelength. The measures which are shown in Figure 4.12 have been corrected for exposure errors and reciprocity failure. There are neutral changes in speed which are sometimes as much as 0.2 magnitude, but the only effect would be to change the zero of the magnitude scale of any reddening curve which has been derived from spectra that have been developed separately. Colour changes appear to be small, except for certain plates where the changes are greater than those found between spectra on individual plates.

To see if the calibrator lamp was responsible for the colour changes, a correlation was sought between the colour and overall speed differences. For an approximate black body radiator, small changes in temperature cause changes in brightness which, on a logarithmic scale, are proportional to reciprocal wavelength. Therefore, if the lamp temperature were the only thing to change from plate to plate, the data in Figure 4.12 could be fitted by straight lines passing through the

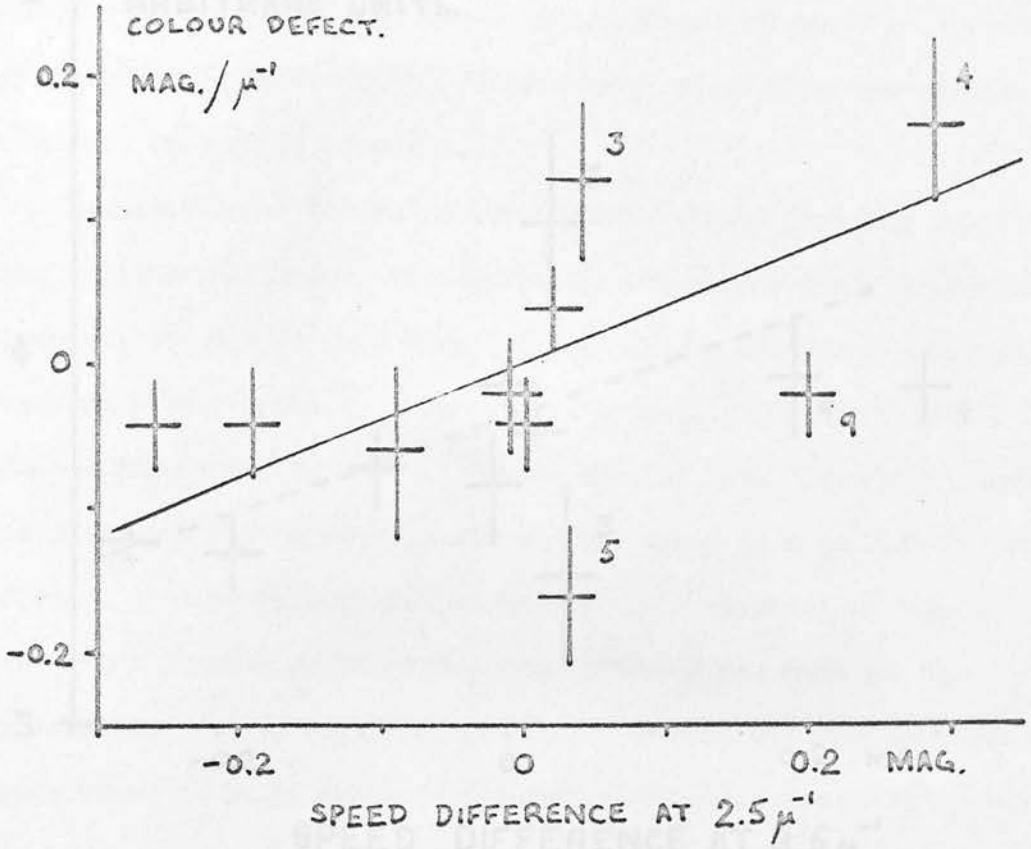

FIGURE 4.13

Apparent correlation of plate speed with colour sensitivity.

Numbers refer to particular calibration plates.

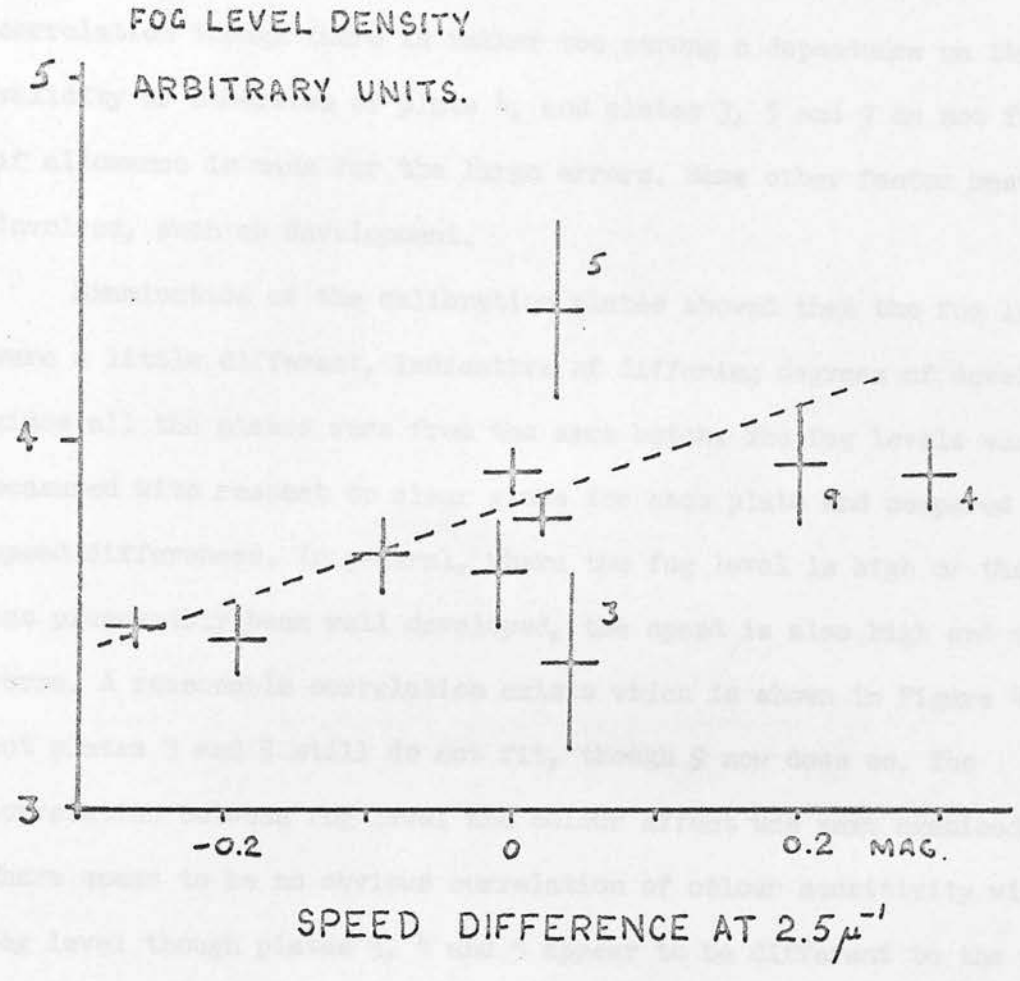

FIGURE 4.14

Correlation of plate speed with fog level.

Numbers refer to particular calibration plates.

origin of the speed and reciprocal wavelength axis. The data can be fitted approximately by straight lines and their slopes, between 2 and 3 μ^{-1}, have been plotted against the speed difference at 2.5 μ^{-1} in Figure 4.13 . Apparently, there is agreement with the expected correlation though there is rather too strong a dependence on the validity or otherwise of plate 4, and plates 3, 5 and 9 do not fit, even if allowance is made for the large errors. Some other factor must be involved, such as development.

Examination of the calibration plates showed that the fog levels were a little different, indicative of differing degrees of development since all the plates were from the same batch. The fog levels were measured with respect to clear glass for each plate and compared to the speed differences. In general, where the fog level is high or the plate has presumeably been well developed, the speed is also high and vice versa. A reasonable correlation exists which is shown in Figure 4.14 but plates 3 and 5 still do not fit, though 9 now does so. The correlation between fog level and colour effect was next examined. There seems to be no obvious correlation of colour sensitivity with fog level though plates 3, 4 and 5 appear to be different to the normal run of plates. If the points for plates 3, 4 and 5 are ignored in Figure 4.13 then the data can be interpreted in terms of development differences rather than lamp temperature changes. Plate 9 now appears to be normal and colour sensitivity is seen to be only slightly dependent, if at all, on overall speed. The spurious points can be explained by a combination of development differences and lamp temperature changes. For example, plate 5 has a high fog level but its speed does not correspond, being some 0.4 magnitude low. However, the negative slope of the speed difference versus reciprocal wavelength curve indicates a drop in lamp output of about 0.4 magnitude.

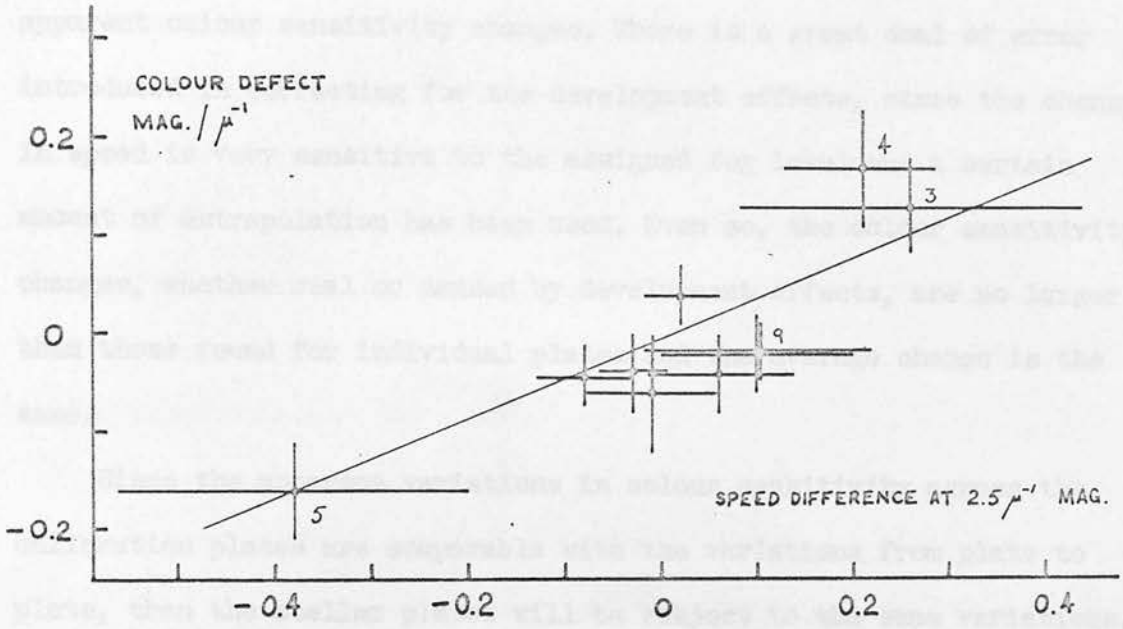

FIGURE 4.15

Colour-speed relation attributed to the calibrator lamp. Numbers refer to particular calibration plates.

To show the effect of lamp variations separated from development effects, the data shown in Figure 4.13 have been corrected for the change in speed caused by different development by using the correlation between speed and fog level. The modified data are shown in Figure 4.15 . The fit of the lamp thermal correlation curve is better than in Figure 4.13 and the dispersion left represents the apparent colour sensitivity changes. There is a great deal of error introduced in correcting for the development effects, since the change in speed is very sensitive to the assigned fog level and a certain amount of extrapolation has been used. Even so, the colour sensitivity changes, whether real or caused by development effects, are no larger than those found for individual plates and the average change is the same.

Since the apparent variations in colour sensitivity across the calibration plates are comparable with the variations from plate to plate, then the stellar plates will be subject to the same variations. Nothing is gained, in terms of the correct derived colour for a stellar spectrum, by applying data from individual calibration spectra, even though the calibration and stellar spectra were developed together. Therefore, stellar spectra on different plates can be differenced directly. On average, the error introduced into the reddening curve obtained from a pair of spectra, by variations in colour sensitivity, will be about 0.04 magnitude between 2 and 3 μ^{-1}.

4.7 SUMMARY.

Although the calibrator lamp did not prove to be as stable as was hoped for, the short term stability was sufficient to enable relatively larger variations in the colour sensitivity of individual calibration plates to be detected. Further, the changes in lamp output and colour

between different periods of operation, though troublesome, can be allowed for by assuming that the lamp is approximately a black body radiator.

There are apparent variations across and between the calibration plates of the shape of the characteristic curves, of colour sensitivity and contrast which, presumeably, occur also for the stellar plates. It is not possible to determine to what extent the variations are intrinsic or caused by non uniform development, though there is some evidence of irregular development. Within the limitations imposed by these uncertainties, and for the purpose of reducing the stellar spectra, the calibration material is best represented as having a fixed colour sensitivity, with the shape of the characteristics and contrast given by the means from all the plates.

5 REDUCTION OF THE STELLAR SPECTRA AND SOURCES OF ERROR.

5.1 MAGNITUDE DIFFERENCES FOR A STAR PAIR.

According to the results of the analysis of the calibration plates, their photometric properties are fairly constant. In particular, all characteristic curves can be reduced to straight lines which have the same slope or contrast at a given wavelength. The only changes in sensitivity that occur are caused by reciprocity failure which is independent of wavelength. While the actual properties of the stellar plates can be expected to be a little variable, the reduction of the stellar spectra must be undertaken using the mean properties derived from the calibration material. The consequences of doing so are investigated in Section 6.

At the end of Section 4.3 a function of blackening was derived which plots linearly against intensities expressed on a magnitude scale. Values of the function will be simply referred to as linear densities. If the density differences between two stellar spectra are divided by the contrast appropriate to each wavelength, a series of magnitudes are obtained. The change in magnitude from one wavelength to another is equal to that required in the magnitude difference curve of the two stars. This is so, because the emulsion wavelength sensitivity and the transmission of the telescope and spectrograph are the same for both stars. However, since the exposures and exposure times are, in general, not the same, the zero point of the derived magnitudes is not correct. In this case this is of no importance.

The magnitude difference curve derived from a pair of spectra refers to light entering the telescope after transmission through the atmosphere and must therefore be corrected for differential atmospheric extinction, since this is a function of wavelength. It is sufficiently accurate to assume a secant zenith distance law of extinction.

The required magnitude difference, at wavelength λ, between stars of apparent magnitudes m and m' is therefore:-

$$m_\lambda - m'_\lambda = (d'_\lambda - d_\lambda) F_\lambda + a_\lambda (\sec Z - \sec Z') + \text{constant}.$$

where d is the spectrum linear density, F the emulsion contrast, a the zenith extinction and Z is the zenith distance.

5.2 THE SUMMED REDDENING CURVES.

To obtain individual reddening curves and then sum these to obtain a mean reddening curve would have involved a great deal of unnecessary labour. Therefore, the differences in the linear densities of paired spectra were summed before converting to magnitudes and the total extinction corrections applied to the end result. To further reduce the amount of labour, data for wavelengths short of 3565A were omitted.

The readings from the tracings of the stellar spectra were converted to linear densities with the aid of a table prepared from the data used for Figure 4.4 . Spectra were paired off according to the scheme shown in Table 5.1 so that, as far as possible, spectra occuring together on the same plate were paired in preference to those occuring on different plates. As will be shown in Section 6, this reduces photometric errors a little, even though the analysis of the calibration material does not seem to suggest this. Each pair of spectra were then differenced point by point and the results plotted out in terms of distance from H_γ. Obvious discrepancies in the alignment of strong spectrum lines were then easily corrected. An indication of the corner of the reddening curve is apparent on some of the difference curves as is also residual Balmer jump. The 26 difference curves were then added together and converted to magnitudes by multiplying the density at each point by reciprocal contrast which was obtained from Table 4.2 by graphical interpolation.

TABLE 5.1

Spectra paired to form reddening curves.

Reddened star.	Plate.	Tracing.	Comparison star.	Plate.	Tracing.
1	3/66	24	3	38/65	29
1	4/66	25	3	6/66	28
2	5/66	26	3	38/65	29
2	4/66	27	3	6/66	28
5	37/65	34	6	37/65	36
5	9/66	33	6	44/65	35
7	36/65	2	9	36/65	1
7	46/65	4	9	46/65	3
8	46/65	31	9	46/65	3
8	4/66	32	9	44/65	30
10	39/65	9	12	39/65	10
10	44/65	38	12	39/65	10
10	47/65	39	12	4/66	37
11	39/65	11	12	39/65	10
11	47/65	40	12	4/66	37
13	40/65	17	15	4/66	22
13	9/66	18	15	9/66	21
14	40/65	19	15	4/66	22
14	41/65	20	15	9/66	21
16	42/65	14	18	42/65	15
17	42/65	16	18	42/65	15
19	42/65	6	21	42/65	5
19	1/66	8	21	1/66	7
20	1/66	12	21	1/66	7
20	10/66	13	21	44/65	23
22	2/66	42	24	45/65	41

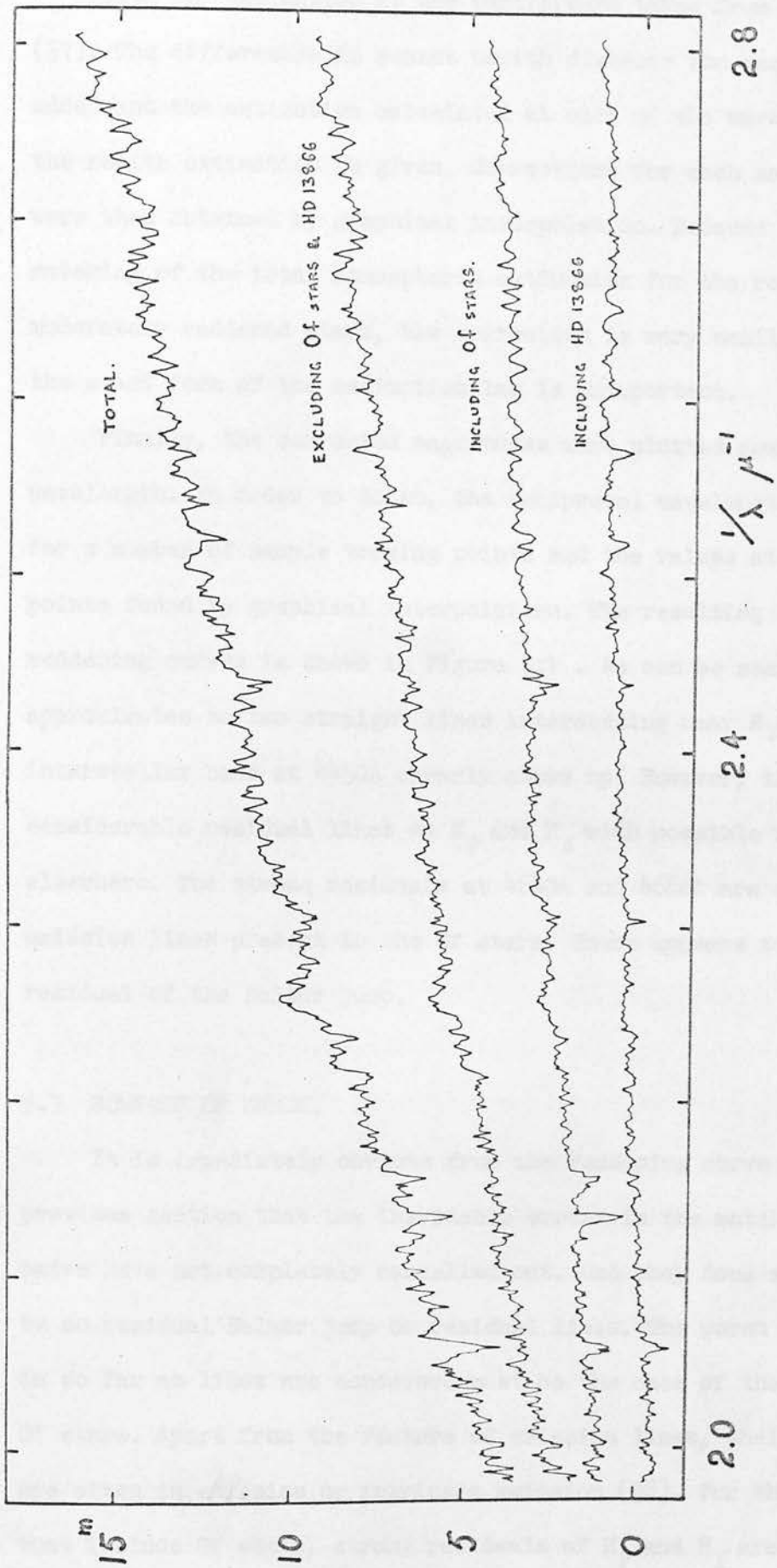

FIGURE 5.1

Sum of reddening curves (hand reduced).

Showing the effect of the inclusion of Of stars and HD 13866.

Data for extinction at the zenith were taken from the literature (37). The differences in secant zenith distance for each star pair were added and the extinction calculated at each of the wavelengths for which the zenith extinction is given. Corrections for each sample point were then obtained by graphical interpolation. Because of fortuitous matching of the total atmospheric extinction for the reddened and moderately reddened stars, the correction is very small and therefore the exact form of the extinction law is unimportant.

Finally, the corrected magnitudes were plotted against reciprocal wavelength. In order to do so, the reciprocal wavelength was calculated for a number of sample tracing points and the values at the intermediate points found by graphical interpolation. The resulting sum of the 26 reddening curves is shown in Figure 5.1 . As can be seen, the curve approximates to two straight lines intersecting near H_γ and the interstellar band at 4430A clearly shows up. However, there are considerable residual lines at H_β and H_γ with possible residuals elsewhere. The strong residuals at 4640A and 4686A are due to the emission lines present in the Of stars. There appears to be some residual of the Balmer jump.

5.3 SOURCES OF ERROR.

It is immediately obvious from the reddening curve derived in the previous section that the inevitable errors in the matching of star pairs have not completely cancelled out. Had they done so, there would be no residual Balmer jump or residual lines. The worst case of matching in so far as lines are concerned must be the case of the inclusion of Of stars. Apart from the feature of emission lines, their Balmer lines are often in emission or intrinsic emission (38). For the star pairs that include Of stars, strong residuals of H_β and H_γ are quite apparent

on the individual density difference curves. The star HD 13866 which is used as a comparison star also seems to have anomalous hydrogen lines. When it is paired with two reddened stars, the differences show well defined residuals of nearly all the hydrogen lines. To demonstrate the effects of this star and of the Of stars on the composite reddening curve, the individual density curves have been divided into three groups and summed separately. The resulting three reddening curves for the group including HD 13866, the group including Of stars and that for the rest of the stars are shown in Figure 5.1 . It is clear that the material must be divided into these groups and be treated separately.

Since no two stars can be quite the same, there must always be a residual of lines and the Balmer jump present in the reddening curve. When residuals are strong enough, as with the lines already considered, they may show above the general level of noise and be allowed for. Weaker residuals will not be visible but their extent must still be estimated if they are at all significant compared to the noise level. A distinction can be made between systematic residuals, which result from known stellar classification mismatch and random residuals which arise from the inaccuracies of classification.

Whatever the other sources of error, every point is strongly affected by grain noise. Although a simple estimate of grain noise made in Section 3.2 showed the general relation to photographic density, the noise should be derived from the actual stellar spectra. This automatically includes noise from sampling and the general effect of very weak lines.

The most serious error and the most difficult to estimate, comes from a combination of irregular development and variations in the properties of the photographic emulsion. If fluctuations occur over

small distances on the stellar plates, the effect is similar to low frequency grain noise. However, if fluctuations occur for distances comparable to the length of the spectra, the shape of the reddening curve would be distorted. Such photometric errors were ascertained for the calibration plates but may not be entirely applicable to the stellar plates on account of the difference in size of the calibration and stellar spectra.

Line residuals, grain noise and photometric errors are examined in detail in Section 6.

5.4 COMPUTER REDUCTION.

Having regard to the number of data points derived from the stellar spectra (29,400), the methods of analysis and reduction of the calibration and stellar plates were chosen with a view to reducing the amount of computation. Even so, this was considerable. It became apparent that at least an equal amount of computation would be required to study and estimate the various errors associated with the mean reddening curve. Fortunately, at this time, ready access to a computer was obtained and the computer was used for all further calculations. To make the spectrum measures available to the computer, the results of their conversion to the linear density scale were put on punched paper tape.

Since the reddening curves already derived were required later in a form suitable for analysis in the computer, they were recalculated. Comparison of the computer and hand calculations provides a useful check, particularly on the effects of misalignment of strong lines. The actual reductions were done in a different manner to allow for easy manipulation of the data in the determination of errors.

The 42 density spectra were individually converted to a series of

magnitudes by multiplying by reciprocal contrast. These magnitudes are relative to the emulsion wavelength sensitivity function which, though unknown, is assumed to be constant. The zero of the magnitude scale is different for each spectrum because the exposure times are not the same. To obtain the reciprocal contrast at each point along a spectrum, the data in Table 4.2 were interpreted in terms of positions on the spectra and then fitted by a polynomial. Orthogonal polynomial curve fitting was used (39) and the polynomials were terminated at the fifth degree after inspection of the residuals. In the same way, the zenith extinction data referred to in Section 5.2 were fitted by a third degree polynomial and used to correct each spectrum for extinction. The resulting 42 sets of data, giving magnitudes at each sample point along the spectrum were then transferred to magnetic tape to form the raw data for all subsequent calculations. Also recorded for each sample point was the zenith extinction, reciprocal contrast and reciprocal wavelength. The latter was found as described in Section 3.3 .

The same difference scheme was used as before to give the three reddening curves described in the previous section. To facilitate plotting of the curves, the data were modified by interpolation and averaging to give extinction at regular intervals of reciprocal wavelength ($0.002\ \mu^{-1}$). Thus the 700 sample points were reduced to 500 on a reciprocal wavelength scale. A small correction was made to each reddening curve for thermal reddening errors arising from known classification differences. Data were taken from the spectrophotometric gradients of Chalonge (40). An attempt was also made to correct for Balmer jump differences as described in Section 6.4 .

6 ERRORS AND THEIR DETERMINATION.

6.1 ESTIMATE OF LINE RESIDUALS.

Line residuals have been estimated by comparison of the spectral types with the variation in line strengths as a function of spectral type given by Sinnerstad (41). Since line strengths and profiles for low dispersion spectra depend on the dispersion and instrumental conditions, they have been derived from a consideration of the actual spectra. For this purpose, the spectra were summed in three groups on the same reciprocal wavelength basis as the three reddening curves. After removal of a low degree polynomial fit, designed to reduce the considerable continuum curvature, the summed spectra were plotted out and all the visible lines, about 50, were identified and measured. It can be assumed that where there is no line visible above the noise in the summed spectra, then none will be present or significant in the reddening curve derived from differencing the same set of spectra. The converse is not necessarily true.

The published relationships between line strengths and spectral types were approximated by straight lines to accord with the qualitative description of the behaviour of spectrum lines, which is the basis of visual estimates of spectral types. That is to say, a particular line is at a maximum at a certain spectral type and goes to zero at two other spectral types. From these linear relations a weight can be calculated for each line in the summed spectra depending on the number of times the spectrum of a star is used and its spectral type. Comparison with the line in the summed spectra then gives an average of the line profile and depth for the spectral type at which it is a maximum. From this, the profile at other types can be estimated. Because the behaviour of the lines has been reduced to an approximate description and the range of spectral type and luminosity class is limited, all the different

lines of a particular ion are assumed to act in the same manner. Further, where a line is not positively identified or through lack of resolution is caused by a blend of lines, its behaviour has been taken as intermediate between those ions showing extremes of behaviour for the group of stars.

Where the types in a reddening pair have been classified as being different, then estimates of systematic line residuals have been made and their contribution to the mean reddening curves found. In general, these systematic errors are quite small, being of the same order as grain noise.

Random error line residuals have been calculated by assuming that spectral type classification is accurate to 0.7 sub-class. The line residuals are supposed to add statistically except where a star is used more than once. In this case, the variance adds as the square of the number of times the star is used.

6.2 GRAIN NOISE AND DIGITISATION ERRORS.

Preliminary measures of grain noise were made from calibration spectra before the spectrograms were digitised, as explained in Section 3.2 . However, these are not nearly representative enough of the stellar spectra and do not include digitisation errors.

Ten clearly defined regions of continuum were chosen on the mean spectrum of all the stars which was used also to find lines for the dispersion curve (Section 3.3). The regions were chosen to be well distributed both in wavelength and density and to include roughly the same number of points. For every individual linear density spectrum, the density measures for each region were fitted with straight lines by the method of least squares and the mean density and standard deviation about the line computed. The resulting plot of R.M.S.

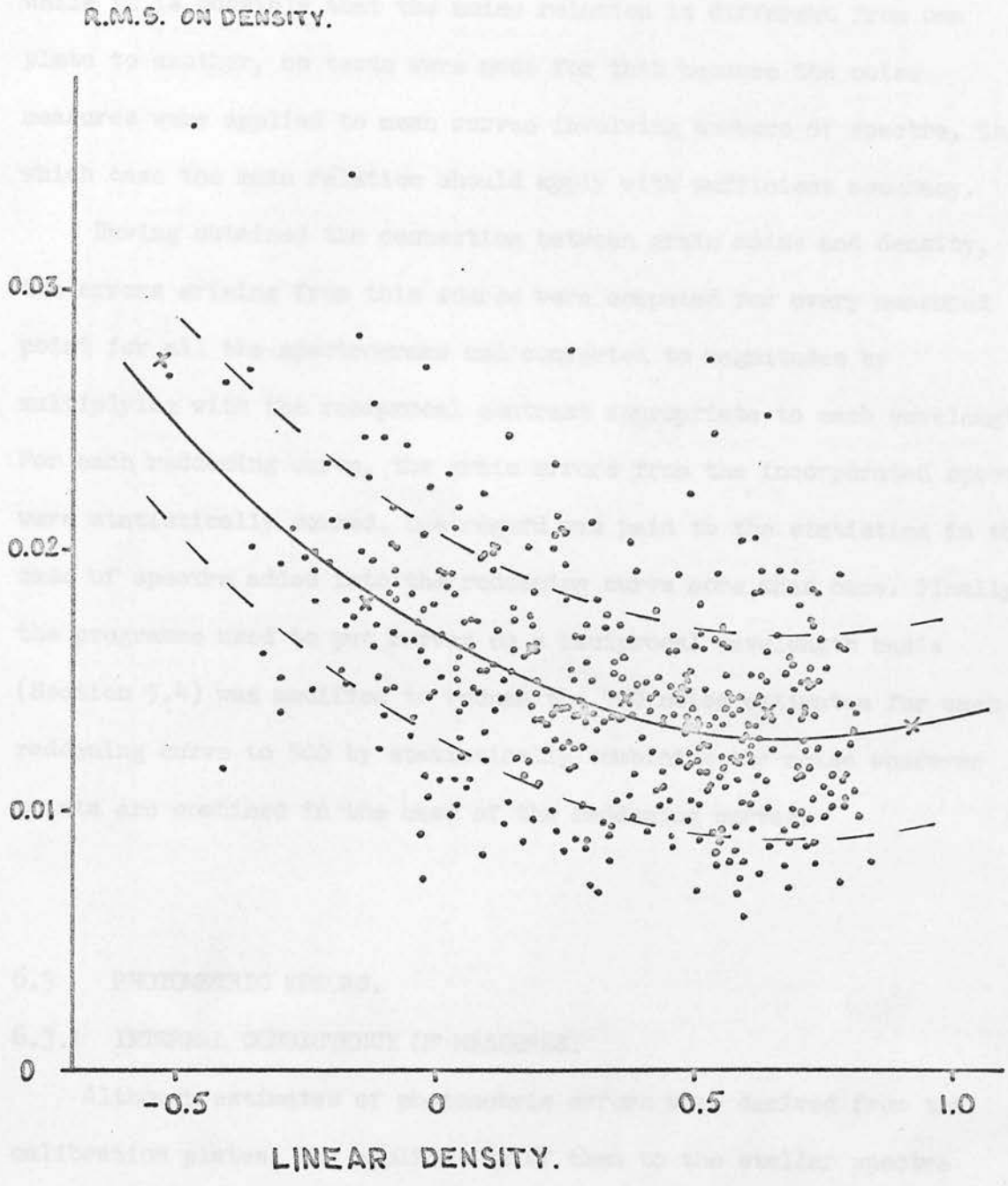

FIGURE 6.1

Photographic grain noise as a function of density.

dispersion against density is shown in Figure 6.1 . For comparison, the earlier measures are shown by crosses. A second degree polynomial was taken to represent the mean relation between noise and density. While it is possible that the noise relation is different from one plate to another, no tests were made for this because the noise measures were applied to mean curves involving numbers of spectra, in which case the mean relation should apply with sufficient accuracy.

Having obtained the connection between grain noise and density, the errors arising from this source were computed for every measured point for all the spectrograms and converted to magnitudes by multiplying with the reciprocal contrast appropriate to each wavelength. For each reddening curve, the grain errors from the incorporated spectra were statistically summed. Due regard was paid to the statistics in the case of spectra added into the reddening curve more than once. Finally, the programme used to put curves on a reciprocal wavelength basis (Section 5.4) was modified to reduce the 700 noise estimates for each reddening curve to 500 by statistically combining the noise wherever points are combined in the case of the reddening curves.

6.3 PHOTOMETRIC ERRORS.

6.3.1 INTERNAL CONSISTENCY OF MEASURES.

Although estimates of photometric errors were derived from the calibration plates, the application of them to the stellar spectra is not straightforward. They serve only to show that photometric properties obtained from individual calibration spectra carry no great weight and give a general indication of the expected level and behaviour of errors associated with the stellar measures. The actual form that the errors take is best found from an examination of the internal consistency of the measures. The most obvious way of doing this is to

PLATE.

STAR.

	36	37	38	39	40	41	42	44	45	46	47	1	2	3	4	5	6	9	10
1														24	25				
2															27	26			
3			29														28		
5		34																33	
6		36						35											
7	2									4									
8										31					32				
9	1							30		3									
10				9				38			39								
11				11							40								
12				10											37				
13					17													18	
14					19	20													
15															22			21	
16							14												
17							16												
18							15												
19							6					8							
20												12							13
21							5	23				7							
22													42						
24									41										

TABLE 6.1

Showing the disposition of spectra of a given star among the plates.

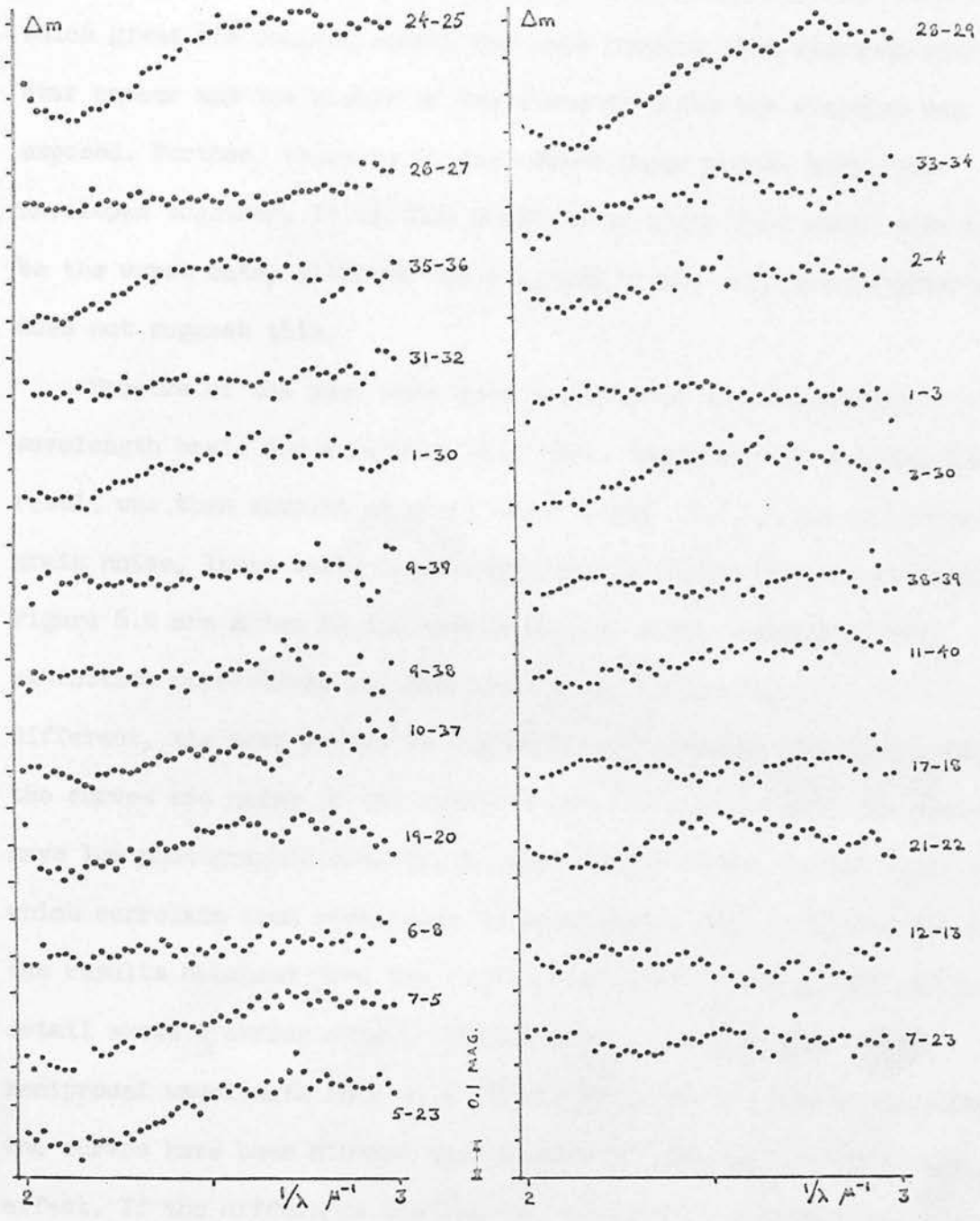

FIGURE 6.2

Photometric error curves.

Each is the difference of the spectrum of a particular star obtained on separate plates. Numbers are spectrum tracing numbers.

compare spectra of the same star.

Where there are two or more spectra of a given star, they have always been taken on different plates, as can be seen from Table 6.1 which gives the running number for each tracing of a spectrum with the star number and the number of the plate on which the spectrum was exposed. Further, there is no case where these plates have been developed together. It is thus possible to study what would seem to be the worst case, although the analysis of the calibration material does not suggest this.

Spectra of the same star were differenced on a reciprocal wavelength basis and a running mean taken involving ten points. The result was then sampled at every tenth point. Due to the reduction in grain noise, large scale photometric errors should not be obscured. In Figure 6.2 are shown 23 difference curves. Since exposure times, extinction corrections and development are in general all a little different, the zero points on the magnitude axis are arbitrary. Where the curves are noisy in the ultra-violet, this is because the spectra have low photographic density. A large number of the curves show defects which correlate from wavelength to wavelength. This is in keeping with the results obtained from the calibration spectra. Here, the greater detail shows a characteristic colour effect which is linear with reciprocal wavelength only to a first approximation. Where necessary, the curves have been plotted upside down in order to emphasise the effect. If the difference between the curves is one of scaling factor, then the first two curves show the effect in its most pronounced form. Since the curves show a strong resemblance to the emulsion contrast curve, the effect is no doubt connected with development.

Evidently, individual reddening curves obtained from spectra on different plates may be seriously distorted by photometric colour

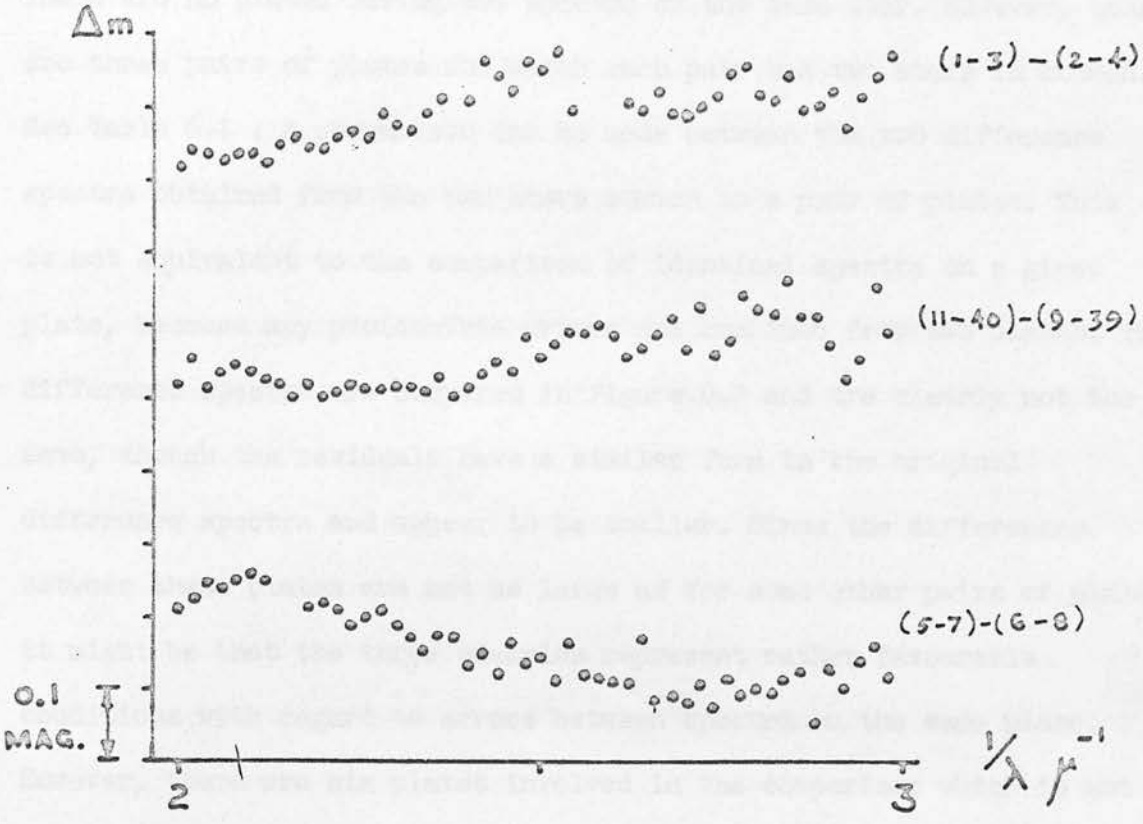

FIGURE 6.3

Comparison of photometric error curves.

The difference between the error curves in Figure 6.2, where a pair of plates give more than one error curve. Numbers refer to spectra.

errors. Not only will the sharpness of the corner be diminished or exaggerated but spurious corners can be introduced.

The presence or otherwise of photometric errors other than grain noise between spectra on the same plate cannot be checked directly. There are no plates having two spectra of the same star. However, there are three pairs of plates for which each pair has two stars in common. See Table 6.1 . A comparison can be made between the two difference spectra obtained from the two stars common to a pair of plates. This is not equivalent to the comparison of identical spectra on a given plate, because any photometric errors are combined from two plates. The difference spectra are compared in Figure 6.3 and are clearly not the same, though the residuals have a similar form to the original difference spectra and appear to be smaller. Since the differences between these plates are not as large as for some other pairs of plates, it might be that the three examples represent rather favourable conditions with regard to errors between spectra on the same plate. However, there are six plates involved in the comparison which is not a too unrepresentative fraction of the total of nineteen. Therefore, it would not be unreasonable to suggest that errors are reduced when spectra on the same plate are compared.

The twelve spectra referred to above form close pairs on individual plates and of these five are spaced by 0.6 mm while the remaining pair are spaced by 1.2 mm. It is thus unlikely that the development of the members of a pair is substantially different. If this is so, then the reason for the discrepancies must be sought in terms of either the incorrect use of mean photometric data or intrinsic variations of photometric properties.

The use of mean photometric data, rather than that derived from the particular calibration plate developed together with the stellar

plate, is based on the observation that the dispersion in such data from plate to plate appears to be no greater than the dispersion across an individual plate. Clearly, the use of mean properties for the photographic process will give rise to errors, even if two spectra are adjacent and the properties of the emulsion identical for the two spectra. When spectra are on different plates, the situation may be worse because of differences in emulsion properties or development. The first two curves in Figure 6.2 are no doubt extreme examples of such cases.

It seems probable that variations in emulsion properties, whether real or caused by non uniform development, occur in a partly random fashion across plates so that only in a given small area or zone can the properties be considered uniform. If spectra are to be accurately compared, then common wavelengths must fall within the characteristic area of a zone and the actual photometric properties of the zone must be known. The characteristic size of zones is perhaps of the order of a centimetre or so across (42). This means that the size of the stellar spectrum plates is border line, while the calibration spectra by nature of their size can only give average values of photometric properties.

6.3.2 SPECTROPHOTOMETRIC GRADIENTS AND COMPARISON WITH UBV COLOURS.

The last section shows the form of the photometric errors but their size is only known reliably for the comparison of spectra occuring on different plates. In order to establish the degree of improvement obtained when spectra are on the same plate and to provide a further check on the accuracy of the photographic measures, it is necessary to make a comparison with independent measures. Therefore, spectrophotometric gradients were derived and compared to UBV photoelectric colours. The gradients and their errors are also of some

interest in connection with the ratio of the slopes of the reddening curves and the effect of the Balmer jump. Although the broad band photoelectric measures are more accurate than the photographic, their interpretation in terms of continuum gradients is not as straightforward. There is the question of the effective wavelengths of the filters and the effect of absorption lines and the Balmer jump. Hence the photoelectric colours are best suited to comparisons with the relative gradients of groups of stars of the same type, which tends to be the case for spectra occuring on the same plate.

When the continuum intensities of stellar spectra represented on a magnitude scale are differenced, the result plots nearly linearly against reciprocal wavelength. This will still be true for reddened stars if the reddening law can be represented by straight lines on a magnitude reciprocal wavelength plot. Therefore, for difference spectra covering the range 3300A to 5000A, the continuum can be represented by three straight lines; two intersecting at the corner of the reddening curve and the third beyond the Balmer jump in the ultra-violet. For convenience these regions can be called Blue, Violet and Ultra-violet. They cover the reciprocal wavelength ranges 2.0 to 2.3 μ^{-1}, 2.3 to 2.7 μ^{-1} and 2.7 to 3.0 μ^{-1} respectively.

Since the stars cover a comparatively small range of spectral types and luminosity classes, it is only necessary to omit strong spectrum lines in order to define a continuum on a difference spectrum. If the stars form a reddening pair, then they are supposed to be closely matched and omission of lines is merely a precautionary measure against residual lines in the difference. The lines omitted are the Balmer lines, neutral helium, the interstellar band at 4430A and the helium and nitrogen lines which are in emission in Of stars. What is left is then fitted by straight lines by the method of least squares.

If the spectra of individual stars are differenced from a suitable comparison such as the mean spectrum of all the stars, then the blue gradients of the difference spectra should be nearly linearly related to the colour indices (B – V) of the stars. Since the effective wavelength of the B filter is on the corner of the reddening curve, there should be no significant difference in (B – V) colour for any possible variations in the ratio of violet to blue gradient. A plot of blue gradients versus colour indices (B – V) should be a straight line of slope 2.13 if the effective reciprocal wavelengths of the B and V filters are separated by 0.47 μ^{-1}. The effective wavelengths of the filters are functions of the colour indices, so that the difference between the effective wavelengths decreases with increasing (B – V) colour index. Rozis–Saulgeot (43) has calculated the relation between colour excess and mass of interstellar absorbing material. Since thermal and interstellar reddening are equivalent for the wavelengths under consideration, Rozis–Saulgeot's data gives the change in effective wavelengths with change in colour index. For the reddest star, the difference in effective reciprocal wavelengths decreases by 3 per cent and therefore the effect can be neglected. The blue gradients have been plotted against (B – V) colour indices in Figure 6.4 . Though the trend of the points is correct, there is considerable scatter which may be slightly spectral type dependent. However, for pairs of stars that have exposures on the same plate, the correlation is much better. Evidently, the blue gradient errors are large from plate to plate but relatively constant across a given plate. This being so, a plot of the difference of blue gradients and colour indices of pairs of stars, for cases where both stars in the pair occur on the same plate, will tend to have smaller gradient errors. Such a plot is shown in Figure 6.5 . Mixing of spectral types might be expected to produce scatter because

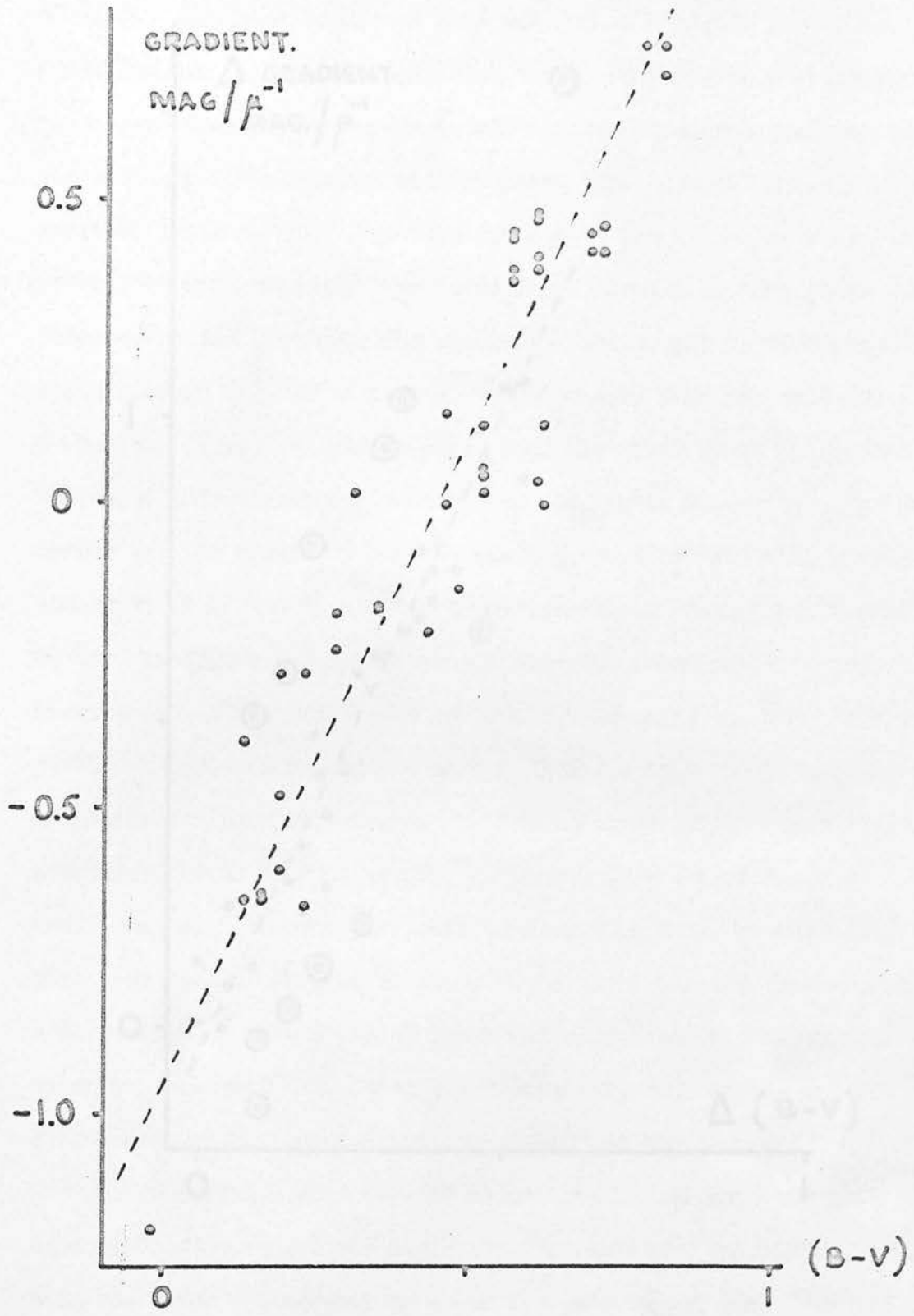

FIGURE 6.4

Blue gradient and (B – V) colour.

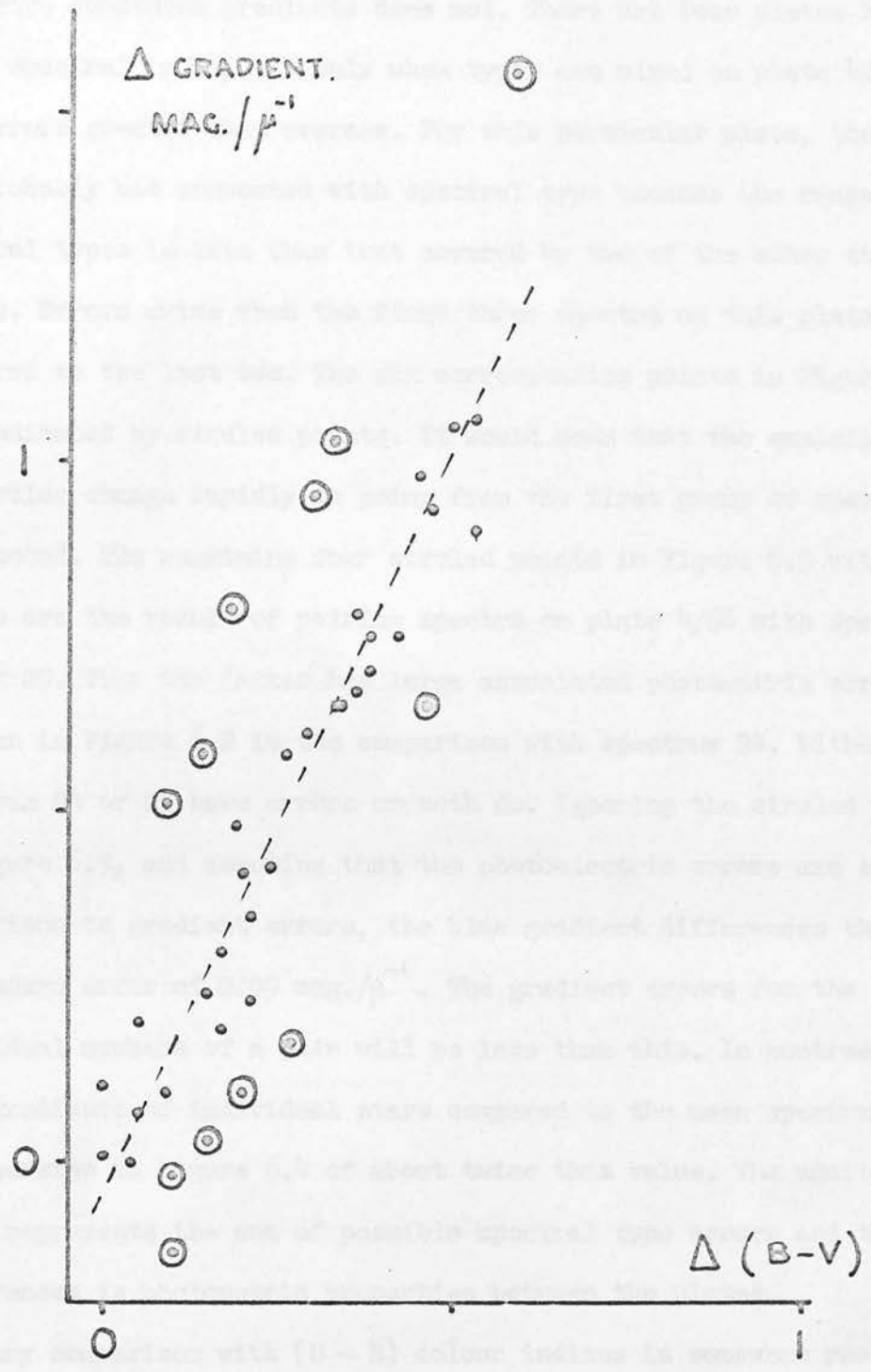

FIGURE 6.5

Comparison of Blue gradient differences with (B – V) differences.

broad band photometry includes spectral lines whereas the method used to derive continuum gradients does not. There are four plates having mixed spectral types, but only when types are mixed on plate 42/65 are the errors greater than average. For this particular plate, the errors are probably not connected with spectral type because the range of spectral types is less than that covered by two of the other three plates. Errors arise when the first three spectra on this plate are compared to the last two. The six corresponding points in Figure 6.5 are indicated by circled points. It would seem that the emulsion properties change rapidly in going from the first group of spectra to the second. The remaining four circled points in Figure 6.5 with large errors are the result of pairing spectra on plate 4/66 with spectrum number 25. That the latter has large associated photometric errors can be seen in Figure 6.2 in the comparison with spectrum 24. Either spectrum 24 or 25 have errors or both do. Ignoring the circled points in Figure 6.5, and assuming that the photoelectric errors are small in comparison to gradient errors, the blue gradient differences then have a standard error of 0.09 mag./μ^{-1}. The gradient errors for the individual members of a pair will be less than this. In contrast, the blue gradients of individual stars compared to the mean spectrum show a dispersion in Figure 6.4 of about twice this value. The additional error represents the sum of possible spectral type errors and the differences in photometric properties between the plates.

Any comparison with (U – B) colour indices is somewhat restricted because the U measures are more strongly dependent on spectral types than the B and V measures, on account of the Balmer jump. For the (U – B) colours, the difference between the effective wavelengths of the filters increases with the amount of interstellar reddening (43). Apart from the effect of the Balmer jump and absorption lines,

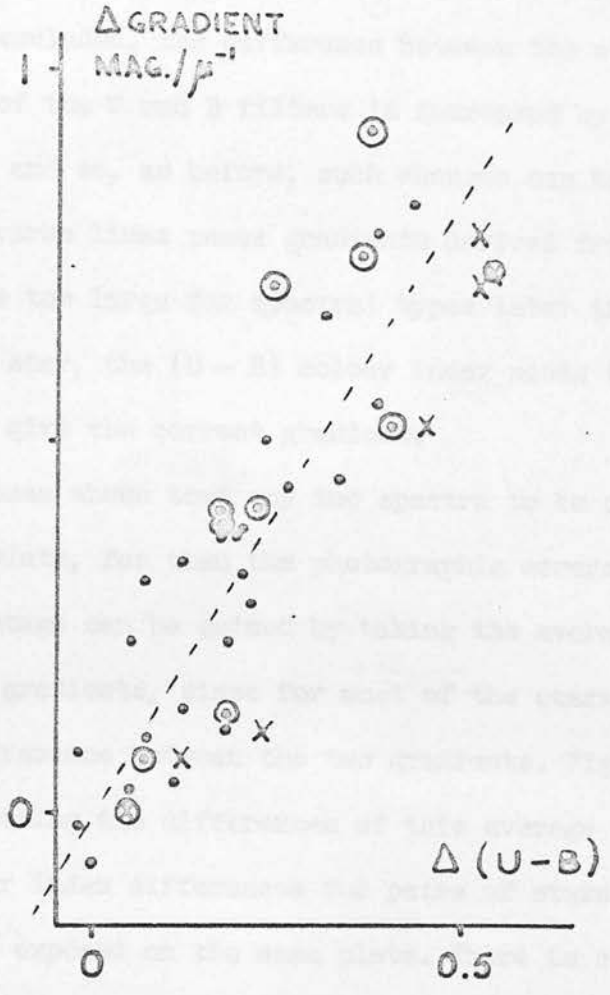

FIGURE 6.6

Differences in the mean violet gradient compared to those for (U – B).

interstellar and thermal reddening are nearly equivalent for these wavelengths. There is a slight complication which arises from the difference in continuum colour temperature each side of the Balmer jump (44). However, the difference is small and should only be significant for the B8 stars used in the programme. With the effect of lines and the Balmer jump excluded, the difference between the effective reciprocal wavelengths of the U and B filters is increased by 3 per cent for the reddest star and so, as before, such changes can be ignored. The Balmer jump and spectrum lines cause gradients derived from the (U – B) colour indices to be too large for spectral types later than about B1. In the case of a B8 star, the (U – B) colour index needs to be reduced by 0.19 magnitude to give the correct gradient.

It has been shown that any two spectra to be compared should be on the same plate, for then the photographic errors are smaller. A further advantage can be gained by taking the average of the violet and ultra-violet gradients, since for most of the stars there is very little intrinsic difference between the two gradients. Figure 6.6 shows the result of plotting the differences of this average gradient against (U – B) colour index differences for pairs of stars where both stars of a pair are exposed on the same plate. There is considerable scatter but most of the points are consistent with the correlation shown, which represents an effective reciprocal wavelength for the U filter of $2.90\ \mu^{-1}$.

For most of the star pairs that show the greatest deviations from the expected correlation, the differential violet and ultra-violet gradients are in poor agreement, though the converse is not necessarily true. There are three cases where there are two sets of measurements that can be compared. In each case the measurements do not agree very well and they happen to include three of the points that do not

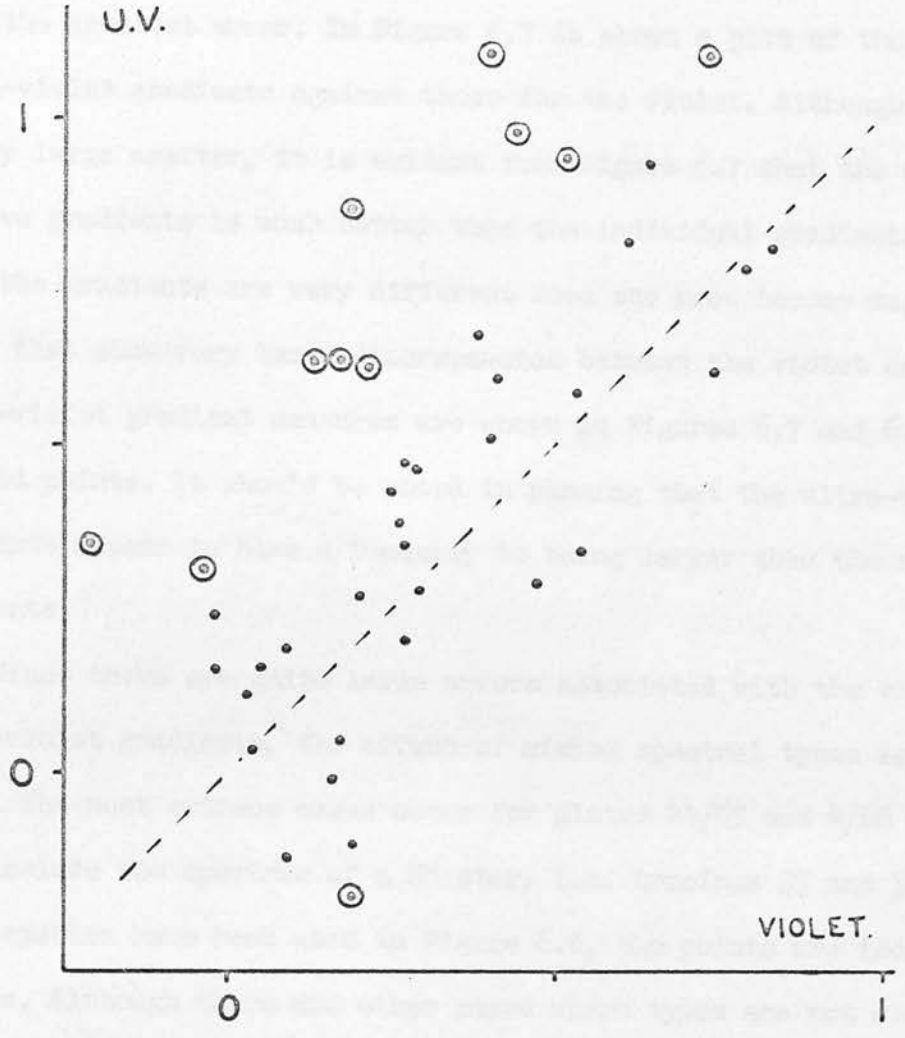

FIGURE 6.7

Correlation between Violet and Ultra-violet gradients.

correlate well with (U – B) colours. Therefore the difference between the two gradients is probably due to photometric errors. According to the error curves shown in the previous section, it is quite likely there will be a difference in the gradients and that the violet gradient will have the greatest error. In Figure 6.7 is shown a plot of the ultra-violet gradients against those for the violet. Although there is a very large scatter, it is evident from Figure 6.7 that the mean of the two gradients is much better than the individual gradients. Only when the gradients are very different does the mean become suspect. The pairs that show very large discrepancies between the violet and ultra-violet gradient measures are shown in Figures 6.7 and 6.6 by circled points. It should be noted in passing that the ultra-violet gradients appear to have a tendency to being larger than the violet gradients.

Since there are quite large errors associated with the violet and ultra-violet gradients, the effect of mixing spectral types is not clear. The most extreme cases occur for plates 44/65 and 4/66 which each include the spectrum of a B8 star, i.e. tracings 37 and 38. Where these spectra have been used in Figure 6.6, the points are indicated by crosses. Although there are other cases where types are not closely matched, it is only for the points represented by the crosses that the errors involved in mixing types are comparable to the gradient errors.

If it is assumed that the photographic errors predominate in Figure 6.6, then an estimate can be made of the errors in the mean gradient measures. Omitting both the crossed and circled points, the R.M.S. deviation from the correlation shown is 0.11 mag./μ^{-1}.

Because the gradients correlate reasonably well with the photoelectric colours, using the accepted values of effective wavelengths, the photographic magnitude scales are thought to be

correct. The estimates of difference gradient errors between spectra occuring on the same plate are probably a little in error because of the uncertainties in interpreting wide band photometry and the arbitrary rejection of points with suspected larger than average errors. They may well be slightly underestimated. This is particularly true of the combined violet and ultra-violet gradients.

In order to show the reduction in errors obtained by having a group of spectra exposed on the same plate, gradient errors have been derived from the error curves of the previous section for comparison. When the spectra are on different plates the blue, violet and ultra-violet gradient standard errors are respectively 0.16, 0.23 and 0.19 mag./ μ^{-1} . The error for the mean of the two violet gradients is then 0.15 mag./ μ^{-1} . These figures are to be compared to those derived above which are 0.09 mag./ μ^{-1} for the blue and 0.11 mag./ μ^{-1} for the mean of the violet gradients. In view of the uncertainty of the errors, the apparent difference in the improvement of the two ends of the spectrum is probably not significant. The similarity of the photometric error curves obtained across plates and between plates was noted in the last section. Therefore, the degreee of improvement is of the order of 1.6 .

6.3.3 PHOTOMETRIC ERRORS ASSOCIATED WITH THE REDDENING CURVE.

If the mean of the 23 curves shown in Figure 6.2 is formed, then the resulting curve shown in Figure 6.8 represents the typical error curve which one can expect when two spectra on different plates are differenced. Of course, the sign is not known and the curve may differ from the actual error curve by a difference of degreee or by another wavelength dependent curve. Since the form of individual error curves is not required but only the effect for a number of difference spectra

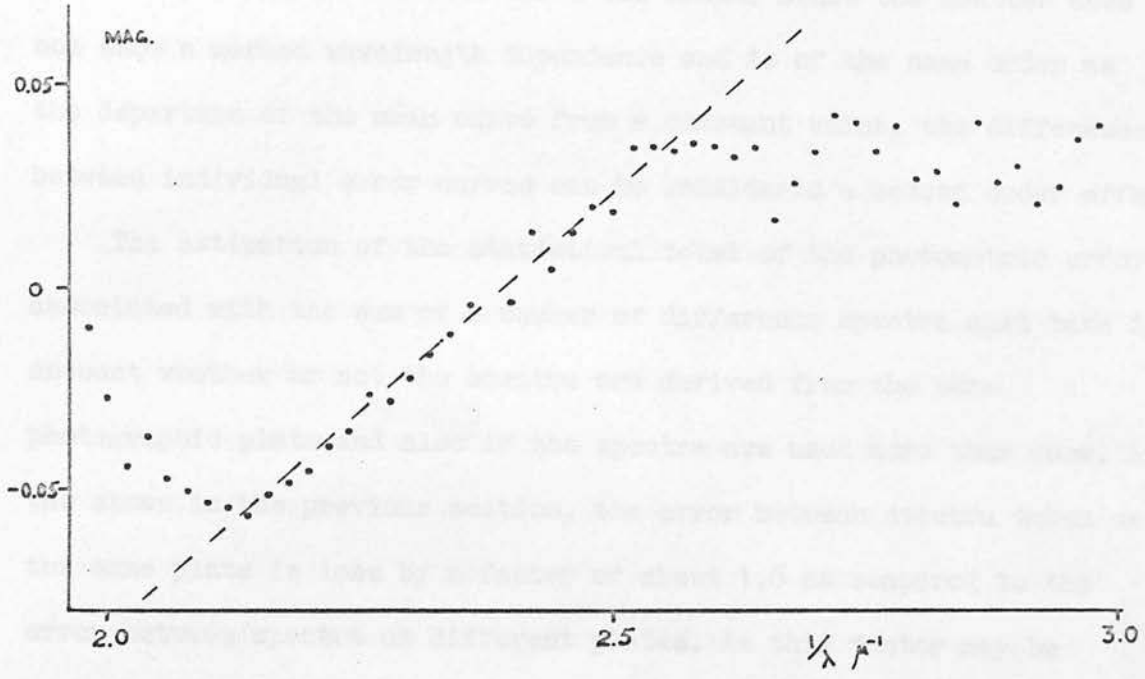

FIGURE 6.8

The mean photometric error curve.

added together, the behaviour of the error curve was not further investigated other than to observe the scatter of individual curves about the mean. To do this, the zero point of each curve was adjusted to minimise the sum of the squares of the deviations of the curve from the mean curve. From all the individual curves, so adjusted, the scatter about each point on the mean curve was found. Since the scatter does not show a marked wavelength dependence and is of the same order as the departure of the mean curve from a constant value, the differences between individual error curves can be considered a second order effect.

The estimation of the statistical total of the photometric errors associated with the sum of a number of difference spectra must take into account whether or not the spectra are derived from the same photographic plate and also if the spectra are used more than once. As was shown in the previous section, the error between spectra taken on the same plate is less by a factor of about 1.6 as compared to the error between spectra on different plates. As this factor may be slightly overestimated it has been reduced to 1.4 . This makes the variances differ by a factor of two which is both convenient and quite justified by the nature of the other assumptions and approximations which follow. Most of the comparison spectra are used more than once which means that the errors are not statistically independent and the variance adds as the square of the number of times the spectrum is used. There are many mixed cases where a comparison spectrum is used more than once and the spectra for comparison may or may not be on the same plate. It is therefore necessary to estimate the error associated with a single spectrum. This has been obtained from the estimates of the error between two spectra by assuming that, on average, the variance is contributed to equally by the two members of the pair. For the three reddening curves formed by dividing the spectra into three groups, the

mean photometric error curve must be multiplied by the appropriate factors to give the standard photometric error curves. The 16 pairs excluding Of stars and HD 13866 give the factor $\sqrt{17.5}$, the 6 pairs including Of stars give $\sqrt{6.5}$ and the 4 pairs including HD 13866 give $\sqrt{3.0}$.

6.4 THE BALMER JUMP.

In general, the shape of the reddening curve obtained from the comparison of the spectra of two stars will be affected by lack of matching of spectral type and luminosity class of the two stars. For each star used in this investigation and over the wavelength region of interest near the corner, the continuum colour temperature can be considered constant. This should also apply to the Balmer continuum. Therefore, although the relation between the section of the reddening curve each side of the Balmer jump may not be correct, the shape of each section should be correct. The two parts of the curve can be properly connected if, for each star, the Balmer jump and change in spectrophotometric gradient across the jump are known. While these parameters can be found from the relation with spectral types and luminosity class given in the literature, it was thought advisable to determine them directly from the spectra. A further check is then obtained of the validity of the photometry. Because the shape of the reddening curve at and beyond the Balmer jump has no bearing on the shape of the corner, examination of the Balmer jump was not extensive. No attempt was made to measure the position of the jump since this is mostly influenced by luminosity and nearly all the stars used are supergiants.

The size of the jump was found from the data derived in section 6.3.2., where the spectra of individual stars were compared to the

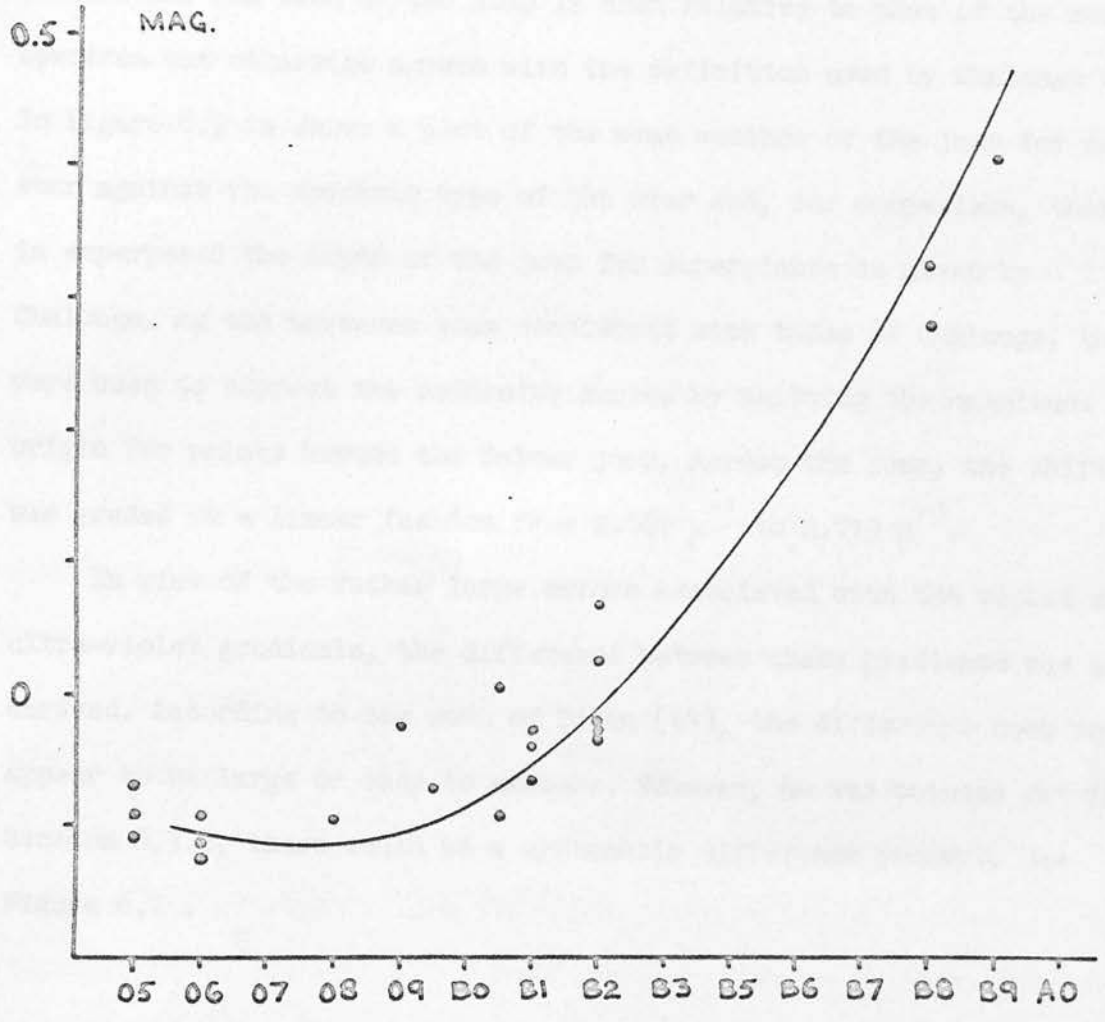

FIGURE 6.9

The relation between Balmer jump and spectral type.

The curve is obtained by Chalonge.

mean spectrum of all the stars. The straight lines fitted to the difference spectra, which were used to find the violet and ultra-violet gradients, were extrapolated to 2.7 μ^{-1} and the difference in magnitudes calculated. The size of the jump is then relative to that of the mean spectrum but otherwise agrees with the definition used by Chalonge (40). In Figure 6.9 is shown a plot of the mean measure of the jump for each star against the spectral type of the star and, for comparison, there is superposed the depth of the jump for supergiants as given by Chalonge. As the measures seem consistent with those of Chalonge, they were used to correct the reddening curves by shifting the magnitude origin for points beyond the Balmer jump. Across the jump, the shift was graded in a linear fashion from 2.661 μ^{-1} to 2.719 μ^{-1}.

In view of the rather large errors associated with the violet and ultra-violet gradients, the difference between these gradients was not derived. According to the work of Divan (44), the difference does not appear to be large or easy to measure. However, as was pointed out in Section 6.3.2, there could be a systematic difference present. See Figure 6.7 .

7. RESULTS AND CONCLUSION.

7.1 COMPARISON OF RESULTS WITH OTHER OBSERVATIONS.

The curve derived from the difference between the spectra of a particular pair of stars is an approximation to the reddening law and, being independent of the method of observation, it should be the same for all observers. It is therefore interesting to compare the results for individual reddening curves with those obtained by other observers, particularly if their instruments and methods of reduction are at all different. However, suitable spectroscopic material is scarce in the Perseus region and comparisons of any value can be made for only eight stars which are in common with those investigated by Nandy (11). Five pairs of stars have been selected from these eight stars and the resulting reddening curves are shown in Figure 7.1 together with the corresponding curves given by Nandy. To make the comparison more meaningful, the resolution has been degraded to approximate Nandy's. The 700 points for each difference spectrum give some 500 after conversion to a reciprocal wavelength basis. After taking a running mean of ten points, the data is sampled every tenth point. Since the zero points on the author's curves are quite arbitrary, they have been adjusted so that the curves pass through the run of Nandy's points where this is possible. The run of points is generally much smoother than Nandy's, as might be expected, because the greater number of measured points involved reduce errors due to grain. On the other hand, it is clear that there are systematic differences present. In this work it has been shown that differences may be expected to arise from wavelength dependent photometric errors, and corresponding errors may be presumed to exist in Nandy's results. Such errors obviously limit the interpretation of individual reddening curves. It is possible that there are small residuals of extinction corrections present on the author's

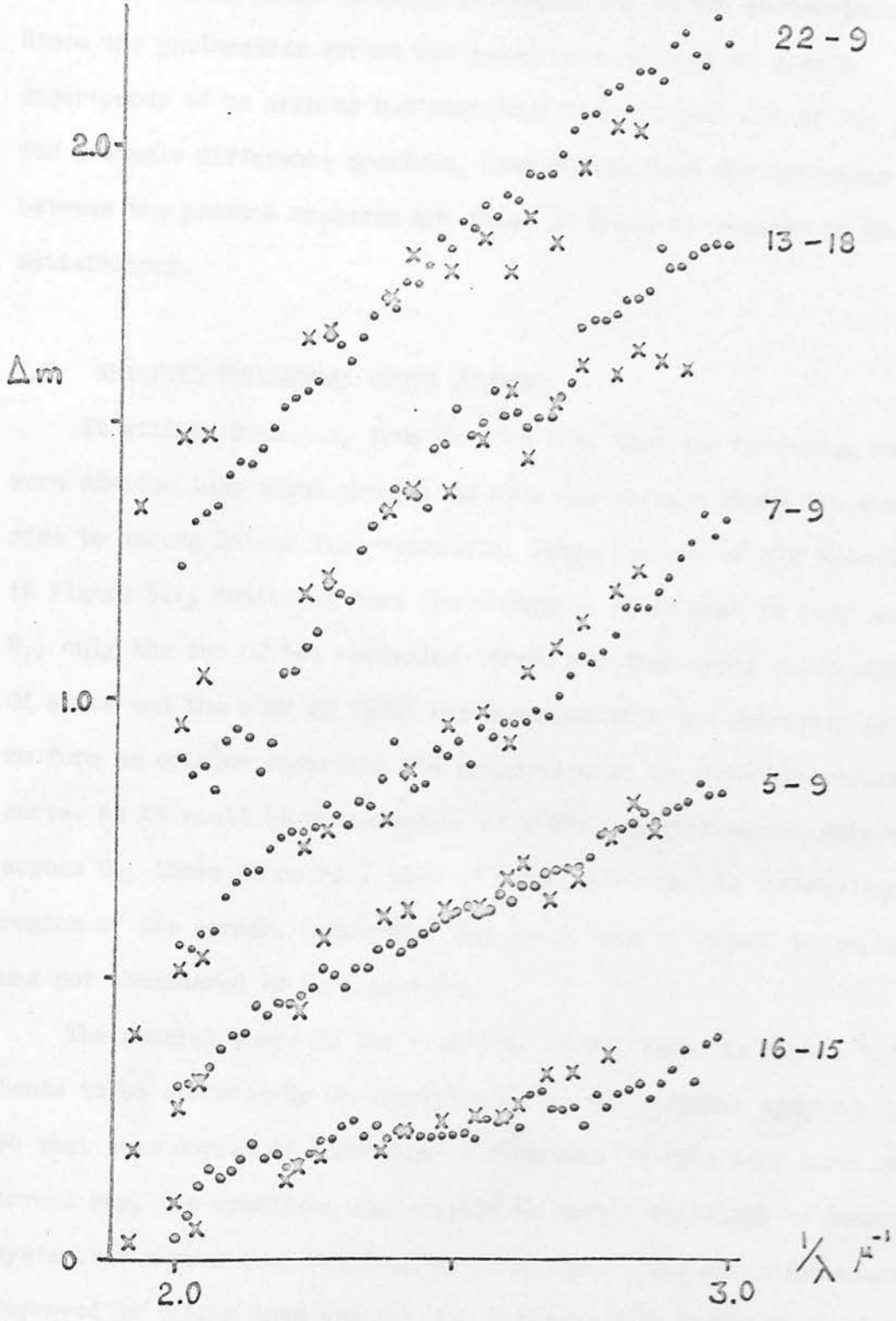

FIGURE 7.1

Comparison of reddening curves with those obtained by Nandy.

Crosses denote Nandy's points.

curves but these would be small in comparison to the photometric errors. Since the photometric errors are known on occasions to give a discrepancy of as much as 0.3 magnitude between each end of the spectrum for a single difference spectrum, (see Figure 6.2) the agreement between the present measures and those of Nandy is thought to be very satisfactory.

7.2 WEIGHTED POLYNOMIAL CURVE FITTING.

It will be recalled, from Section 5.3, that the reddening curves were divided into three groups, to show how certain stars can give rise to strong Balmer line residuals. Since the sum of all curves, shown in Figure 5.1, indicates that the change of slope must be very near to H_γ, only the sum of the reddening curves for that group which excludes Of stars and the star HD 13866 was examined with the necessary detail to form an opinion regarding the properties of the mean extinction curve. As it would be necessary to give the rejected curves zero weight across H_γ, there is no real loss of information in the interesting region of the corner. Elsewhere, the small loss of signal to noise ratio was not considered to be important.

The general shape of the reddening curve, shown in Figure 7.2 , tends to be obscured by photographic noise and residual spectrum lines so that some degree of smoothing is required. If this were done in the normal way, the resulting curve would be rather sensitive to localised systematic errors i.e. residual spectrum lines. The situation would be improved by taking into account the expected size of the errors by some method of weighting the data points. However, using a curve fitting technique reduces the local error dependence, the overall shape of the curve being determined to some extent by all the data. By properly weighting the data points, the fitted curve can be made

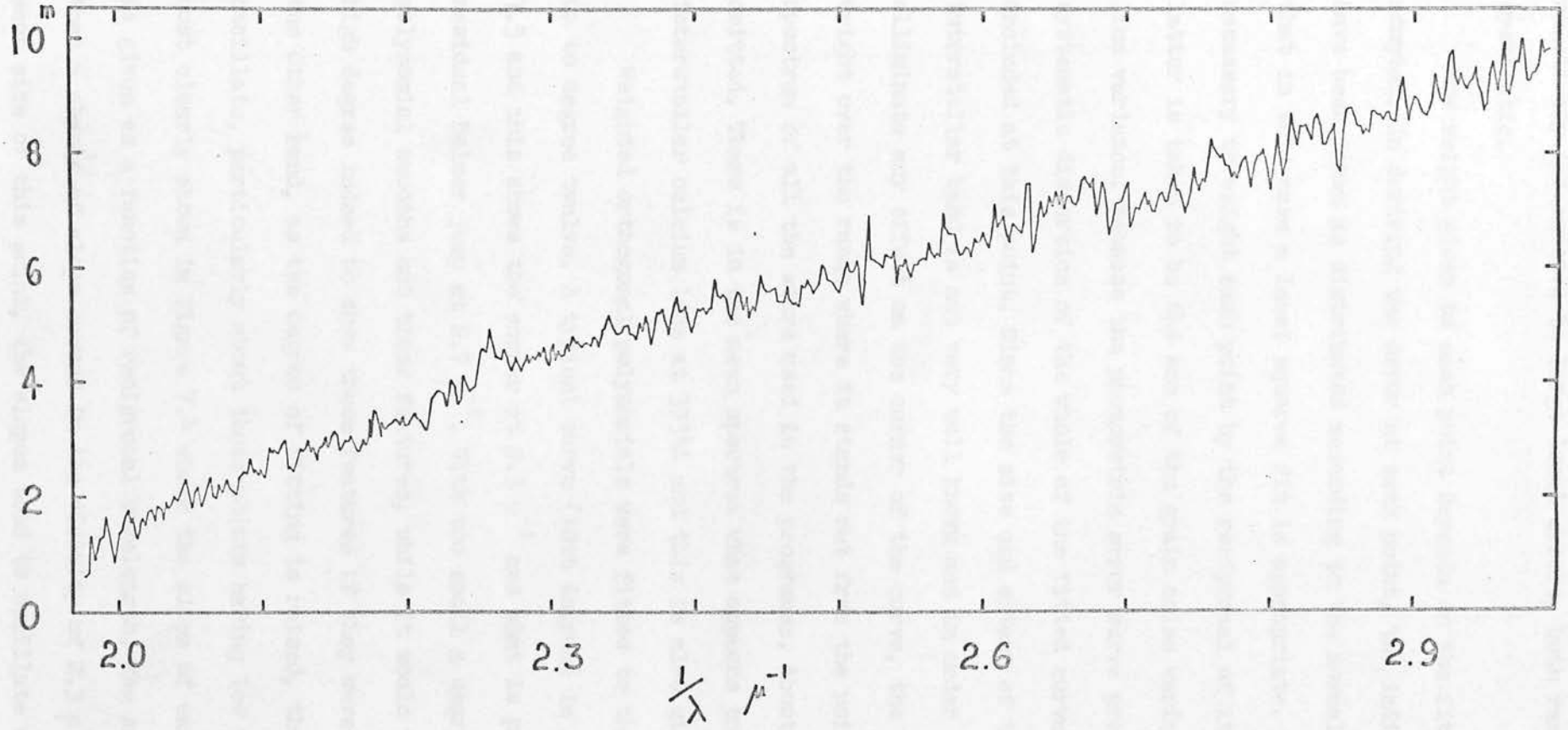

FIGURE 7.2

Sum of reddening curves derived from 8 reddened and 5 comparison stars.

relatively insensitive to large local errors, both random and systematic.

The weight given to each point depends on the fitting criterion adopted. In deriving the error at each point, the individual errors have been taken as distributed according to the normal error law, so that in this case a least squares fit is appropriate. It is then necessary to weight each point by the reciprocal of its variance. The latter is taken to be the sum of the grain noise variance and residual line variance. Because the photometric error curve produces a systematic distortion of the whole of the fitted curve, it is not included at this point. Since the size and extent of the residual 4430A interstellar band is not very well known and in order to clearly elliminate any effect on the corner of the curve, the band is given zero weight over the range where it stands out from the noise in the mean spectrum of all the stars used in the programme. About 50A are thereby omitted. There is in the mean spectrum what appears to be the interstellar calcium line at 3934A and this is also given zero weight.

Weighted orthogonal polynomials were fitted to the reddening curve up to degree twelve. A typical curve (10th degree) is given in Figure 7.3 and this shows the corner at 2.3 μ^{-1} and what is presumably a residual Balmer jump at 2.7 μ^{-1}. With too small a degree, the fitted polynomial smooths out these features, while it would require a very high degree indeed to show these features if they were very sharp. On the other hand, as the degree of fitting is raised, the curve tends to oscillate, particularly about those points having low weight. This is most clearly shown in Figure 7.4 where the slope of each fitted curve is given as a function of reciprocal wavelength. The same figure shows that a change of slope occurs in the vicinity of 2.3 μ^{-1} and that to each side of this point, the slopes tend to oscillate about constant

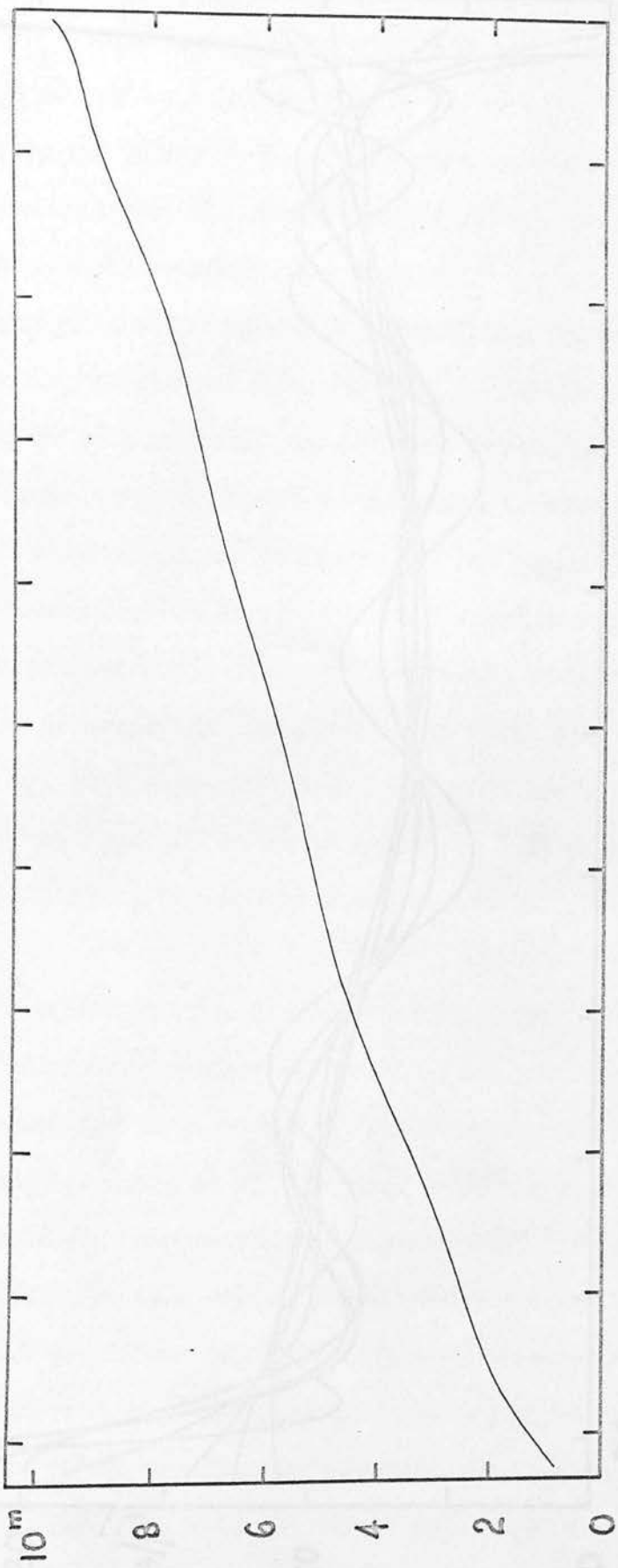

FIGURE 7.3

Tenth degree polynomial fit to reddening curve.

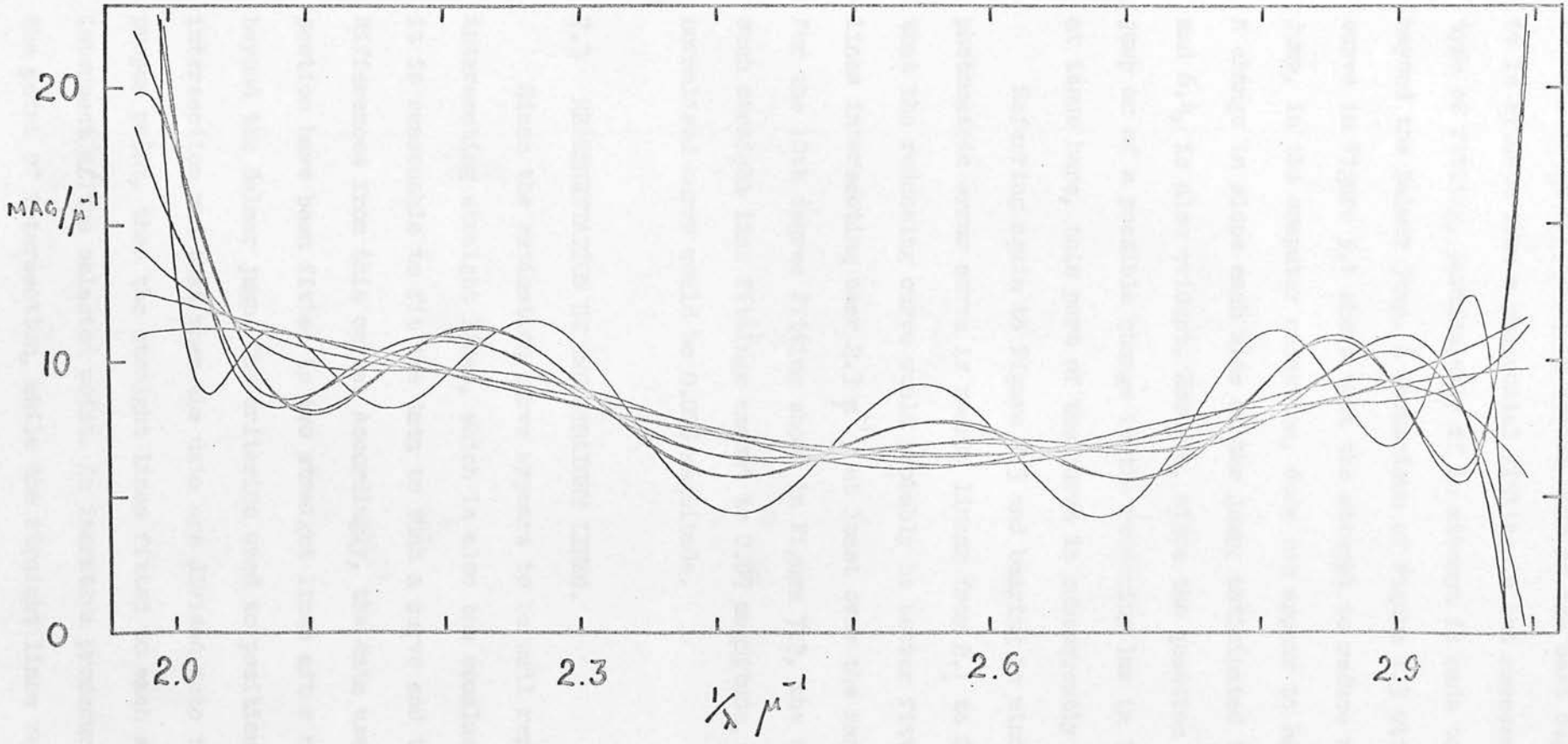

FIGURE 7.4

Slopes of polynomials fitted to reddening curve.

The differential coefficients are given for degrees 4 to 12.

values. It is difficult to decide what is the best degree of fit, while it is evident that a polynomial fitting is not necessarily the best type of fitting, particularly if an attempt is made to include data beyond the Balmer jump. A comparison of Figure 7.3 with the appropriate curve in Figure 5.1 shows that the attempt to reduce residual Balmer jump, in the computer reduction, does not appear to have been a success. A change in slope each side of the jump, anticipated in Section 6.3.2 and 6.4, is also evident. However, since the question of residual Balmer jump or of a possible change in the reddening law in this region is not at issue here, this part of the curve is subsequently ignored.

Referring again to Figure 7.3 and bearing in mind that the mean photometric error curve is nearly linear from 2.1 to 2.6 μ^{-1} it is clear that the reddening curve would probably be better fitted by two straight lines intersecting near 2.3 μ^{-1}, at least over the range 2.0 to 2.7 μ^{-1}. For the 10th degree fitting shown in Figure 7.3, the deviations from such straight line fittings amount to 0.05 magnitude, which on a normalised curve would be 0.005 magnitude.

7.3 REPRESENTATION BY TWO STRAIGHT LINES.

Since the extinction curve appears to be well represented by two intersecting straight lines, which is also the conclusion of Nandy (11), it is reasonable to fit the data to such a curve and then look for differences from this curve. Accordingly, the data used in the last section have been fitted to two straight lines after removal of the data beyond the Balmer jump. The criterion used to position the point of intersection was that when the data are divided into two parts at the proper point, then the straight lines fitted to each section of data intersect at the selected point. An iterative procedure was used to find the point of intersection, while the straight lines were fitted by the

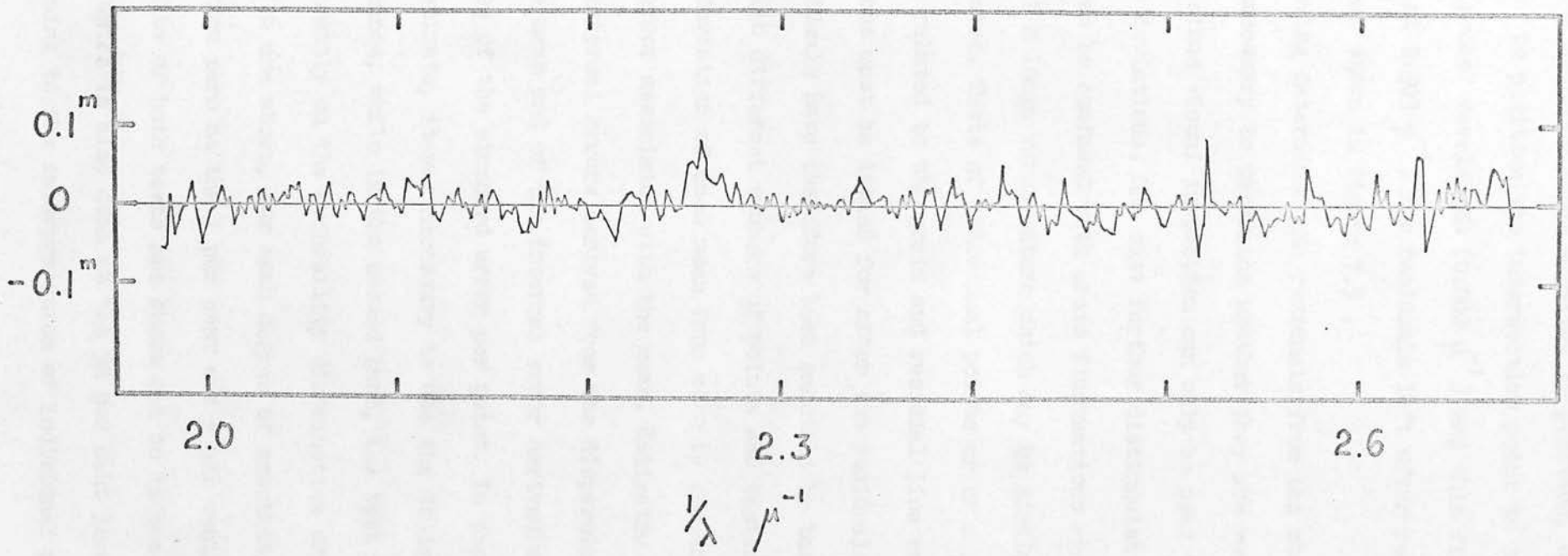

FIGURE 7.5

Residuals from the two straight lines fitted to the reddening curve.
The intersection point for this initial fitting is at 2.302 μ^{-1}.

method of weighted least squares. In practice, only four iterations were required to position the intersection point to the nearest increment of reciprocal wavelength ($0.002\ \mu^{-1}$) and this first fitting puts the corner at $2.303\ \mu^{-1}$. The residuals left after removal of the fitted curve are shown in Figure 7.5 .

Having determined the residuals from the straight line fitting, it is necessary to determine whether they are real or not by statistical tests, since visual inspection can only be used to sort out the most obvious deviations. One must further distinguish between deviations which can be confused with grain fluctuations and residual lines, and those of a longe range nature which may be similar to the photometric error curve. Tests of individual points or of a few adjacent points must be related to the grain and residual line errors, while long range deviations must be looked for after the residuals are suitably smoothed. The residuals have therefore been smoothed by taking weighted running means with different numbers of points and testing for the significance of the deviation of each mean from zero by comparing it to an estimate of the error associated with the mean. Estimates have been made both of the external errors derived from the dispersion of individual points from the mean and of the internal error derived entirely from previous estimates of the standard error per point. In the case of the external error estimate, it was necessary to use the Student T test of significance, while in the second case, the test was the usual one based directly on the probability distribution of normal errors. In Figure 7.6 are shown, for each degree of smoothing, those points which differ from zero at the 1 per cent and 5 per cent levels of significance. The results of both tests are shown and so is the test of individual points, which is also done at the 32 per cent level of significance.

Turning to the interpretation of individual points first, it is

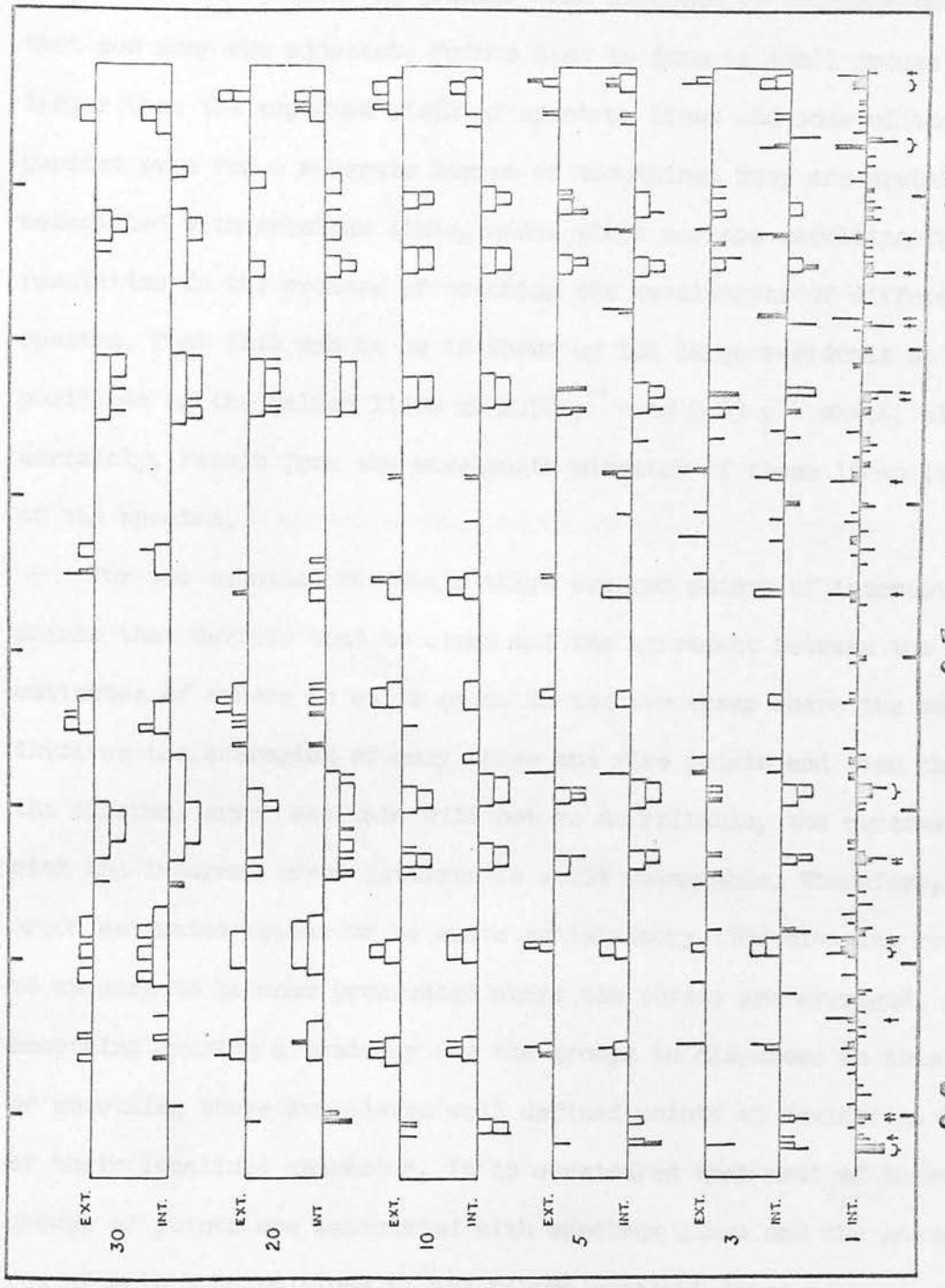

FIGURE 7.6

Significance of residuals for different running means. Ordinate numbers indicate number of intervals of 0.002 μ^{-1} in each mean. Arrows at the foot of the figure show points considered for rejection.

noted that their number is greater than expected by chance alone and that too many are adjacent. Points tend to form in small groups a little larger than the expected width of spectrum lines and some of the groups persist even for a moderate degree of smoothing. They are probably associated with spectrum lines, undue width perhaps resulting from lost resolution in the process of matching the wavelengths of different spectra. That this can be so is shown by the large residuals at the positions of the Balmer lines at 2.52 μ^{-1} and 2.63 μ^{-1} which, almost certainly, result from the wavelength mismatch of these lines in some of the spectra.

For the smoothed residuals there are two points of interest; the points that deviate tend to clump and the agreement between the two estimates of errors is quite good. In the two cases where the smoothing involves the averaging of only three and five points and even though the external error estimate will not be so reliable, the agreement with the internal error estimate is still reasonable. Therefore, the error estimates appear to be quite satisfactory. The clumping referred to appears to be most pronounced where ten points are averaged, greater smoothing causing a tendency for the groups to disperse. At this degree of smoothing there are eleven well defined points of deviation. Because of their localised character, it is considered that most of these groups of points are associated with spectrum lines and the general run of points to be close to the fitted straight lines.

In considering the influence of the photometric error curve, any overall slope that the curve may have is to be ignored in the present context, since it would have no effect on the intersecting straight line fitting other than to alter the slope of the two lines. With this in mind it can be seen, by reference to the mean photometric error curve shown in Figure 6.8 , that by excluding data beyond 2.7 μ^{-1} there is

a reduction in the deviations left after removal of the general slope of the remaining curve. This means that such deviations are only of the order of 0.04 magnitude for the reddening curve under consideration, which is less than the average grain noise level of 0.15 magnitude. (Note that these figures are reduced by a factor of ten when the data is normalised.) With sufficient smoothing, the noise level can be so reduced as to make deviations detectable and at the 5 per cent level of significance this implies that the running mean must include about 50 points. However, at such large degrees of smoothing, the deviations sought for will themselves start to be smoothed out and are likely to be swamped by the prominent deviations already found with less smoothing. The latter could of course be associated with the photometric error curve but the pattern of points does not in any way correspond. For these reasons the photometric errors are considered to be undetectable.

Of the eleven deviating groups of points, three can be explained. That at 2.04 μ^{-1} corresponds to the interstellar band at 4890A while 2.67 μ^{-1} is too close to the Balmer jump at a point where the overlapping Balmer lines cause difficulties. At the very longest wavelengths covered, the photometric errors rise very rapidly and it is therefore possible that here the errors are not correctly assessed and the deviation is spuriously detected. The other deviations are difficult to explain on account of their ill defined wavelengths, though some can be tentatively identified with spectrum lines. As they have the appearance of lines it is suggested that this is what they are and that they arise from incomplete matching of spectral types rather than being of interstellar origin since they would have been identified already in the spectra of heavily reddened stars and half of them appear in emission.

With the exception of the deviating points already dealt with, it seems that within the limits of observational errors, the extinction curve is very well represented by two intersecting straight lines. On a normalised curve, and at a resolution of 0.002 μ^{-1}, the curves are straight to better than 0.019 magnitude on average. Since the data points across the interstellar band at 4430A were specifically excluded, it appears that the corner of the curve is not caused by this band. The all important position and sharpness of the corner can now be calculated in terms of all the data points which appear to lie on the two straight lines.

The position of the corner is, of course, the point of intersection of the two straight lines, while the sharpness may be defined by the statistical limits in both wavelength and absorption over which the point of intersection is possible. These limits can be derived from the statistical errors on the two coefficients connected with each straight line. However, before doing so, it was necessary to consider whether the fit of the lines could be improved by suitable rejection of the data points. Had the distribution of large residuals been less favourable, this would have been required in some degree in order to establish the form of the extinction curve. Examination of the residuals for individual points shows that some 10 per cent of points could be rejected on the grounds that the residuals are very significant (1 per cent level) or that adjacent points have significant (5 per cent level) residuals of the same sign. These points are indicated in Figure 7.6 . When rejected in total and the intersecting straight lines fitting repeated, using the iterative procedure already outlined, the R.M.S. errors are considerably reduced, and the point of intersection is shifted a little to a longer wavelength at 2.294 μ^{-1}. A more useful statistic than the R.M.S. error of fitting is the ratio of the R.M.S.

error to the root mean expected variance. If the adopted curve and the error estimates are both correct, then this ratio is unity. In fact, the ratio is reduced from some 30 per cent or so above unity to a few per cent below unity. It is therefore evident that for the bulk of the data, the intersecting straight lines fitting and the independent error estimates are very consistent with one another. Because the ratio turns out to be less than unity, it is thought that the rejection of data is too severe so that data which come under the rejection criteria by chance alone have been rejected. As a rough guide to what happens to the ratio and also to the position of the intersection point, when the rejection criteria are relaxed, it is easier to change the degree of rejection than modify the criteria. This has been done by scaling the weights associated with the previously rejected data points.

TABLE 7.1

Change of fitted parameters with scale of rejection of points.

Scaling factor.	1.0	0.5	0.1	0.0
Intersection point.	2.302 μ^{-1}	2.300 μ^{-1}	2.294 μ^{-1}	2.294 μ^{-1}
Blue fitting:-				
Ratio of errors.	1.371	1.190	1.016	0.967
R.M.S. error.	0.178	0.160	0.141	0.135
Gradient.	10.24 ± 0.16	10.24 ± 0.14	10.30 ± 0.13	10.31 ± 0.13
Intercept at 2.3 μ^{-1}	4.01 ± 0.03	4.01 ± 0.03	4.03 ± 0.02	4.03 ± 0.02
Violet fitting:-				
Ratio of errors.	1.378	1.199	1.028	0.982
R.M.S. error.	0.205	0.182	0.158	0.152
Gradient.	7.04 ± 0.14	7.00 ± 0.12	6.96 ± 0.10	6.95 ± 0.10
Intercept at 2.3 μ^{-1}	4.01 ± 0.03	4.01 ± 0.02	4.01 ± 0.02	4.01 ± 0.02

Table 7.1 shows various parameters for the scaling factors 0.1 and 0.5 together with the cases of total and no rejection. When it is remembered that the scaling factor operates on the squares of the residuals in the curve fitting, it is clear that once some two thirds of suspect points are rejected, the fitted parameters become relatively insensitive to further rejection. This is partly on account of the good distribution in position and sign of such points. The best fitting curve is therefore fairly well defined over a range of rejection but may be taken to be the curve that fits the data when the degree of rejection is such as to make the mean error of fitting equal to the mean expected error. This requires the scaling factor to be about 0.05 . Of course, the mean expected error may be incorrectly estimated but the above considerations seem more important and, if anything, point to an over estimation of the expected error. However, since grain noise predominates in the error estimate, there is not thought to be any particular bias.

With the suggested level of rejection of suspect points and the blue gradient normalised to unity, the blue part of the reddening curve is straight to 0.013 magnitude and the violet to 0.015 magnitude. The most probable position of the intersection point is calculated to be $2.294\ \mu^{-1}$, as shown in Table 7.1 . The sharpness of the corner is related to the distribution in wavelength and absorption of the probability of intersection of the fitted lines. Each of the two lines has errors associated with the derived coefficients and the interaction of these errors gives rise to the probability distribution. There are two coefficients fitted to the data for each line and the zero order coefficient represents the absorption at the zero of the reciprocal wavelength scale while the first order coefficient is the line gradient. Therefore, there are four errors to be considered but by shifting the

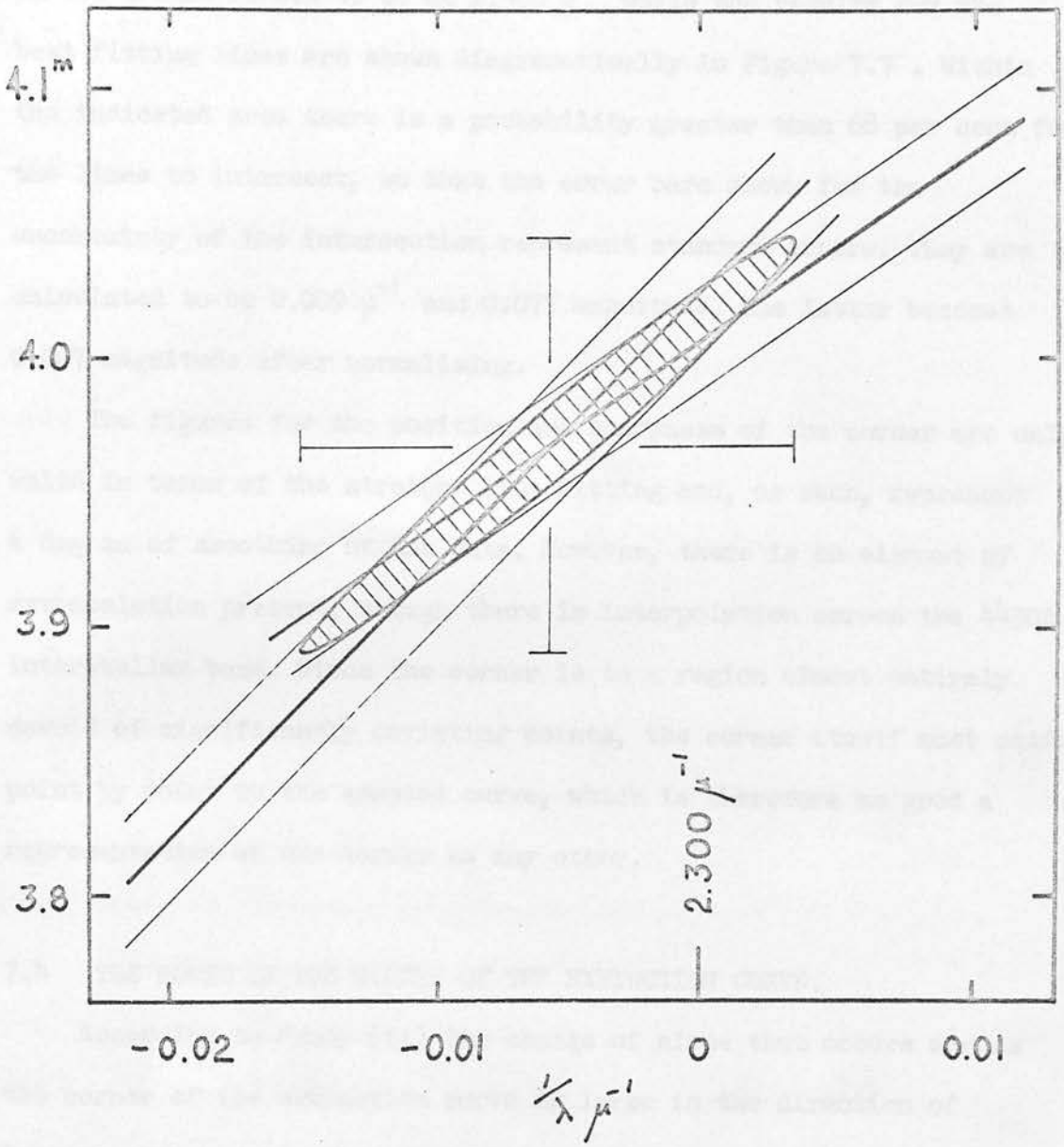

FIGURE 7.7

Errors associated with the fitted straight lines and their intersection.

origin of the wavelength scale to the region of interest, the effects of the gradient errors become negligible in comparison with the errors on the zero order coefficient. The data given in Table 7.1 are based on the origin chosen to be at 2.300 μ^{-1} while the results for the best fitting lines are shown diagramatically in Figure 7.7 . Within the indicated area there is a probability greater than 68 per cent for the lines to intersect, so that the error bars shown for the uncertainty of the intersection represent standard errors. They are calculated to be 0.009 μ^{-1} and 0.077 magnitude. The latter becomes 0.007 magnitude after normalising.

The figures for the position and sharpness of the corner are only valid in terms of the straight line fitting and, as such, represent a degree of smoothing of the data. However, there is no element of extrapolation present, though there is interpolation across the 4430A interstellar band. Since the corner is in a region almost entirely devoid of significantly deviating points, the corner itself must conform point by point to the adopted curve, which is therefore as good a representation of the corner as any other.

7.4 THE RATIO OF THE SLOPES OF THE EXTINCTION CURVE.

According to Nandy (11) the change of slope that occurs across the corner of the extinction curve is large in the direction of Perseus. Perseus was therefore chosen for this work in order to emphasise the corner. However, it became clear, during the course of the hand reduction of the spectra, that the corner was more apparent on some reddening curves than on others, while the mean ratio of the violet slope relative to the blue was found to be 0.61 . This is high when compared to Nandy's value of 0.46 and is more typical of Cygnus, for which he gives the value 0.64 . An even higher value of 0.67 results

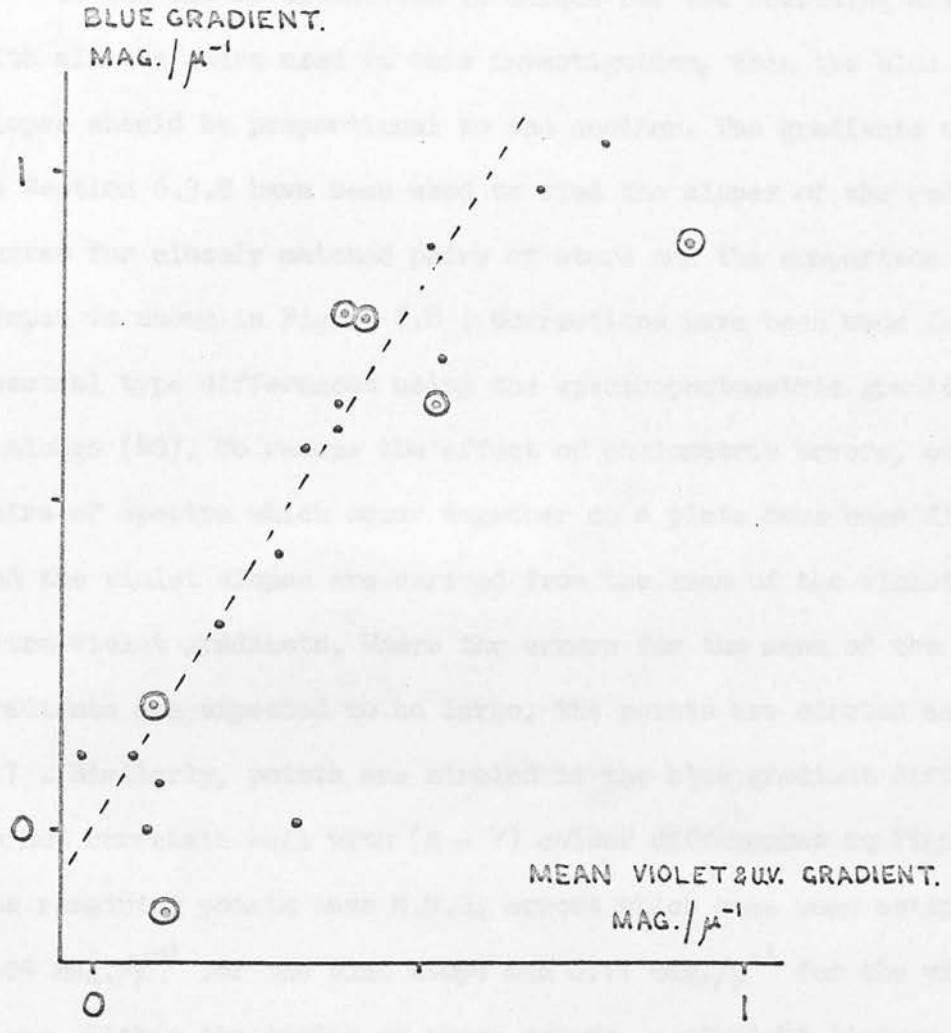

FIGURE 7.8

The two slopes of the reddening curve for different star pairs.

from the detailed examination of just over a half of the spectra which is given in the previous section. The discrepancy is explained in terms of photometric errors and observational selection, as follows.

If the law of extinction is unique for the reddening associated with all the stars used in this investigation, then the blue and violet slopes should be proportional to one another. The gradients obtained in Section 6.3.2 have been used to find the slopes of the reddening curves for closely matched pairs of stars and the comparison of the two slopes is shown in Figure 7.8 . Corrections have been made for small spectral type differences using the spectrophotometric gradients of Chalonge (40). To reduce the effect of photometric errors, only those pairs of spectra which occur together on a plate have been differenced and the violet slopes are derived from the mean of the violet and ultra-violet gradients. Where the errors for the mean of the two violet gradients are expected to be large, the points are circled as in Figure 6.7 . Similarly, points are circled if the blue gradient differences do not correlate well with (B - V) colour differences in Figure 6.5 . The remaining points have R.M.S. errors which have been estimated as 0.09 mag./μ^{-1} for the blue slope and 0.11 mag./μ^{-1} for the violet slope. Within the limits of these errors, a straight line can be drawn through the points and through the origin, with the exception of only one point. This implies that the relative slopes of the extinction curves are much the same, with a mean value for the ratio of 0.6, which is the value found for the mean curve derived by hand. However, the uncertainty of about 0.1 barely places this in agreement with Nandy's figure of 0.46 .

It was concluded in the previous section that the mean reddening curve used there was hardly affected by the photometric error curve. The high value for the ratio of the slopes must therefore be connected

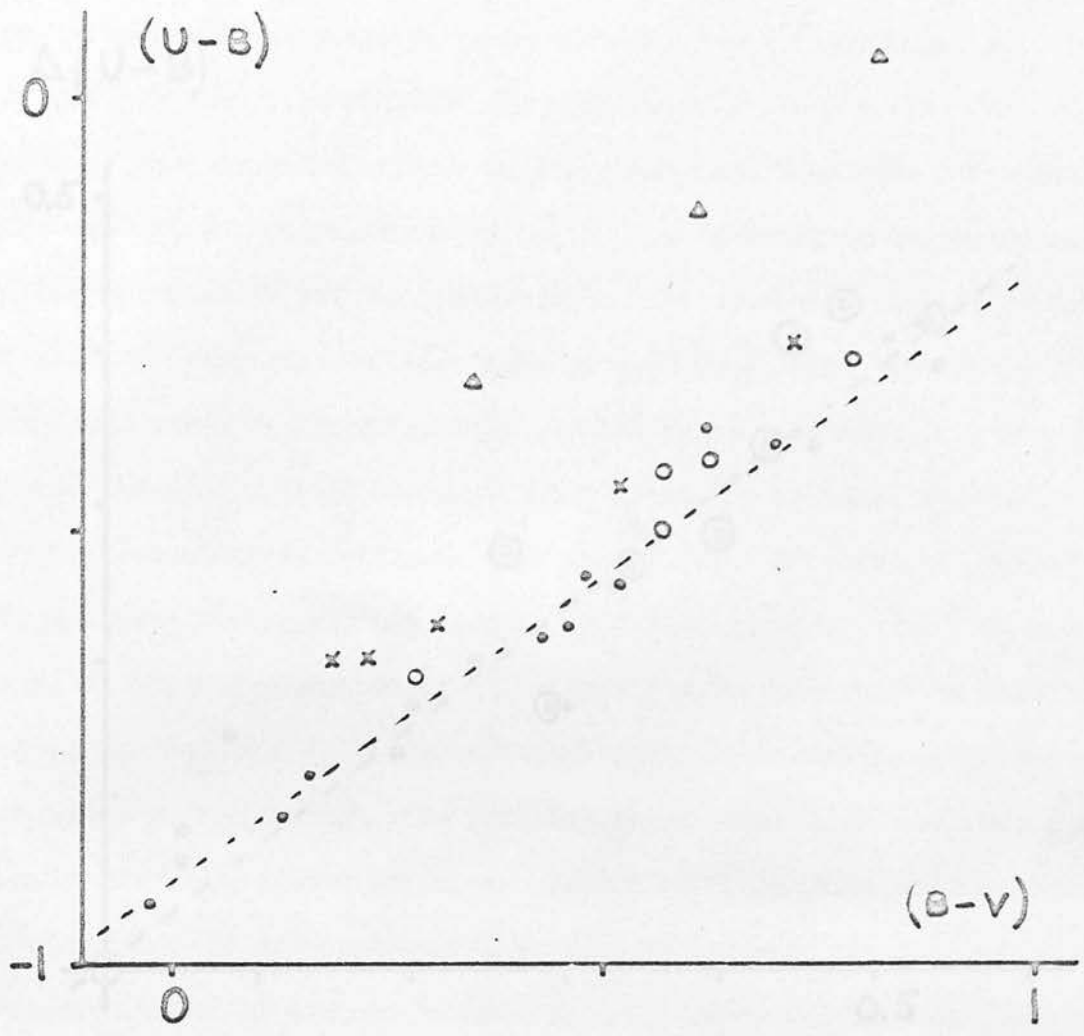

FIGURE 7.9

Two colour diagram for programme stars.

Δ denotes stars of type B8 and B9, X denotes B2, o denotes B1 and B0.5 , while ⊙ denotes the O stars.

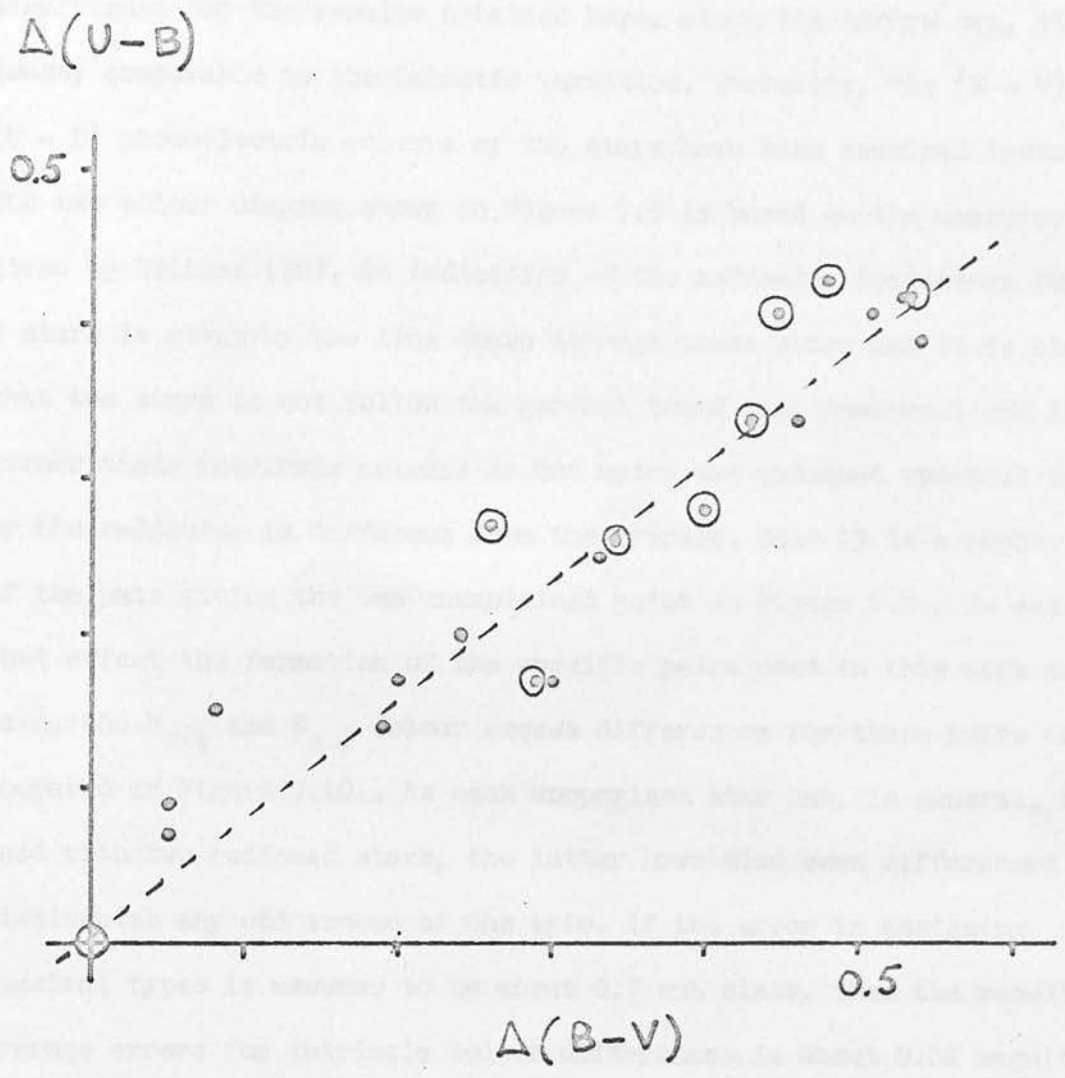

FIGURE 7.10

Comparison of E_{B-V} and E_{U-B} colour excess differences for star pairs.

with the stars or their associated reddening and this may be partly so for the remainder of the stars. Apparent differences in the ratio of the slopes of reddening curves of individual star pairs are not very significant for the results obtained here, since the errors are, at least, comparable to the Galactic variation. Therefore, the (B – V) and (U – B) photoelectric colours of the stars have been examined instead. The two colour diagram shown in Figure 7.9 is based on the measures given by Hiltner (30). An indication of the reddening trajectory for O stars is given by the line drawn through these stars and it is clear that two stars do not follow the general trend i.e. numbers 1 and 19. Either their intrinsic colours do not match the assigned spectral types or the reddening is different from the average. Star 19 is a member of the pair giving the one unexplained point in Figure 7.8 . To see what effect the formation of the specific pairs used in this work may have, the E_{U-B} and E_{B-V} colour excess differences for these pairs are compared in Figure 7.10 . As each comparison star has, in general, been used with two reddened stars, the latter have also been differenced to distinguish any odd member of the trio. If the error in assigning spectral types is assumed to be about 0.7 sub class, then the resulting average errors for intrinsic colour differences is about 0.02 magnitude and this is quite sufficient to allow the majority of points to fit the correlation shown. The remaining points seem to arise from the inclusion of four particular stars, namely numbers 1 and 19 as found before, 12 and possibly number 15. Since star 12 is of spectral type B8, the discrepancy can well come from the large intrinsic colour correction. It is therefore apparent that, in the absence of photometric errors the ratio of the slopes derived from the photographic measures would be nearly the same for most reddening curves but certain pairs of stars would give divergent values. Thus the high value obtained in the

previous section is caused by the particular selection of star pairs which correspond to the circled points in Figure 7.10 .

The correlation shown in Figure 7.10 is found to be consistent with the mean reddening trajectory for O stars in the Milky Way, which is given by Hiltner and Johnson (45) as:-

$$E_{U-B} / E_{B-V} = 0.72 + 0.05 E_{B-V}$$

Because the blue filter is close to the corner of the extinction curve, the first term depends only on the ratio of the slopes of the extinction curve while the second term represents the changes in effective wavelengths of the filters. The gradient of the line in Figure 7.10 was therefore corrected with the aid of the curvature term to derive the gradient of the reddening trajectory for little reddened stars. Since the latter gradient agrees with the mean value for the Milky Way, it appears that most of the stars used in this programme are associated with reddening which is typical, rather than of the type found in Perseus. This is confirmed by the agreement between the mean ratio of the slopes and the average of the ratios for different parts of the sky, as given by Nandy, weighted according to the number of reddened stars observed. The stars are necessarily brighter than those used by Nandy, so they may not be distant enough to give Perseus type reddening. It is also interesting to note that the difference may be due to the proximity of this area of the sky to the Galactic discontinuity at 140 degrees longitude (46) where rapid changes in the properties of the interstellar medium have been observed.

7.5 CONCLUSION.

The principal sources of error in the present work are the photographic recording process and the matching of pairs of stars. It has been shown that changes in the effective sensitivity across

photographic plates give rise to wavelength dependent photometric errors. These are such that the indirect calibration of the stellar plates, which the use of a slit spectrograph necessitates, is hardly inferior to the direct methods of objective prism spectrophotometry. Further, for a homogeneous set of plates, a standard reference spectrum on each stellar plate is not required. Because the Balmer lines of Of stars and, to some extent, O stars are not well behaved, it is now evident that, at the level of resolution used here, they are not very suitable for forming pairs, since strong residuals of H_γ so close to the corner of the extinction curve are undesirable. Observing time would have been better spent in obtaining additional spectra of early B stars, though the difficulty caused by the Balmer lines of the B2 star HD 13866 has been noted. In practice, the errors which most influence the interpretation of the extinction curve prove to be those due to photographic grain and residual spectrum lines. They are of about the same size in the final curve but, as significant lines only occur at certain wavelengths, the grain noise dominates.

The three conclusions of astronomical interest are based mainly on 26 spectra of 13 stars, the resulting extinction curve having a resolution of 6A and some three magnitudes difference of extinction between 2.0 and 2.3 μ^{-1}. It has been shown that the interstellar band at 4430A does not cause the observed corner of the extinction curve, the resolution attained here being quite sufficient to show the band and the corner as separate features. This tends to be confirmed by Seddon (47) who shows that the extent of the band is far less than had been supposed. Over the range 2.0 to 2.7 μ^{-1} the extinction law is best represented by two straight lines intersecting at $2.294 + 0.009\ \mu^{-1}$ (4359 + 17A) . When the blue part of the curve is normalised to give a slope of unity, the average deviation of the data points is 0.013^m for

the blue and 0.015^m for the violet part of the curve. It is also shown that at this level of deviation, the intersecting straight lines are a valid representation of the corner itself, the change of slope therefore taking place within the resolution bandwidth of 6A .

It is interesting to note that Nandy (14), having obtained a reddening curve of high photometric accuracy from the spectra of 130 reddened stars, has determined the position of the corner to be at $2.31 + 0.01\ \mu^{-1}$. The agreement with the present value is remarkable when it is considered that the position was found from the extrapolation of straight line fittings and to data which cover more than double the reciprocal wavelength range used here but with one thirtieth the density of data points. Unless the agreement is fortuitous, it points to the straightness of each section of the extinction curve between 1.3 and $2.9\ \mu^{-1}$.

Any physical theory for the optical properties of the interstellar grains must take into account all the observed features of the extinction curve. The linearity of the two sections of the curve already requires that, for models based on scattering, the grains must have fairly specific properties and size distribution. However, since the linearity shows up at the greater resolution and density of points obtained here, the constraints are even greater. The comparatively sharp nature of the corner suggests that the optical properties of the grains change abruptly at the wavelength of the corner and this, coupled with the straightness of the two sections of the curve, may mean that mechanisms other than pure scattering may be responsible, at least in part, for interstellar extinction. In view of this, the definition of the corner should be improved, for the position and profile of the corner may well indicate the exact nature of the extinction mechanism and the composition of the interstellar material.

REFERENCES.

1 Trumpler,R.J., 1930, Lick Obs. Bull., 14 , 154.

2 Stebbins,J., Huffer,C.M. and Whitford,A.E., 1939, Ap.J., 90 , 209.

3 Oort,J.H., 1932, B.A.N., 238 , 249.

4 Lindblad,B., 1935, Nature, 135 , 133.

5 Hulst,H.C. van de, 1949, Rech. Astr. Obs. Utrecht, 11 , Part 2.

6 Platt,J.R., 1956, Ap.J., 123 , 486.

7 Hiltner,W.A. and Hall,J.S., 1949, Science, 109 , 165 and 166.

8 Cayrel,R. and Schatzman,E., 1954, Ann. d'ap., 17 , 555.

9 Hoyle,F. and Wickramasinghe,N.C., 1962, M.N.R.A.S., 124 , 417.

10 Nandy,K., 1964, Publ. Roy. Obs. Edin., 3 , 142.

11 Nandy,K., 1965, Publ. Roy. Obs. Edin., 5 , 13.

12 Nandy,K., 1966, Publ. Roy. Obs. Edin., 5 , 233.

13 Nandy,K., 1967, Publ. Roy. Obs. Edin., 6 , 25.

14 Nandy,K., 1968, Publ. Roy. Obs. Edin., 7 , 169.

15 Johnson,H.L. and Morgan,W.W., 1955, Ap.J., 122 , 142.

16 Borgman,J., 1961, B.A.N., 16 , 99.

17 Wampler,E.J., 1961, Ap.J., 134 , 861.

18 Johnson,H.L. and Borgman,J., 1963, B.A.N., 17 , 115.

19 Johnson,H.L., 1965, ApJ., 141 , 923.

20 Boggess,A. and Borgman,J., 1964, ApJ., 140 , 1636.

21 Stecher,T.P., 1965, ApJ., 142 , 1683.

22 Wickramasinghe,N.C., 1967, Interstellar Grains, (Chapman and Hall, London.)

23 Nandy,K. & Wickramasinghe,N.C., 1965, Publ. Roy. Obs. Edin., 5 ,29.

24 Stecher,T.P. and Donn,B., 1965, ApJ., 142 , 1681.

25 Whitford,A.E., 1958, A.J., 63 , 201.

26 Oke,J.B., 1964, Ap.J., 140 , 689.

27 Willstrop,R.V., 1965, Mem. R.A.S., 69 , 83.

28 Underhill,A.B. and Walker,G.A.H., 1965, M.N.R.A.S., 131 , 475.

29 Weber,A.E., 1914, Ann. Physik, 45 , 801.

30 Hiltner,W.A., 1956, Ap.J. Suppl. Ser., 2 , 389.

31 Kreveld,A. van, and Ornstein,L.S., 1936, Proc. Acad. Sci. Amsterdam, 39 , 477.

32 Webb,J.H., 1936, J.O.S.A., 26 , 12.

33 Webb,J.H., 1933, J.O.S.A., 23 , 317.

34 Hurter,F. and Driffield,V.C., 1890, J. Soc. Chem. Ind., 9 , 455.

35 Baker,E.A., 1925, Proc. Roy. Soc. Edinburgh, 45 , 34.

36 Schwarzschild,K., 1900, Ap.J., 11 , 89.

37 Allen,C.W., 1962, Astronomical Quantities, (Athlone Press, London.)

38 Underhill,A.B., 1966, The Early Type Stars, (Reidel Publishing Co., Dordrecht, Holland.)

39 Froberg,C.E., 1965, Introduction to Numerical Analysis, (Addison – Wesley, London.)

40 Chalonge,D., 1956, Ann. d'ap., 19 , 258.

41 Sinnerstad,U., 1961, Stockholms Obs. Ann., 22 , No. 2.

42 Lawrence,L.C. & Reddish,V.C., 1965, Publ. Roy. Obs. Edin., 3 , 280.

43 Rozis – Saulgeot,A.M., 1956, Ann. d'ap., 19 , 274.

44 Divan,L., 1954, Ann. d'ap., 17 , 456.

45 Hiltner,W.A. and Johnson,H.L., 1956, Ap.J., 124 , 367.

46 Reddish,V.C., 1967, Nature, 213 , 1107.

47 Seddon,H., 1967, Nature, 214 , 257.